Title

Enhancing Grasping in Robotic and Human-robot Systems by Leveraging Intrinsic Functionality

Author

Lee, Jungpyo

Publication Date

2024

Peer reviewed|Thesis/dissertation

Enhancing Grasping in Robotic and Human-robot Systems by Leveraging Intrinsic Functionality

By

Jungpyo Lee

A dissertation submitted in partial satisfaction of the

requirements for the degree of

Doctor of Philosophy

in

Engineering - Mechanical Engineering

in the

Graduate Division

of the

University of California, Berkeley

Committee in charge:

Professor Hannah Stuart, Chair
Professor Kosa Goucher-Lambert
Professor Masayoshi Tomizuka

Summer 2024

Enhancing Grasping in Robotic and Human-robot Systems by Leveraging Intrinsic Functionality

Abstract

Enhancing Grasping in Robotic and Human-robot Systems by Leveraging Intrinsic Functionality

by

Jungpyo Lee

Doctor of Philosophy in Engineering - Mechanical Engineering

University of California, Berkeley

Professor Hannah Stuart, Chair

Robotic grasping and manipulation are essential for applications ranging from industrial automation to assistive technologies. In this dissertation, I address the challenges of improving these capabilities through advancements in gripper design by leveraging intrinsic functionality in the systems. The first focus is on developing a smart suction cup system with pressure-based tactile sensors that detect contact status, enabling real-time adjustments for enhanced grasp success rates. A developed suction cup and its haptic search algorithm leverage suction airflow into tactile feedback to achieve robust robotic grasping. The second focus is on regaining grasping function through the development of an assistive Dorsal Grasper designed for individuals with spinal cord injuries at cervical levels. This device enhances grasping capability by leveraging residual motor functions and providing additional mechanical support, thus improving the ability to perform daily tasks. By leveraging the inherent functions of systems, the dissertation offers a simple but effective approach to advancing robotic and human-robot systems, contributing novel insights and solutions.

Towards Truth

Contents

List of Figures

List of Tables

Acknowledgments

First, I would like to express my gratitude to the funding sources that supported me during my Ph.D. at UC Berkeley. The Korean Government Scholarship for Graduate Study Overseas was my primary funding during the first couple of years of graduate life. It was an honor to receive this funding from my country. Additionally, I was able to work on the Smart Suction Cup with support from InnoHK of the Government of the Hong Kong Special Administrative Region via the Hong Kong Centre for Logistics Robotics.

I deeply appreciate my dissertation committee. Prof. Hannah Stuart, my Ph.D. advisor, accepted me into Berkeley and provided unwavering support throughout my studies. Without her guidance, both academically and personally, I would not have succeeded in my Ph.D. Prof. Kosa Goucher-Lambert, who also served on my Qual committee, provided insightful comments that strengthened my dissertation. Prof. Masayoshi Tomizuka led the funding source that supported me during the latter half of my Ph.D., making him an important figure in my academic journey. I also want to thank other Qual committee members, Prof. Dennis Lieu, Prof. Grace O'Connell, and Prof. Yi Ma. Special thanks to Prof. Dennis Lieu, who chaired my Qual and for whom I was a graduate student instructor for two semesters. It was a great opportunity to learn essential skills for an academic career.

As the first international student in the Embodied Dexterity Group (EDG), my cohorts Sebastian Lee, Juan Romero, and Wilson Torres helped me adapt to the new environment both inside and outside the lab. I had a great time with lab members who provided valuable feedback during lab meetings and sub-group meetings. I would not have been able to write this thesis without their contributions. I would like to thank Michael Abbott, Monica Li, Cyndia Cao, Laura Trees, Sareum Kim, Erin Chang, Drew McPherson, Deaho Moon, Justin Page, Raghid Mardini, Jadesola Aderibigbe, Ben Davis, Andrew Galassi, and Amber Young. I also appreciate the undergraduate students who worked with me on this dissertation. Licheng Yu helped develop the Dorsal Grasper and the initial experimental setup, while Haoxiang Huang assisted with setting up workspace-related experiments with the 3D motion capture system.

Previous postdocs in our lab played a significant role in my research. Dr. Tae Myung Huh developed the Smart Suction Cup, a crucial part of this dissertation, and guided me in researching robotic systems. He mentored me in various aspects, including technical skills, and inspired my research. Dr. Yuri Gloumakov was also a great academic mentor and friend, providing sharp feedback on my research, particularly for the Dorsal Grasper.

Outside the lab, I owe thanks to many people. I am grateful to all my friends who supported me: Daewon Lee, Hotae Lee, Sangjoon Lee, Jason Choi, and all members of the Korean Graduate Student Association (KGSA). Thanks also to the friends who welcomed me whenever I visited Korea. Lastly, I want to express my sincere gratitude to my wife, Eunsun Jang. Her support and encouragement have been essential throughout my Ph.D. journey. Eunsun made the significant sacrifice of moving to the United States to be with me, and her presence has been a constant source of strength. Without her, this dissertation would not have been possible. I am deeply appreciative of her support and dedication.

Chapter 1

Introduction

Grasping and manipulation are not only among the most fundamental capabilities that enable robots to perform a wide range of tasks, from industrial automation to assistive technologies for individuals with disabilities, but also among the most challenging tasks in robotic systems [1, 2]. Considering the infinite variability and uncertainty of the real world, physical interactions and changes in the environment make robust robotic grasping extremely difficult [3]. The pipeline of robotic grasping comprises a series of steps: decision, perception, planning, and grasp execution [4]. For example, in a simple pick-and-place task, the process begins with the decision phase, where the robot identifies the object to be grasped and the goal location. In the perception phase, sensors (usually vision-based) gather information about the environment and the object's properties, such as shape and orientation. Next, in the planning phase, the data from the perception phase is used to determine the optimal grasp strategy, including grasp pose estimation and path planning. Finally, during the grasp execution phase, the robot physically performs the grasp. In this phase, additional feedback control can be used to make adjustments and ensure stability by real-time tactile sensing and observation [5]. This dissertation primarily focuses on the grasp execution phase.

In addition to the steps above, gripper design plays a crucial role in robotic grasping, since it significantly influences the strategies for decision, perception, planning, and particularly execution. Several types of grippers are commonly used in robotic systems with their own strengths/limitations and applications (Fig. 1.1). These include parallel jaw grippers, anthropomorphic multi-finger hands, vacuum suction cups, and other types of grippers, such as the universal gripper with a particle jamming[6] and filament gripper[7]. Parallel jaw grippers are simple and the most common gripper type for various applications involving small and uniform objects, though they may struggle with more complex motion such as in-hand manipulation[2]. Anthropomorphic multi-finger grippers, designed to mimic the human hand, offer greater dexterity and adaptability, making them suitable for tasks requiring fine manipulation, including in-hand manipulation, although many of these hands do not have as many controllable degrees of freedom as the human hand[8]. Suction grippers, which rely on vacuum suction, are specialized for handling smooth, flat surfaces but are less effective on porous or textured objects[9]. One example case of a suction gripper is

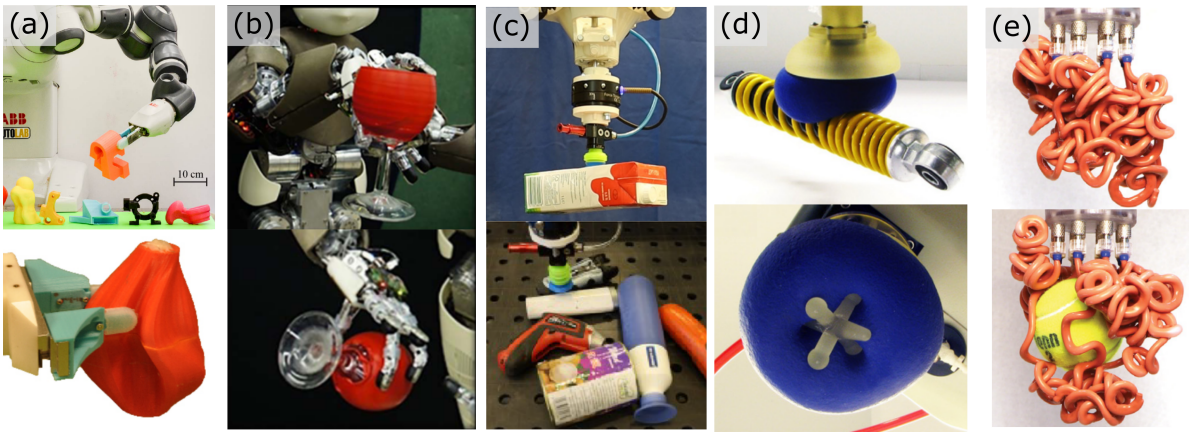

Figure 1.1: Various gripper design in Robot systems. (a) Parellel jaw gripper [10]. (b) Anthromorphic hand from [2] (originally from Learning Algorithms and System Laboratory, EPFL). (c) Vacuum suction cup from [11]. (d) Universal gripper from [6]. (e)Filament gripper [7].

industrial pick-and-place operations in warehouses. Other types of grippers are specialized for specific applications. For example, universal grippers, which use granular materials with particle jamming, provide versatility by conforming to various object shapes through their shape-adaptive mechanisms.

All of these grippers face challenges in determining the robustness of a grasp or even whether the grasp is successful. One way to check the grasp status is to use a force/torque sensor in the wrist of a robot arm, which measures the increased load on the gripper. However, this on/off state measurement does not guarantee grasp quality and can eventually result in a failed grasp. Therefore, real-time feedback from sensor information, such as tactile sensors and vision, is required to achieve robust grasping [12]. Tactile sensing is particularly effective in detecting real-time interactions with objects, such as local contact status or dynamic events like slipping [5]. Consequently, over several decades, many researchers have been developing tactile sensors for robotic end-effectors using a variety of methods [13, 14].

In parallel to fully robotic systems, gripper design also plays a critical role in human-robot systems. These systems leverage human inherent functionality rather than relying solely on robotic manipulators, such as 6 DOF robotic arms or delta robots. Instead, they utilize the human body, including the trunk, arm, and hand, to perform tasks. In terms of sensing, robotic systems primarily use vision and require the development of advanced vision algorithms for perception and planning. In contrast, humans have exceptional multi-modal sensing capabilities, including vision, proprioception, mechano-cutaneous sensors, and even

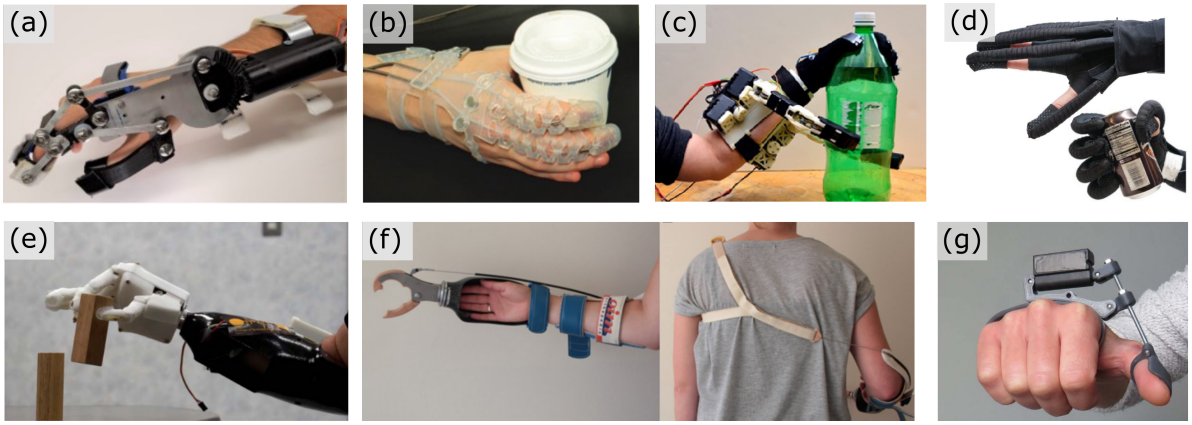

Figure 1.2: Various gripper design in human-robot systems. (a) Motorized wrist-driven orthosis from [15]. (b) Exo-Glove Poly II from [16]. (c) Assistive device with supernumerary fingers from [17]. (d) Fabric-based soft robot glove from [18]. (e) Myoelectric prosthetic hand from [19]. (f) Body-powered prosthetic hand from [20]. (g) T-GRIP thumb exoskeleton from [21].

sound, which enable seamless, adaptive, and real-time interactions with the environment. Grippers in human-robot systems are particularly relevant for augmenting or restoring functions in normative individuals or ones with disabilities, such as those who have experienced a stroke, spinal cord injury, or amputation (Fig. 1.2). These systems aim to restore or enhance the user's ability to perform everyday tasks by complementing their natural movements with robotic assistance. In addition to functional aspects, other considerations are crucial for the success of human-robot systems. These include weight, as the device must be lightweight to prevent fatigue; aesthetics, to ensure that the device is visually acceptable to the user; comfort, to allow for long-term use without discomfort; and donnability, to ensure the device is easy to put on and take off by themselves.

The overall goal of this dissertation is to design grippers that utilize the intrinsic functions of systems to improve grasping efficiency and adaptability. Intrinsic functions refer to the inherent properties and capabilities that a system already has without the need for additional external mechanisms. Leveraging these intrinsic functions has several advantages. First, it leads to more efficient and adaptable solutions compared to integrating extra sensors or actuators. Second, using intrinsic functions reduces the need for complex and expensive components, making the technology more cost-effective and reliable. Also, it results in more intuitive and natural interactions, enhancing user experience and system usability. Thus, by leveraging the intrinsic functions of systems, the designed gripper will effectively adapt to the system and improve its capabilities.

In this dissertation, I introduce two new grippers designed to enhance grasping capabil-

ities in both robotic and human-robot systems by leveraging the intrinsic functionality of these systems. The first gripper, called the Smart Suction Cup, is a vacuum suction gripper specifically designed to address and fine-tune errors arising from the perception and planning phases. By utilizing inherent suction airflow during actuation, additional transducers do not need to be integrated into the suction cup structure in order to gather contact information between the cups and objects. The second gripper, called the Dorsal Grasper, is an assistive wearable device to restore grasping capabilities for individuals with impaired motor function. Since people with disabilities still have significant sensory modalities such as vision, proprioception, and sound, as well as some degree of motor function, the Dorsal Grasper leverages these residual sensorimotor abilities and provides additional mechanical support to help users regain independence and improve their quality of life through enhanced hand functionality.

The Smart Suction cup

Autonomous robot systems often do not have perfect vision systems. Unlike humans, who can rapidly perceive and process visual information, robotic vision systems require extensive training and struggle with dynamic situations and disturbances such as direct light, which can cause significant performance issues. Additionally, during contact, robotic systems cannot see the contact surface, making it difficult to ensure a secure and stable grasp based solely on visual feedback. Traditional suction grasp planners often rely heavily on vision systems, which can fail to capture fine object details, leading to suction failures. To overcome these challenges, Huh et al. integrated tactile sensors into the Smart Suction Cup [22], featuring four internal chambers connected to pressure sensors, enabling us to measure its internal airflow. In this dissertation, I introduce haptic search algorithms with the Smart Suction cup guided by flow-based tactile sensors, allowing real-time monitoring of internal airflow to detect subtle changes in the contact surface so that the robot can adjust its pose to achieve better sealing.

The Dorsal Grasper

Humans, in particular, have an exceptional ability to grasp, owing to the advanced dexterity of our hands [2]. Additionally, our bodies are equipped with a multi-modal sensing system. These systems work together seamlessly, allowing us to adjust and compensate even if one sensory function is impaired. For example, in a dark room, we can still perform grasping and manipulation tasks using only proprioception, sound, and cutaneous sensing on the body. However, the loss of motor function severely impacts our grasping ability, dramatically reducing our capacity to perform everyday tasks. This loss of motor function is a critical factor that significantly affects the quality of life and the most desirable function to restore over other body functions [23]. To address this issue, I introduce the Dorsal Grasper, an assistive wearable device, designed to restore and enhance the grasping capabilities of individuals with impaired motor function. Designed from the perspective of human-robot collaboration, the

Dorsal Grasper augments the user's grasp strength and expands the graspable workspace, enabling them to perform daily tasks with greater ease and independence.

1.1 Dissertation Overview

The structure of this dissertation is as follows. Chapter 2 introduces the concept of haptic search algorithms with the Smart Suction Cup in an automated pick-and-place demonstration with adversarial objects. A state-of-the-art vision-based algorithm initiates suction grasping; however, when the vision system fails, the proposed haptic search algorithm adjusts the suction cup poses on objects. Consequently, our haptic search algorithm with the Smart Suction Cup demonstrates an increased grasping success rate through physical interactions with objects. Next, Chapter 3 focuses on one of the key applications of the Smart Suction Cup, which is haptic regrasping on Printed Circuit Boards (PCBs) using a new control method. This demonstrates the feasibility of the Smart Suction Cup and haptic search algorithm in an industrial application. From those chapters, I show the Smart Suction Cup and haptic search algorithm successfully enhanced grasping capability in suction cup grasping

Chapters 4 and 5 present the Dorsal Grasper, designed for people with Spinal Cord Injury (SCI) to restore the grasping capability of their hands. Specifically, Chapter 4 introduces the first version of the Dorsal Grasper, highlighting the effects of key components such as wrist extension and an artificial palm, and presents the results of the Grasp and Release test with subjects. In Chapter 5, I present the next version of the Dorsal Grasper and discuss how the device affects the grasping workspace and its influence on grasping and manipulation scenarios, using a motion capture system to evaluate these changes with an extended number of subjects. Overall, the Dorsal Grasper successfully leverages the residual sensorimotor functions of individuals with disabilities to enhance their grasping capabilities, addressing the challenges they face. Finally, in Chapter 6, I describe the conclusions of the dissertation and outline future work for the projects.

1.2 List of Publishcation

The results presented in this dissertation are drawn from several publications first-authored or co-first-authored by the dissertation's author. Specifically:

- Chapter 2 contains the full text of a co-first-authored publication as from:
  - J. Lee, S. D. Lee, T. M. Huh, and H. S. Stuart, "Haptic search with the smart suction cup on adversarial objects," IEEE Transactions on Robotics, 2024 vol. 40, pp. 226–239. ©2024 IEEE
  - This work was done in collaboration with graduate student Sebastian Lee. Sebastian Lee focused on the characterization of rotational alignment and experimental

setup, while Jungpyo Lee concentrated on the characterization of lateral positioning and conducted bin-picking experiments.

- Chapter 3 contains the full text of an accepted paper from:
  - J. Lee, Z. Sun, Z. Dong, F. Chen, H. S. Stuart, "Regrasping on Printed Circuit Boards with the Smart Suction Cup," IEEE International Conference on Robotics and Automation (ICRA), 2024. [Accepted]
- Chapter 4 contains the full text of a publication from:
  - J. Lee, L. Yu, L. Derbier, and H. S. Stuart, "Assistive supernumerary grasping with the back of the hand," in 2021 IEEE International Conference on Robotics and Automation (ICRA). 2021, pp. 6154–6160. ©2021 IEEE
- Chapter 5 contains the full text of a preprint (in revision) from:
  - J. Lee, A. I.W. McPherson, H. Huang, L. Yu, Y. Gloumakov, and H. S. Stuart, "The Supernumerary *Dorsal Grasper* for people with C5-C7 spinal cord injury," IEEE Transactions on Neural Systems and Rehabilitation Engineering. [In revision, DOI (preprint): 10.36227/techrxiv.171625805.56926586/v1]

Chapter 2

The Smart Suction Cup: Haptic search introduction

Suction cups are an important gripper type in industrial robot applications, and prior literature focuses on using vision-based planners to improve grasping success in these tasks. Vision-based planners can fail due to adversarial objects or lose generalizability for unseen scenarios, without retraining learned algorithms. We propose haptic exploration to improve suction cup grasping when visual grasp planners fail. We present the Smart Suction Cup, an end-effector that utilizes internal flow measurements for tactile sensing. We show that model-based haptic search methods, guided by these flow measurements, improve grasping success by up to 2.5x as compared with using only a vision planner during a bin-picking task. In characterizing the Smart Suction Cup on both geometric edges and curves, we find that flow rate can accurately predict the ideal motion direction even with large postural errors. The Smart Suction Cup includes no electronics on the cup itself, such that the design is easy to fabricate and haptic exploration does not damage the sensor. This work motivates the use of suction cups with autonomous haptic search capabilities in especially adversarial scenarios.

2.1 Introduction

Vacuum grippers, or suction grippers, are widely used in industry for simple pick and place operations. Relying on negative internal pressure that forms when sealed against a surface, the suction gripper can gently handle an object without applying squeezing force, which allows an astrictive handling of various types of objects. If the item to be grasped is smooth and well modelled, as in manufacturing lines, the gripper can repeatably and predictably handle it with high reliability. However, for grasping in unstructured environments, e.g., in e-commerce warehouses, objects vary dramatically and present many different surface conditions that may or may not be easy to visually perceive or grip with a suction cup. Careful planning of grasp contact location is therefore important, and methods for doing so have been

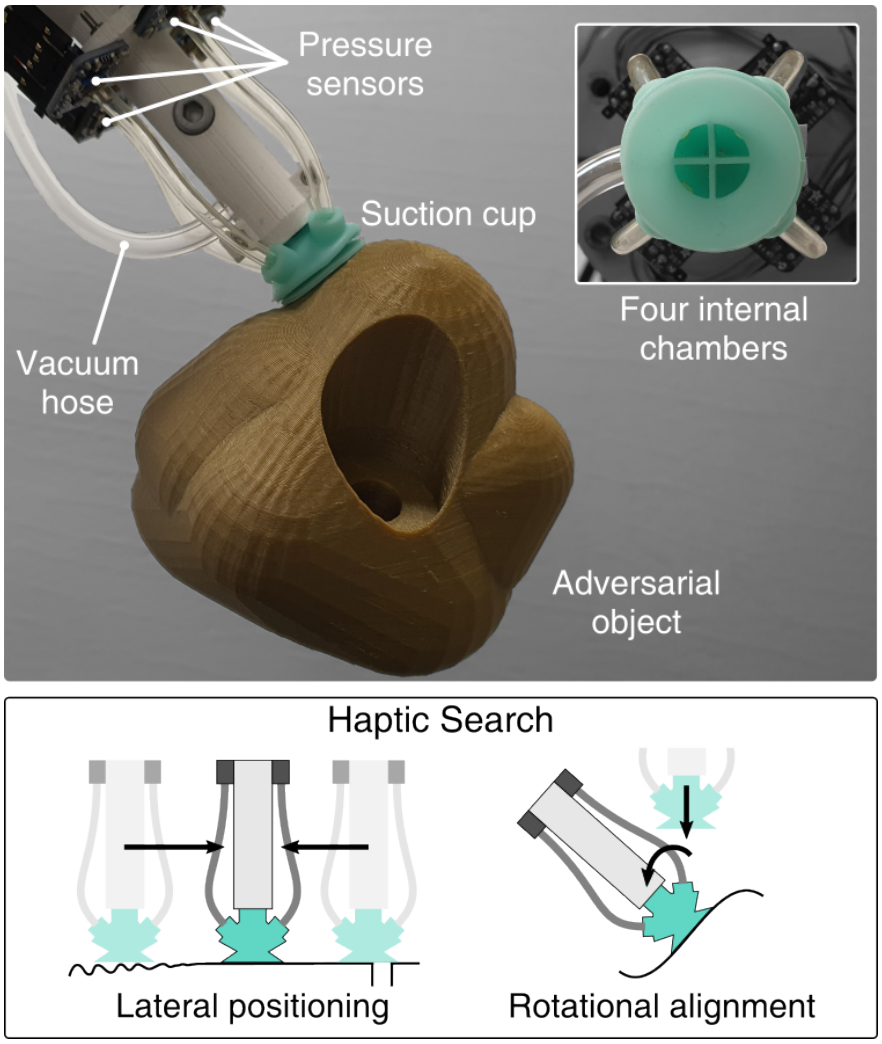

Figure 2.1: The multi-chamber Smart Suction Cup grips an adversarial object. The cup has four internal chambers, each connected to a pressure transducer that provides a measure of internal flow rate. It is able to localize small breaks in the seal due to, for example, the rugosity (e.g., wrinkles, bumps, etc.) of the object surface. Haptic search can allow for successful gripping even when the initial grasping point fails, important for visually-adversarial objects.

widely studied for the past few years. While there have been successful demonstrations of versatile suction grasp planners, these methods often rely on vision, which may not capture fine object details of the geometry and lead to suction failure. Moreover, pre-trained models are typically specific to certain suction cup and camera configurations, making it challenging to transfer these methods to different hardware setups without retraining. Time-consuming retraining currently presents a barrier to adoption.

To address these challenges, we propose the use of autonomous haptic search – or the repositioning of the cup using contact measurements – to supplement vision in suction grasping. This new approach leverages pre-trained vision-based grasp planners to obtain an approximate solution before then fine-tuning the pose after contact occurs until the grasp succeeds. For this method to be effective, we assume that a successful grasp point is close to the pre-trained planner's solution even when errors emerge, as the planner already considers key factors of graspability such as the object's weight distribution and the suction seal formation of a similar suction cup. To adjust the contact location, we use haptic exploration driven by flow-based tactile sensors on our Smart Suction Cup, first presented in [22]. This design has the advantage of no electronics embedded in the cup itself, but remote sensors can still provide valuable information about local suction leakages to overcome grasp failures.

Overview

Section 2.2 provides a review of related works. In Section 2.3, the Smart Suction Cup is described along with computational fluid dynamics models to demonstrate the expected signals; this design and flow analysis was previously presented in our prior work [22]. In the current work, we evolve this concept substantially beyond the prior work by now introducing and implementing autonomous haptic search. Section 2.4 presents our new proposed haptic search algorithm that utilizes the flow readings to improve grasping on adversarial objects. Experimental setup and procedures are described in Section 2.5, including both sensor characterization on primitive fixed objects and a bin-picking task with loose adversarial objects. Section 2.6 presents the results of these experiments; overall, we find that the use of the Smart Suction Cup haptic algorithm provides useful controller estimates and more successful grasping. Discussed in Section 2.7, the model-based haptic exploration encounters failure modes that can be further improved in future work.

The contributions of this paper are as follows:

1. Presentation and characterization of the first Smart Suction Cup that can sense local suction seal leakage on flat and curved surfaces by using remote pressure sensors.

2. Design of a suitable model-based haptic search controller using tactile sensing feedback to improve suction seal in real time.

3. Bin-picking experiments to evaluate performance across adaptive control algorithms with comparison to an existing vision-based grasp planner.

2.2 Related works

Suction grasp planning using vision

One major challenge in suction grasping is how to plan a contact location. Examples of planning methods include the heuristic search for a surface normal[24] and neural network training of grasp affordance using binary success labels[25]. Wan et al. (2020) use CAD model meshes to plan a grasp resisting gravitational wrench[26], and Dex-Net 3.0 learns the best suction contact pose from a point cloud considering both suction seal formation and gravitational wrench resistance[27]. Using a similar approach to Dex-Net, Cao et al. (2021) built a larger suction grasp dataset including RGB images and annotations of a billion suction points[28]. Using physics simulation, Shao et al. (2019) demonstrated a self-supervised learning method that finds suction grasp policies from RGB-D images for cluttered objects[29], and Cao et al. (2022) improved it by implementing dense object descriptors[30]. These aforementioned methods rely on RGB or depth sensors, which may not perceive fine details critical to suction success, e.g., texture, rugosity, porosity, etc. Vision can also become occluded in cluttered environments and heavily distorted with reflective or transparent objects.

Suction cup tactile sensors

Prior tactile sensors designed for use in suction cups provide partial information about object properties and vacuum sealing state. Researchers employ strain sensors on a suction cup by coating PEDOT [31] or carbon nanotube [32], or by installing microfluidic channels filled with carbon grease [33]. These strain sensors measure suction deformation during surface contact, estimating the compression forces and load distributions of suction cups [31], surface angles and stiffness [33], and object weight and center of gravity [32]. Alternatively, the contact of the suction cup can be measured indirectly by proximity sensors, including a capacitive base plate [34], inserted fiber optic cable [35], and micro-LIDAR [36]. However, these methods provide information about the cup deformation and surface proximity, which may not always correspond to a suction seal formation that is subject to fine local geometry and porosity. For direct contact sensing, Muller et al. (2017) report a thin pressure sensor array attached to the suction cup lips, measuring the distributed contact pressures [37]. However, the sensor film on the contact layer may weaken the suction seals.

Another straightforward approach is to monitor the internal vacuum pressure of the suction cup as a discrete measure of suction sealing, as in [38]. However, this prior implementation method does not localize the source of a leak around the lip's edge or measure local surface geometry, which is critical for adaptive haptic exploration for a better grasp.

Adaptive Regrasping using Tactile Sensing

Robust grasping in real-world scenarios has driven research in adaptive regrasping using tactile sensing. Due to uncertainties in vision systems and difficulties capturing detailed object features, tactile sensors are employed to detect contact information and guide improvements in response to unsuccessful grasps. Adaptive regrasp research has predominantly focused on friction-based grippers rather than suction grippers. Simple regrasping approaches include increasing grasp forces or grasp impedance upon detection of perturbations, such as external forces causing slips[5, 39]. For multi-finger grippers, researchers have demonstrated finding better grasping points through finger gaiting [39]. These methods primarily aim to improve handling or increase the stability of objects already held by the gripper. In object-picking processes, deep learning or reinforcement learning techniques have been employed to process complex tactile sensor data. Chebotar et al. (2016) used a multi-finger gripper with a BioTac sensor to demonstrate regrasping of a simple cylindrical object; they analyzed complex spatiotemporal tactile sensor information with PCA and learned a regrasp policy to update the pose[40]. Reinforcement learning was also used to learn hand grasping and regrasping policies in simulation, which are then effectively transferred to real robots [41]. For parallel jaw grippers, vision-based tactile sensors, such as Gelsight, have been used[42, 43]. In [42], the researchers trained a grasp quality metric from a given tactile image and simulated possible image shifts to guide the best regrasping policy. In [43], they directly trained for the best action to achieve the highest grasp success, which could be either a regrasp or pick.

The majority of the approaches mentioned above rely on tactile sensing information processed by deep learning or reinforcement learning algorithms. These methods can be unintuitive and may require significant training data for generalization. These approaches may involve fully reopening the gripper during regrasp actions, which can be time-consuming. Moreover, theses approaches may not be applicable to suction grasping due to differences in grasping mechanisms. In the following sections, we will present a physics- or intuition-based regrasping controller for suction cup grippers, enabling generalization without requiring extensive training data. Our controller operates without losing contact, potentially reducing operation times. To our knowledge, no existing literature addresses adaptive regrasping for suction cup grippers.

2.3 The Smart Suction Cup

The Smart Suction Cup utilizes internal airflow estimates to monitor local contact conditions. Internal wall structures separate the internal cavity of the suction cup into four chambers (Fig. 2.1) – one for each cardinal direction. Overall suction airflow is therefore separated between each chamber and the pressure sensor connected to each chamber provides an estimate of the local flow rate. We implement the wall structure inside a single-bellows suction cup for its versatility on different curvatures and orientations of objects. The internal wall structure only spans the proximal portion of the suction cup, in order to maintain typical

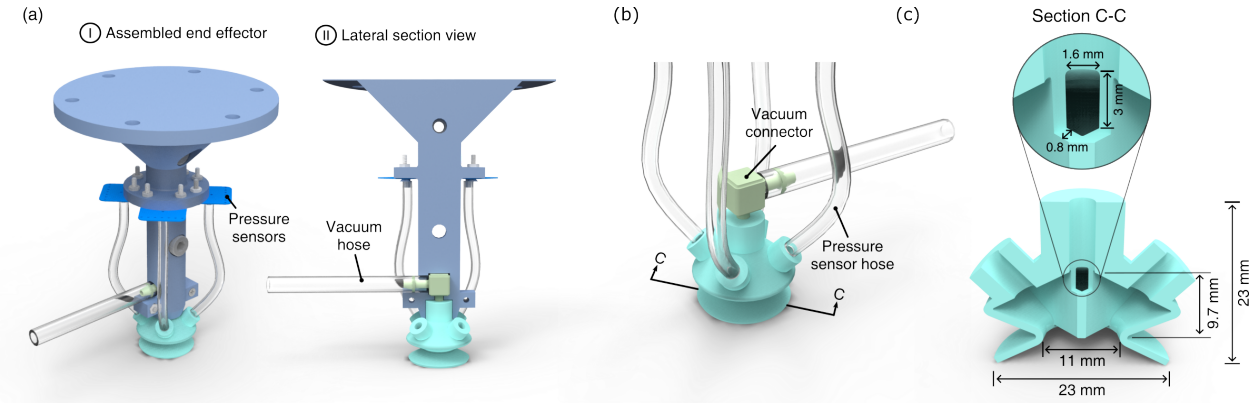

Figure 2.2: Design of the end effector and the suction cup. (a) The end effector integration with the suction cup. (b) A close up of the suction cup shows how it is connected with a vacuum connector and hoses to the pressure sensors. (c) Cross-sectional view of the suction cup shows internal and outer dimensions.

flexibility, deformation and seal formation at the distal lip. As shown in Fig. 2.2a-b, the suction cup is mounted to an end effector fixture piece and connected with pressure transducers and a single vacuum hose with pressure regulation. For experimental trials, this end effector is integrated with a universal robot arm. Dimensions and internal geometry of the compliant cup are shown in Fig. 2.2c. A single prototype is used throughout experimental testing, without incurring damage or needing replacement.

Fabrication

We fabricate this 3D rubber structure including the chamber walls as in Fig. 2.3, with a single-step casting of silicone rubber. The casting mold comprises three parts, two outer shells and one core, that are 3D printed using an SLA 3D printer (Formlabs, Form2). These are assembled together using stainless steel dowel pins and bolts. To ensure the clean casting of the thin internal wall structures (0.8 mm thick), we used a syringe with a blunt needle (gauge 14) to inject uncured RTV silicone rubber (Smooth-On, MoldMax 40) and then vacuum-degassed it. After curing, the outer shells are removed and the silicone suction cup is stretched and peeled off of the inner core mold. Tearing of the silicone can occur during this step, especially with harder rubbers. Cast flashing around the lip of the cup can occur at the interface between the core and outer shells; deflashing is performed manually after demolding using a razor blade.

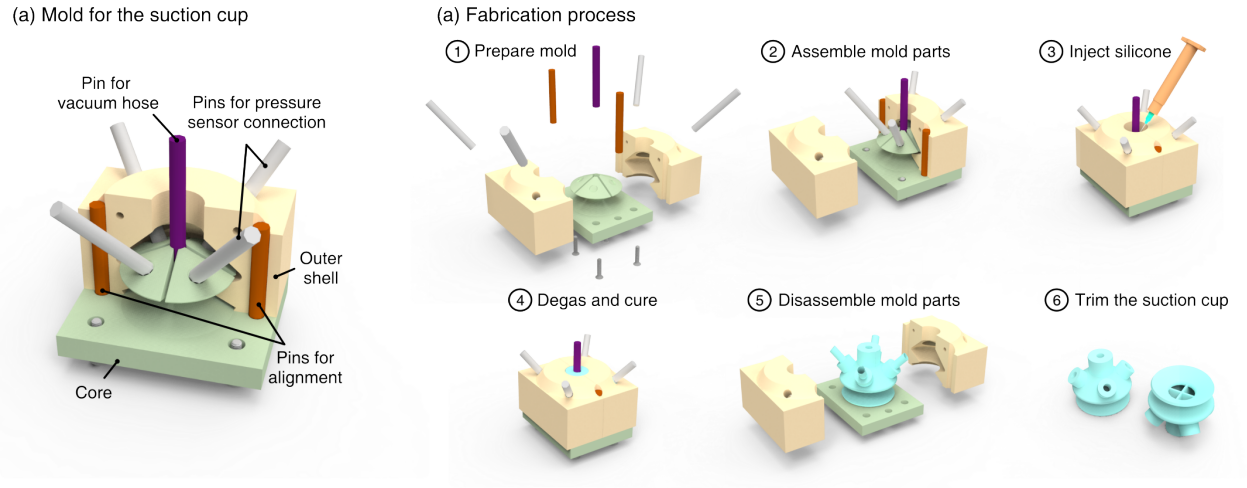

Figure 2.3: Casting mold and fabrication of the suction cup. (a) The casting mold has three parts (2 Outer shells and 1 core). Molds are aligned and fixed by pins and bottom bolts. (b) The fabrication process of the suction cup.

CFD Simulation

Using Computational Fluid Dynamics (CFD) simulation (COMSOL Multiphysics, $k-\epsilon$ turbulence model), we evaluate the gripper in two example suction flow cases: *vertical* and *horizontal* flow (Fig. 2.4a and b, respectively). The vertical flow case emulates when the suction cup only partially contacts a surface, or when the surface's shape inhibits sealing. However, when the suction cup engages with a smooth flat surface, flow can only move inward from the outer edges of the cup, as in the horizontal flow case. This horizontal leak is common as the suction cup is wrenched from the surface after a suction seal is formed. Although the suction cup will deform under vacuum pressure, we use modeled rigid geometry in the CFD simulation. For each case, we approximate the leak flow direction with a small pipe (D = 1 mm, L = 7 mm) intersecting with one of the internal chamber volumes as shown in Fig. 2.4a-b. The boundary conditions of the vacuum pump pressures and flow rates match the experimental setup.

The simulation results suggest that the gripper can detect leakage flows using differences between the four pressure transducers. We defined vacuum pressure (P_{vac}) as

$$P_{vac} = P_{atm} - P_{chamber} \tag{2.1}$$

where P_{atm} is atmospheric pressure. In the vertical leakage flow case, P_{vac} close to the leaking orifice shows the least vacuum pressure than the others (Fig. 2.4c). On the other hand, the horizontal leakage causes the diagonally opposite channel to have the lowest P_{vac} (Fig. 2.4d). These trends are supported by the flow results in Fig. 2.4e-f, where the vertical and horizontal orifices produce the highest flow rate in opposite chambers. The simulation

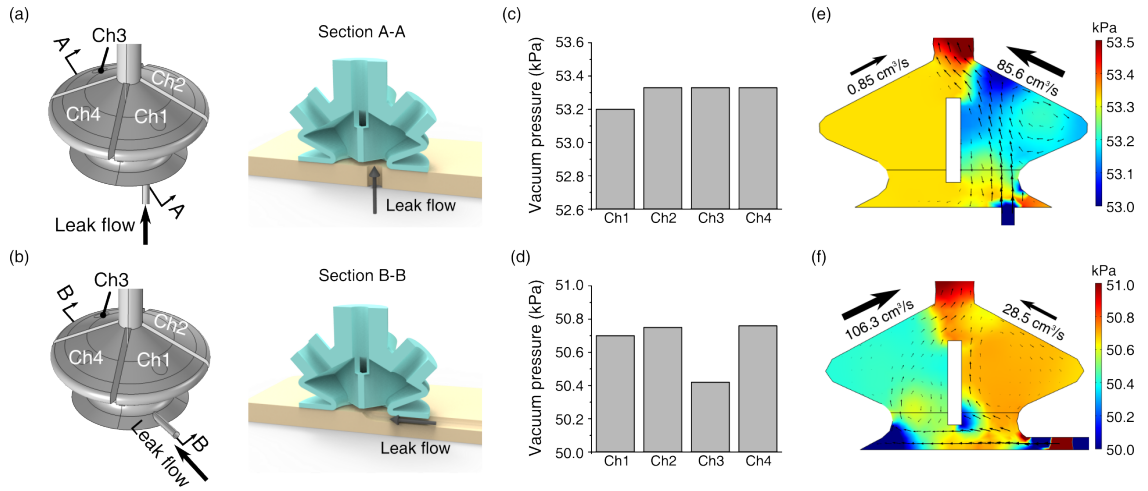

Figure 2.4: (a-b) Two cases of CFD simulation. Light yellow blocks are engaged objects and the cross-sectional view shows leak flow into channel number 1. (c-d) CFD result of the vacuum pressure measured at the sensor locations of each chamber. The bar graphs are from the maximum of the four vacuum pressures. (e-f) Cross-sectional view of the pressure distribution. The arrows inside represent the relative logarithmic scale of airflow velocity.

result also shows an estimate of the pressure difference between chambers (∼0.4kPa) which must be differentiated by the selected pressure sensors.

System integration

Four ported pressure sensors (Adafruit, MPRLS Breakout, 24 bit ADC, 0.01 Pa/count with an RMS noise of 5.0 Pa) connect with the four chambers of the smart suction cup via polyurethane tubes. The suction cup and the pressure sensors attach to a 3D printed fixture (Fig. 2.1a) and this fixture is attached to the wrist F/T sensor (ATI, Axia80, sampling rate 150 Hz) on the robot arm (Universal Robots, UR-10) as in Fig. 2.5. A microcontroller (Cypress, PSoC 4000s) is fixed to the arm proximal to the load cell and communicates with the four pressure sensors via I2C at a 166.7 Hz sampling rate.

A vacuum generator (VacMotion, VM5-NA) converts compressed building air to a vacuum source with a maximum vacuum of 85 kPa. A solenoid valve (SMC pneumatics, VQ110, On/off time = 3.5 / 2 ms), commanded by a microcontroller, regulates the compressed air as a means of moderating vacuum intensity. The vacuum hose that applies suction to the cup is attached at both the suction cup vacuum connector and proximal to the load cell to reduce tube movement and subsequent F/T coupling.

The experiments are conducted on a desktop computer running Ubuntu 20.04 with a 3.00-GHz Intel Core i5-7400 quad-core CPU and an Intel HD Graphics 630 GPU. The UR-

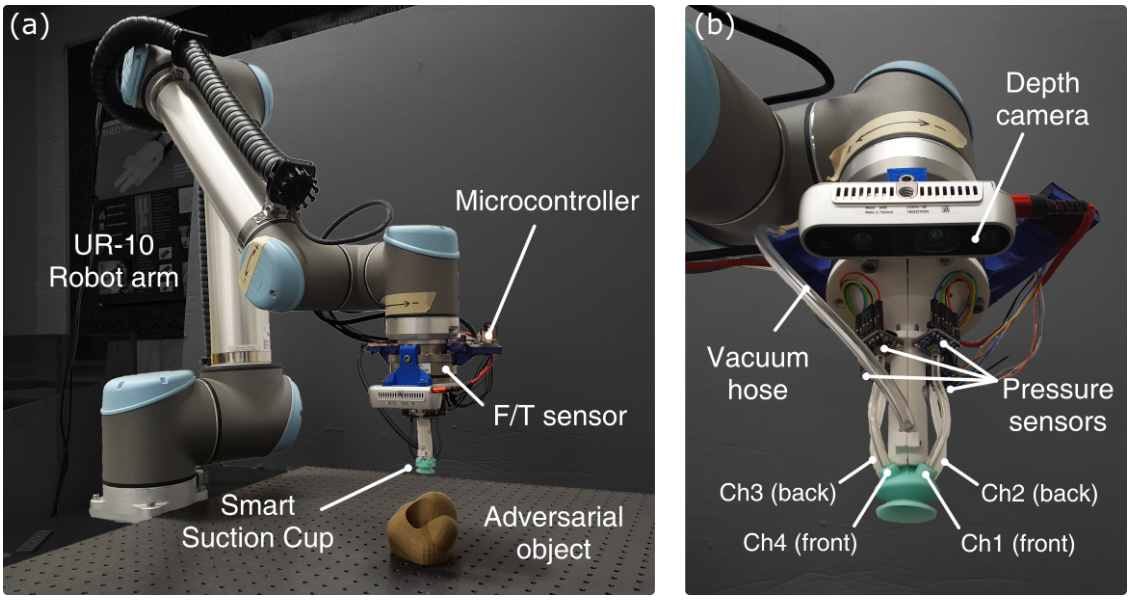

Figure 2.5: System integration of the Smart Suction Cup. (a) the smart suction cup system integrated on UR-10 robotic arm with a 6 DOF F/T sensor and a microcontroller. (b) Close up of end-effector, including the depth camera.

10 controller is responsible for moving the robot to the target pose, while communication between the desktop computer and the UR-10 robot uses Real-Time Data Exchange (RTDE) over a standard TCP/IP connection. We used ROS (Noetic) to collect both pressure sensor and wrist force/torque (F/T) sensor data during experiments. An RBG-D camera (Intel, RealSense D435) is additionally mounted to the robot arm wrist such that it does not apply any wrenches on the F/T sensor. It takes photos (640x480 RGB resolution, 0.1 mm depth resolution), which are used in the bin-picking experiments.

2.4 Autonomous Haptic Search

The control goal is to enable the robot arm to make small end-effector pose adjustments in the direction that will eventually seal the suction cup, in other words bring the vacuum pressure of all channels closer to the maximum vacuum–85kPa for the fully sealed condition. We decompose autonomous haptic search motions into three direction unit vectors defined in the tool basis, shown in Figure 2.6: (1) *lateral positioning* or translation along $\hat{v}$ in the $\hat{x}$-$\hat{y}$ plane, (2) *rotational alignment* or rotation about $\hat{\omega}$ in the $\hat{x}$-$\hat{y}$ plane, and (3) *axial movement* or movement along $\hat{z}$. The lateral positioning assumes partial contact of the suction cup with an object or the presence of small holes underneath the cup. The rotational alignment assumes a misalignment between the suction cup and the surface normal of the object contact point. In both situations, we assume there is significant misalignment or the existence of

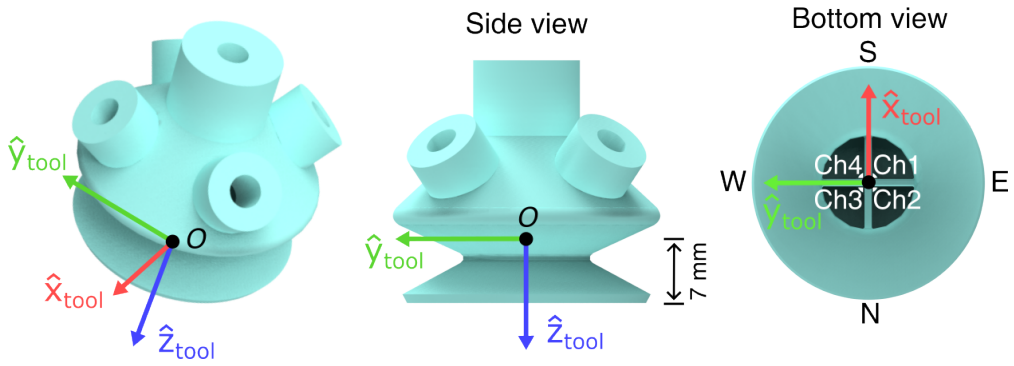

Figure 2.6: The reference frame associated with the tool end is shown, including the origin point (O) located relative to the unloaded cup lip. The cardinal directions of the cup are oriented along the walls of the inner chamber, shown in the bottom view.

bottom holes, resulting in vertical leak flows as depicted in Fig. 2.4(a). The axial movement ensures a consistent normal force, or $\hat{z}$-force, that is necessary to engage the suction with an object and maintain contact.

Both lateral positioning and rotational alignment search for a better grasping pose using smart suction cup pressure signals. To do so, pressures are first calculated for each cardinal direction by taking the average of the two chambers that correspond to that direction:[1]

$$P_E = (P_1 + P_2)/2 \tag{2.2a}$$
$$P_N = (P_2 + P_3)/2 \tag{2.2b}$$
$$P_W = (P_3 + P_4)/2 \tag{2.2c}$$
$$P_S = (P_4 + P_1)/2. \tag{2.2d}$$

Pressure differentials across cardinal directions are then calculated as:

$$\Delta P_{WE} = P_W - P_E \tag{2.3a}$$
$$\Delta P_{NS} = P_N - P_S. \tag{2.3b}$$

Using these values, the vectors $\hat{v}$ and $\hat{\omega}$ are calculated at each time step, in real time at a control rate of 125Hz.

Pressure Signal to Lateral Positioning

The lateral direction vector, $\hat{v}$, is defined to move the suction cup towards the channels with less leakage flow, i.e., higher vacuum pressure, as follows:

[1]This first step aligns the cardinal points with the wall interfaces of the cup. Alternatively, one can directly assign chambers to cardinal directions, e.g., $P_E = P_1$; this would result in a tool basis rotation of 45° about the $\hat{z}$ direction compared to our implementation.

$$\vec{v} = -\Delta P_{NS}\hat{x}_{tool} + \Delta P_{WE}\hat{y}_{tool} \tag{2.4a}$$
$$\hat{v} = \vec{v}/||\vec{v}||. \tag{2.4b}$$

Then the lateral repositioning increments, ΔL_x and ΔL_y, are defined as follows:

$$\Delta L_x(\hat{v}, \Delta L) = \Delta L\hat{v} \cdot \hat{x}_{tool} \tag{2.5a}$$
$$\Delta L_y(\hat{v}, \Delta L) = \Delta L\hat{v} \cdot \hat{y}_{tool} \tag{2.5b}$$

where $\Delta L = 0.5$ mm, is the overall lateral positioning step size per control loop.

Pressure Signal to Rotational Alignment

The rotational direction vector (axis of rotation), $\hat{\omega}$, is defined to close the gap between the object and channels with high leakage flow, i.e., low vacuum pressure, as follows:

$$\vec{\omega} = -\Delta P_{WE}\hat{x}_{tool} - \Delta P_{NS}\hat{y}_{tool} \tag{2.6a}$$
$$\hat{\omega} = \vec{\omega}/||\vec{\omega}|| = [\omega_1, \omega_2, 0]^T. \tag{2.6b}$$

Given an overall rotational alignment step size of $\Delta\theta = 0.5°$, the rotation matrix R is calculated as follows:

$$R(\hat{\omega}, \Delta\theta) = e^{\Delta\theta S(\hat{\omega})} \in SO(3), \tag{2.7}$$

where S is the skew-symmetric operator,

$$S(\hat{\omega}) = \begin{bmatrix} 0 & 0 & \omega_2 \\ 0 & 0 & -\omega_1 \\ -\omega_2 & \omega_1 & 0 \end{bmatrix} \tag{2.8}$$

Rotations are applied about the axis of rotation, along $\hat{\omega}$, which is always in the $\hat{x}$-$\hat{y}$ plane and always intersects point O.

Force Signal to Axial Motion

The axial step size ΔL_z, is calculated as follows,

$$\Delta L_z = \left\{ \begin{array}{ll} -\Delta z, & \text{if } F_z \leq F_{z,min} = 1.5N \\ 0, & \text{if } F_{z,min} < F_z < F_{z,max} \\ \Delta z, & \text{if } F_z \geq F_{z,max} = 2.0N \end{array} \right\} \tag{2.9}$$

where $\Delta z = 0.1$ mm is the axial step size per control loop.

Composition of Motion Primitives

To test different combinations of lateral and rotational motion in experiments, step sizes in the lateral and rotational directions are scaled as:

$$\Delta\theta_\alpha = \Delta\theta\alpha \tag{2.10a}$$
$$\Delta L_\alpha = \Delta L(1-\alpha) \tag{2.10b}$$

where $\Delta\theta_\alpha$ and ΔL_α are new step sizes weighed by α, which in turn change ΔL_x, ΔL_y, and R, producing an overall transformation matrix, T:

$$T = \left[\begin{array}{ccc|c} & R(\hat{\omega}, \Delta\theta_\alpha) & & \begin{array}{c}\Delta L_x(\hat{v}, \Delta L_\alpha)\\ \Delta L_y(\hat{v}, \Delta L_\alpha)\\ \Delta L_z\end{array} \\ \hline 0 & 0 & 0 & 1 \end{array}\right] \in SE(3) \tag{2.11}$$

If $\alpha = 0$, then $\Delta\theta_\alpha = 0$ and $\Delta L_\alpha = 1$, which results in pure lateral positioning. If $\alpha = 1$, then $\Delta\theta_\alpha = 1$ and $\Delta L_\alpha = 0$, which results in pure rotational alignment. For any α, axial force control remains unchanged to ensure contact with a surface.

2.5 Experimental Methods

Sensing Characterization for Haptic Search

To characterize the Smart Suction Cup sensing performance relevant for (1) lateral positioning and (2) rotational alignment, we perform two characterization experiments, one for each. We swept lateral and rotational offsets from known reference points and analyzed the resulting pressure signals. From these pressure signals in each experiment, we compute measured $\hat{v} = \hat{v}_{meas}$ and $\hat{\omega} = \hat{\omega}_{meas}$, respectively. Based on the physical experimental setups, we know the ground truth $\hat{v}_{true}$ and $\hat{\omega}_{true}$ that would move the suction cup towards a successful suction grasp with the shortest displacement. As shown in Fig. 2.7a-b, we report direction error as the unsigned angle between the measured and true direction vectors:

$$e_v = \cos^{-1}(\hat{v}_{true} \cdot \hat{v}_{meas}) \tag{2.12a}$$
$$e_\omega = \cos^{-1}(\hat{\omega}_{true} \cdot \hat{\omega}_{meas}) \tag{2.12b}$$

for lateral positioning and rotational alignment, respectively, where e_v, $e_\omega \in [0°, 180°]$.

Lateral Positioning characterization procedure

In the lateral haptic characterization experiments, we positioned and oriented the suction cup relative to the edge of a flat plate, as shown in Fig. 2.7c-d. We define the lateral offset δ as the exposed lip length, and the orientation is parameterized by the yaw angle $\phi \in [0°, 360°]$ to test for asymmetry in the pressure sensor response. A yaw angle of $\phi = 0°$ corresponds to

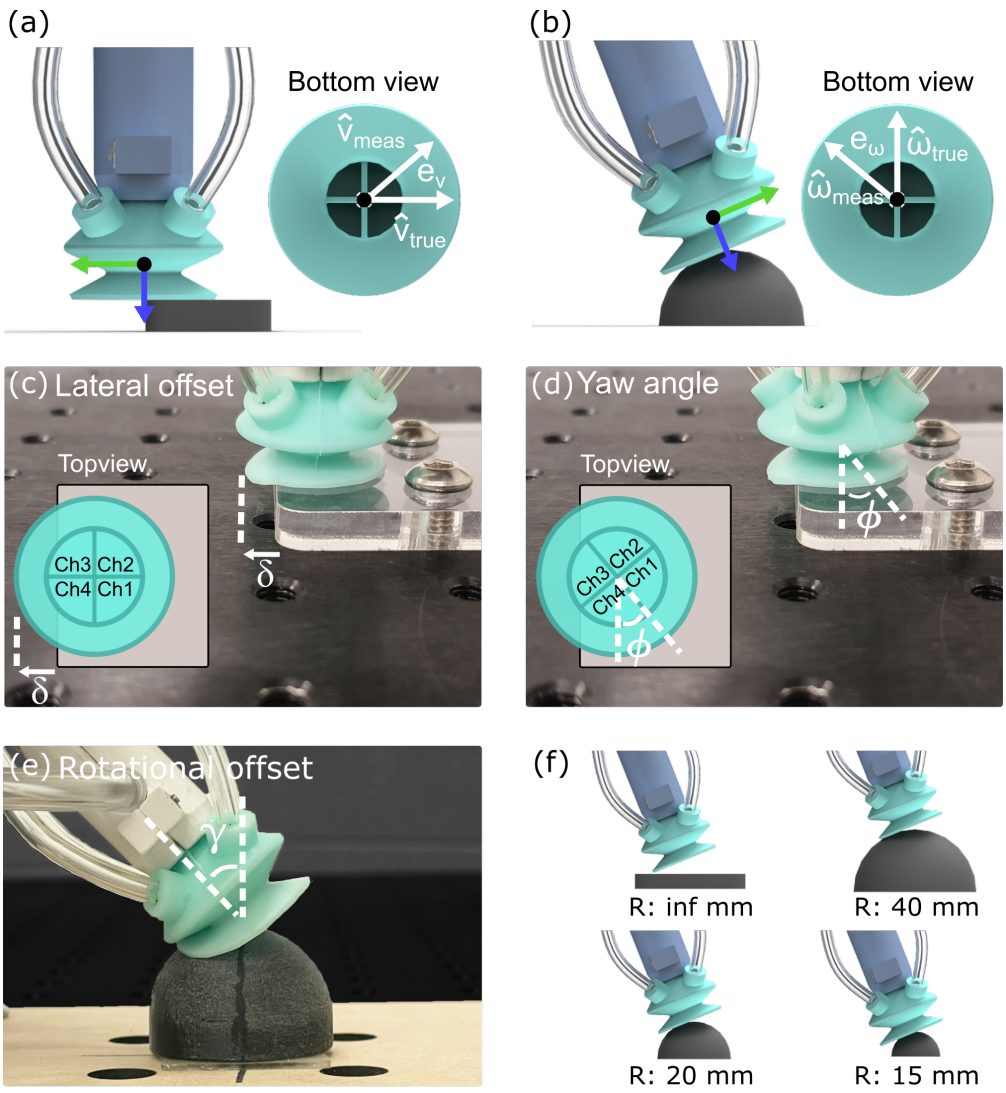

Figure 2.7: Schematic image of direction error for (a) lateral positioning and (b) rotational alignment. (c) Experimental image of the suction cup with lateral offset, defined as the exposed lip length δ, and (d) yaw angle ϕ about the symmetric axis of the cup. (e) Experimental image of the suction cup with a rotational offset angle γ on a dome. (f) Four different radius domes for characterization of rotational alignment.

$\hat{v}_{true} = -\hat{y}_{tool}$. To maintain a constant vertical distance between the flat plate and suction cup across all trials, we apply a normal force of 1.5 N at a lateral offset of 0 mm and fix this height of the suction cup. We sweep the lateral offset from 0 to 23 mm with a 1 mm increment, noting that an offset of 11.5 mm is when the point O is vertically aligned with the edge of the plate, and sweep the yaw angle from 0° to 360° with a 5° increment. In each test pose, we average the sensor data over a measurement period of 2 seconds.

Rotational Alignment characterization procedure

In rotational haptic characterization, the suction cup was placed on and oriented relative to a sphere, as in Fig. 2.7e, such that the point O is vertically aligned with the highest point of the dome. We define the rotational offset γ as the angle between the true surface normal at this highest point (vertically upward) and $-\hat{z}_{tool}$. Domes with different diameters (15 mm, 20 mm, 40 mm, and flat plate) are selected, as in Fig. 2.7f, with the 15mm radius dome representing the smallest sphere that the suction cup can grasp in this study. In this experimental setup, $\hat{\omega}_{true} = \hat{x}_{tool}$. To initialize an experiment, we use force control to reach a target 1.5±0.1 N normal load[2], with $\gamma = 0$. We record the position of O in space at this moment, and then pivot about it while regulating the force along $\hat{z}_{tool}$. We sweep γ from 45° to 0° with 1° steps. At each offset, we average pressure measurements for 2 seconds of steady state readings.

Bin-picking

We set up a bin-picking task similar to that of [44] to evaluate the functional performance of the proposed haptic search algorithms. The robot system was programmed to pick objects up from a bin and transport them to a designated container, as shown in Fig. 2.8. For a given trial, the robot was first set with a particular controller. The system was then presented with 19 adversarial objects in a bin. Five of the objects were 3D-printed objects taken directly from the list of Adversarial objects from [27]. Eight of them were taken directly from the Level 3 object set in [44], which includes both 3D-printed and commercial objects. The rest of the objects were picked based on difficulty for a vision-based planner, specifically adversarial objects with imperceptible features like transparency, reflectivity, and small surface features.

Before the start of each trial, the operator placed the complete set of objects into the bin by first shaking them loosely in the container, inverting that container to drop them into the bin, and manually adjusting objects only to ensure that they were below the rim of the bin. The robot then continuously attempted to perform the pick-and-place task until an end-trial condition was met, and the number of successfully grasped objects was recorded. In each trial, 57 attempts (three times the number of objects) were performed, and the trial

[2]This type of force control to an exact value often leads to system vibrations. For the parameters used in our controller, with the tolerance of ±0.1 N and control rate of 125 Hz, we did not observe substantial vibrations.

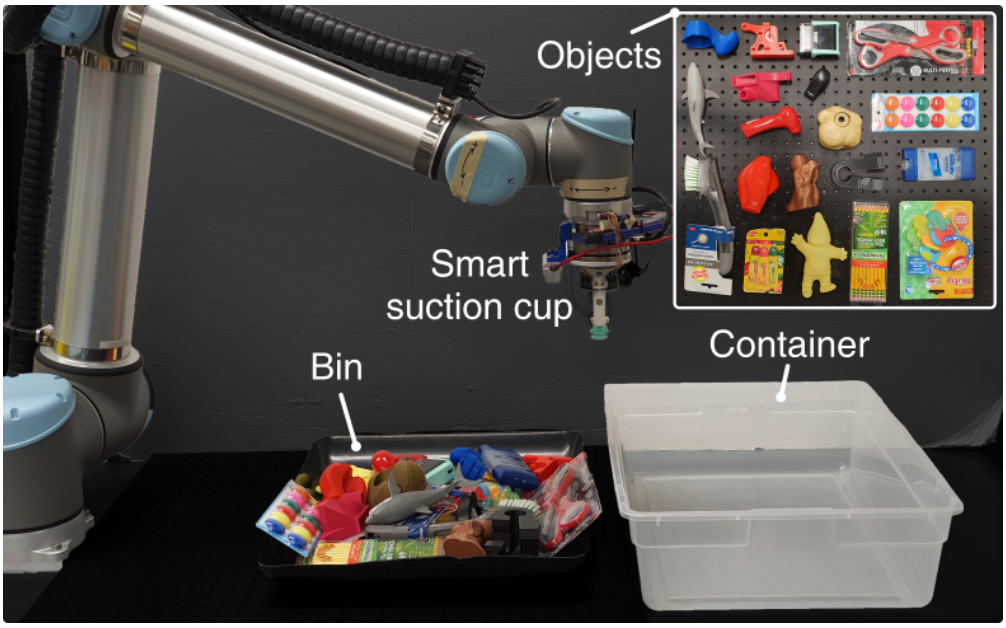

Figure 2.8: Tabletop setup for bin picking experiments. Inset: a dataset of 19 adversarial objects, showing eight 3D printed objects, six real objects with packaging, and five real objects without a package.

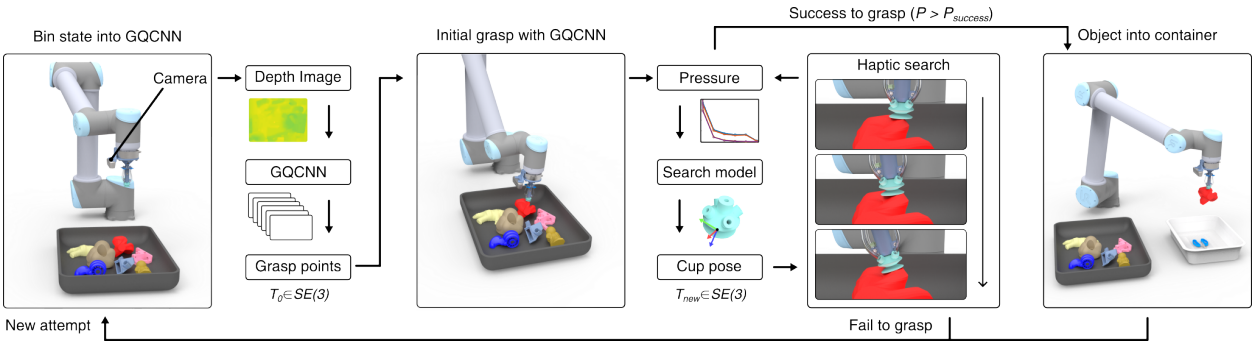

Figure 2.9: Flow chart of robotic behavior during bin picking experiments.[3]

stopped when 10 consecutive grasp attempts failed or no feasible grasping points remained available. We conducted five bin-picking trials for each tested control method.

The process for each trial is shown in Fig. 2.9. On each grasp attempt within a given trial, a point cloud of the bin state with objects is inputted into the Grasp Quality Convolutional

[3]Visual renderings are used for illustrative purposes only. All characterization and bin-picking experiments were done with physical hardware, and not in simulation.

Neural Networks (GQCNN) [45] to generate 30 grasp point candidates with a grasp quality value ranging from 0 to 1 and corresponding suction cup pose. Among the candidates, the pose with the highest quality value and no previous failures is attempted. We implement a simple memory system to avoid repeated failures at the same grasp point. When a grasp is unsuccessful, the grasp point is stored and any points within 3 cm of previous failure points are considered non-feasible. The system stores up to three previous failures and is reset when the suction cup successfully grasps an object. Note that we have not re-trained this algorithm for our particular robot system or object set. The robot approaches the selected grasp point with a 15 mm offset in the estimated surface normal direction. Then, it approaches the surface along the estimated normal until normal force reaches 1.5 N. The suction cup then initiates vacuum suction and checks the vacuum pressure of all channels to determine whether it has successfully grasped an object. We define a grasp success if the mean vacuum pressure is greater than $P_{success}$ =15 kPa, equivalent to holding ∼350 g with our suction cup. This estimate assumes the seal ring diameter is at the midpoint of the suction cup lip, or 17 mm across. The heaviest object lifted in experiments weighs less than 200 g, providing a safety margin of at least 150 g.

If a successful grasp is not detected after the initial grasp attempt with GQCNN, then the robot starts its specified search strategy to adjust the cup pose. During this search phase, a grasp is considered a failure if the suction cup moves away from the initial grasp point by more than 3 cm, rotates by more than 45° from the initial pose, or if the search time exceeds 15 seconds.[4] If the robot fails to grasp an object, it returns to the initial position and starts a new attempt. However, if at any point during the search procedure a successful grasp is detected, the robot then attempts to lift and move the object. Grasp failure is recorded if the object is dropped prior to the intentional release of the object into the container.

We evaluate eight total experiments: six with different haptic searching methods and two experimental controls. We implement five haptic search strategies by modifying the value of α from 0 to 1 in increments of 0.25. Specifically, we denote the values of α_1, α_2, α_3, α_4, and α_5 as an α of 0, 0.25, 0.5, 0.75, and 1, respectively. Also, we include a haptic search strategy which alternates a weight value between α_1 and α_5 every 0.5 s, denoted as $\alpha_{1\&5}$ in order to test the decoupling of motion between lateral positioning and rotational alignment. The first control condition is the application of GQCNN without any additional search method applied. As another experimental control case, we conduct a random search with Brownian motion (BM), or Weiner process, in the lateral direction; the lateral scalar step sizes in Eq. (2.11) , ΔL_x and ΔL_y, are chosen to make the standard deviation of the distance to be 3 cm from the initial grasp point after 15s of searching time.

[4]This maximum search time of 15 seconds was selected after preliminary experiments yielded diminishing grasp success after this time frame. In applications where speed is important, it would be impractical to search for an un-ending amount of time without a successful grasp.

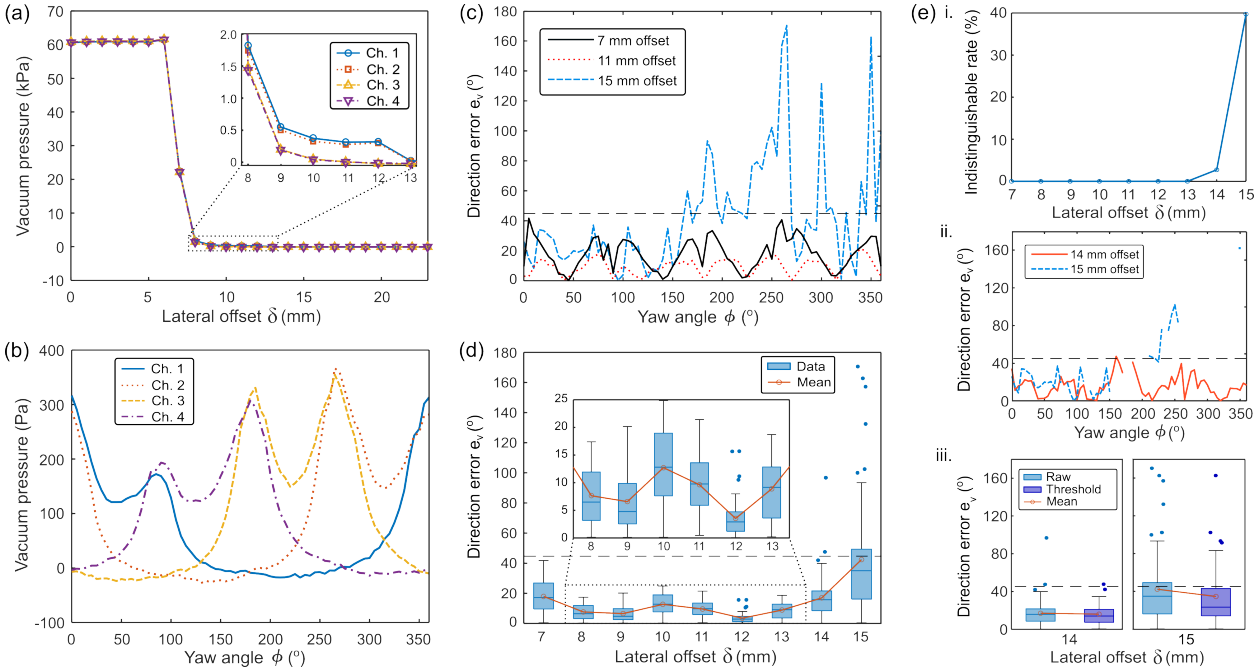

Figure 2.10: The pressure sensor readings for a sweep of lateral offset, δ, and yaw angle, ϕ, for the lateral positioning. (a) Vacuum pressure for a sweep of lateral offset from 0 to 23 mm at 0° yaw angle. (b) Vacuum pressure reading for a sweep of yaw angle from 0° to 360° at the center of the suction cup by averaging pressure reading at 11 and 12 mm lateral offset. (c) The direction error of various lateral offset. (d) Direction error data and mean. (e) Results from thresholding pressure readings by 10 Pa. i. The indistinguishable rate for a sweep of lateral offset. ii. The direction error at 14 mm and 15 mm lateral offset without indistinguishable data by thresholding pressure readings. iii. Direction error data and mean before and after thresholding pressure readings at 14 mm and 15 mm lateral offset. Dashed lines in the figure represent 45°.

2.6 Results

Lateral Positioning sensor characterization

The characterization results of lateral positioning are presented in Fig. 2.10. In Fig. 2.10a, the vacuum pressures from all channels are shown as lateral offset changes while yaw angle is held constant at $\phi = 0°$. All four channels remain over 60 kPa until the lateral offset reaches 6 mm; at these offsets, less than 7 mm, the suction cup seals completely with the plate and no haptic search is needed to grasp successfully. Note that the entire lip of this cup design does not necessarily need to be in full contact to generate a seal. Vacuum pressures decrease starting from a 7 mm lateral offset. The figure inset shows the region of offsets in which notable pressure differences exist between different chambers. Between 16 mm and 23 mm

lateral offset, pressure readings remain at 0 kPa across all chambers. It is therefore expected that directional signals will be most informative between 7 and 15 mm of offset.

To demonstrate how the pressure readings vary with the yaw angle, we vary ϕ from 0° to 360° with the edge of the plate located at the center of the suction cup (11.5 mm offset); we average the pressure readings at 11 mm and 12 mm lateral offset to estimate this cup alignment. As shown in Fig. 2.10b, the vacuum pressures in each chamber vary periodically with the change in yaw angle. At 0° yaw angle, chambers 1 and 2 overlap with the plate, showing higher vacuum pressure than the pressures from chambers 3 and 4. At every 90° of yaw angle, two chambers seal on the plate's surface, causing vacuum pressures to show peaks of two chambers. Given the chamber geometry of the cup, there will be higher overall vacuum pressure applied to the cup when more of the 4 chambers become sealed. This explains why we see two peaks per chamber, rather than just one, as the two adjacent chambers simultaneously break seal between local maxima. Variability between chambers is also seen, for example the maxima at $\phi = 90°$ is smaller than the others. Small variation could be caused by fabrication and assembly, as well as compliance in the suction cup, leading to asymmetric buckling deflections of the internal chamber dividers upon contact, as observed in prior work [22]. Regardless of chamber-to-chamber interaction and nonidealities, at each tested yaw orientation the 4 chambers provide a unique combination of readings to support the estimation of the ϕ state.

In order to understand the interpretation of these signals in our control algorithm, across both δ and ϕ, we visualize direction errors e_v with pressure sensor readings using Eq. (2.12a) in Fig. 2.10c-d. Direction errors from lateral offsets between 7 mm and 15 mm with 4 mm increments are shown in Fig. 2.10c. The 45° boundary indicates the directions that would enable faster haptic search for a better grasping point, by moving the cup towards the plate at a rate faster than along the edge of the plate. At 7 mm and 11 mm lateral offset, the direction errors show that all data is below the 45° boundary line. At a 15 mm lateral offset, some errors go above the boundary. The result shows that direction errors have a cyclic pattern every 45°, reflecting the internal wall structure of the suction cup with four chambers.

In Fig. 2.7d, we report the direction error for all trials between 7 and 15 mm offset. Each lateral offset has 73 data points, where we sweep yaw angles from 0° to 360° with a 5° increment. The result shows box plots with the means of the data. No data exceeds the 45° boundary from 7 mm to 13 mm lateral offset. However, within this range, error is greatest at 7 mm. It makes sense that direction error increases as the offset approaches 6 mm, as the suction cup becomes fully sealed and flow stops altogether. For the 7 mm case, as demonstrated in Fig. 2.4d-f, flow can become predominantly horizontal at the transition to the fully-sealed state, thereby decreasing the pressure difference between the exposed and covered chambers. At both 14 and 15 mm lateral offset, where pressure differences become small, several data points show error over 45°, yet the mean of the direction error remains below this threshold.

At large offsets, greater than 15 mm, the pressure approaches 0 Pa and e_v increases further, meaning that all four channels are open and not forming effective differential pressures.

We therefore apply a threshold condition of 10 Pa during controller implementation such that, when all chambers are below this level, the direction estimate is set to $\hat{0}$ (no motion). The rate at which this condition is met, which we call the indistinguishable rate, at different lateral offsets is shown in Fig. 2.10e i. The indistinguishable rates from thresholding are found to be 2.7% and 39.73% at 14 mm and 15 mm lateral offset, respectively, while no data are indistinguishable between 7 mm and 13 mm lateral offset. Fig. 2.10e ii shows the corresponding result of direction errors e_v at 14 mm and 15 mm lateral offset, where the indistinguishable data points are eliminated. Fig. 2.10e iii shows the change in e_v resulting from the threshold condition. Before thresholding, the mean of direction error at 14 mm lateral offset is 16.99°, which decreases to 15.70° after thresholding. At a 15 mm lateral offset, the mean direction error changes from 42.42° to 34.71°. In practice, motion will only occur when at least one channel measures a degree of flow restriction – if there is no measurable suction contact the cup will remain stationary.

Rotational Alignment sensor characterization

The characterization results of rotational alignment are presented in Fig. 2.11. Since the suction starts without a seal, we read the plot with decreasing rotational offset from left to right. The cup initially starts at $\gamma = 45°$ and all channels read close to 0 kPa. The critical rotational offset, where the vacuum seal is formed, is seen by a rapid increase in the vacuum pressure (Fig. 2.11a). This critical offset angle becomes smaller as the radius of the dome decreases, indicating that smaller radius domes require more precise alignment with the surface normal to successfully grasp. At rotational offsets smaller than the critical offset angle, the vacuum pressures are consistently near 60 kPa across all channels. The control condition for successful grasping, $P > P_{success}$, is shown as the horizontal dashed line. The region of interest for haptic search occurs when there is the presence of pressure differentials within the cup, detailed in the figure, comparing P_W and P_E. The difference is directly plotted as ΔP_{WE} in Fig. 2.11b after removing data points where $P > P_{success}$. For the 15 and 20 mm radius domes, signals rise as high as 1.5 and 1.2 kPa, respectively, over larger rotational offset ranges than the 40 mm dome or flat plate. The pressure differential for the flat plate in particular never even reaches a ΔP_{WE} of 20 Pa, because the compliant lip rapidly deforms and pulls itself into the surface before substantial differential flows can occur inside the cup due to chamber occlusion. We therefore expect tactile sensing to provide more useful prediction of $\hat{\omega}$ on higher curvature objects, where smaller domes can better occlude chambers before the critical angle is reached and more careful alignment with surface normal is required.

As shown in Fig. 2.11c, the test results indicate that the direction error (e_ω, Eqn. 2.12b) is lower for objects with smaller radii. Each subplot i-iv represents a trial on a different object and data for which $P > P_{success}$ is omitted. When we add a dashed boundary line of 45°, similar to in lateral search characterization, we see that errors consistently drop below 45° at rotational offsets of 30°, 31°, 23° for domes with radii of 15 mm, 20 mm, and 40 mm, respectively. On the other hand, the flat plate error does not fall below this threshold

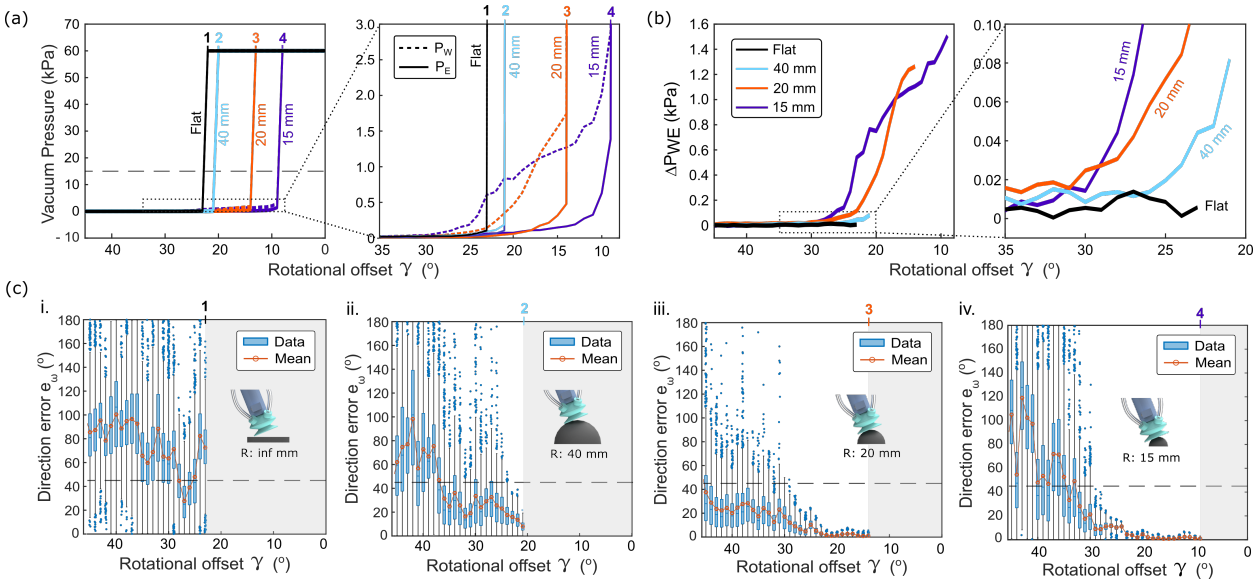

Figure 2.11: Vacuum pressure and pressure differential measurements for a sweep of rotational offsets γ, and direction error, e_ω, for four different objects - a flat plate and spheres with 40 mm, 20 mm, and 15 mm radii. (a) Vacuum pressures for $\gamma \in [45°, 0°]$. Pressure increases sharply at different critical offset angles as the vacuum seals on the surface, points numbered 1-4. Before sealing occurs, differences between P_W and P_E are visible, especially for the 20 mm and 15 mm objects. (b) Pressure differential between west and east chambers for each curved surface. Differential signals rise faster for high curvature objects. (c) i-iv. Direction error data and mean for the four objects. Included is the 45° direction error boundary line. The shaded regions indicate the rotational offsets at which the suction cup passively grasps the object, smaller than the critical offset angle. Direction error past 90° corresponds to motion perpendicular to the true desired direction.

consistently on the flat plate because ΔP_{WE} remains small up to the critical angle. The smaller radii objects (R=15 mm and 20 mm) show the most accurate predictions ($e_\omega < 10°$) close to the critical rotational offset. This result suggests that the proposed haptic search method can successfully grasp objects with small critical offset angles (e.g., 8° in R=15 mm object), even with high visual perception error of surface normal up to 30°.

Bin-picking

We evaluate the bin-picking test conditions defined in Section 2.5, with results shown in Fig. 2.12. The picks-per-attempts mean average from across five independent trials for each condition is reported in Fig. 2.12a; the six haptic search conditions are in shades of red while the the two experimental control cases are in shades of blue. All trials are reported for each

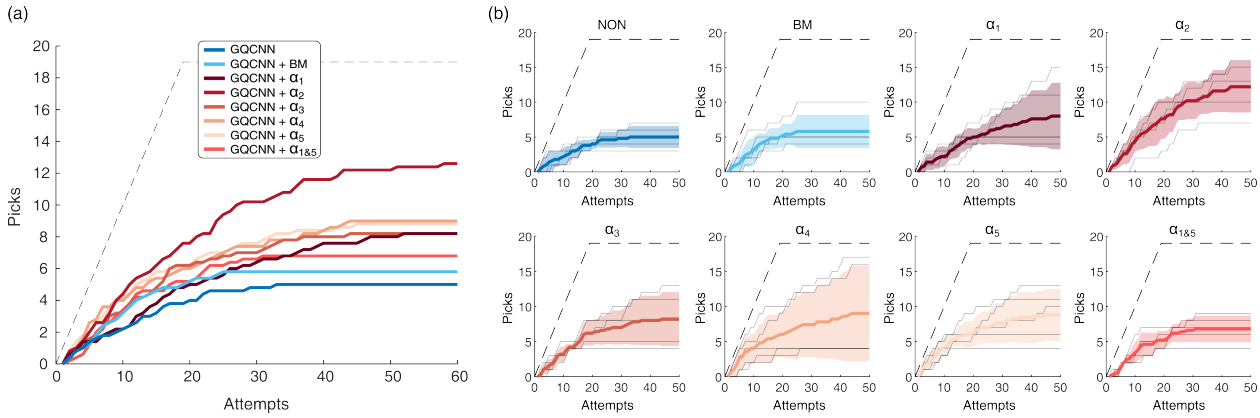

Figure 2.12: Results of bin picking experiments. (a) The average number of successful picks across all grasping methods. (b) The individual results for each grasping strategy, with solid colored lines indicating the average and colored areas representing the standard deviation. The grey lines within each grasping method indicate the results of individual trials. As a reference, a dashed black line is used to represent the optimal performance, which is defined as successfully picking every attempt in the bin until it is completely empty.

test condition experiment in Fig. 2.12b. The dashed lines on all plots indicate the ideal case where every grasp attempt is successful without any failures.

The control case "GQCNN" or "NON," which has no search phase, shows an average of 5 $\pm$ 1.58 successful picks. This means the robot system was able to successfully pick-and-place these objects from the bins without any haptic search assistance. The control case "GQCNN + BM," which includes random Brownian motions in lateral direction during the search phase, results in an average of 5.8 $\pm$ 2.39 successful picks. This shows that the introduction of non-haptically-driven motion after the initial grasp attempt can provide minor improvements. Comparing the two control cases with this ideal performance, we see the difficultly of the selected adversarial pick-and-place task. Of the two control cases, we propose that it is more appropriate to compare haptically-driven results with the "GQCNN + BM" control case because it represents baseline benefits from the presence of a search phase.

The proposed haptic search methods are labeled α_1 to α_5 and $\alpha_{1\&5}$. Results show that α_2 provides the highest number of successful picks per trial, with an average of 12.6 $\pm$ 4.16. Lateral positioning (α_1) and rotational alignment (α_5) show reduced results similar to one another, with 8.2 $\pm$ 5.17 and 8.8 $\pm$ 3.70 successful picks, respectively. α_3 results in an average of 8.2 $\pm$ 3.83 successful picks and α_4 provides successful picks (9 $\pm$ 6.86), but with the largest standard deviation. For the performance of the alternating haptic search method $\alpha_{1\&5}$, it shows the lowest successful picks of 6.8 $\pm$ 1.92 among all the haptic search methods evaluated. Overall, these results demonstrate the effectiveness but also the between-trial variability of the proposed haptic search methods. Out of these methods, α_2, which

predominantly performs lateral search but with some rotational alignment, best improves the success rate of bin picking by the robot system. However, between trial variability indicates that the potential benefits of haptic search is sensitive to initial bin state.

We can then compare the autonomous haptic search methods with the experimental control cases. In the region between 0 and 5 pick attempts, there is little difference between all eight methods. This indicates that success is driven by the GQCNN method, mostly because we attempt the grasping pose with the highest quality value first. The methods diverge in performance after 5 attempts, where the GQCNN and α_1 methods show lower performance than the other six methods. At 25 or more bin pick attempts, all six haptically-driven methods outperform the two experimental control methods. This indicates that autonomous haptic search methods are helpful to expand achievable grasp points, to now include those that GQCNN alone is unable to accurately predict.

Here, we quantify how much fine-tuning is executed through haptic search on average. Among the successful haptic search trials, across all six haptically-driven methods, the mean cartesian displacement from the initial pose was 4.8 mm with a maximum of 13.9 mm. Mean path length was 8.7 mm with a maximum of 32.7 mm. Mean angular displacement was 5.9° with a maximum of 25.2°. Mean angular distance traveled was 6.8° with a maximum of 39.1°.

2.7 Discussion

Sensor characteristics

Through varying the lateral displacement and yaw of the cup against a flat plate edge and varying orientation with domes of different sizes, we characterized the scale and types of pressure signals that the Smart Suction Cup produces. We also demonstrated how these raw signals are interpreted using our proposed haptic search procedure. However, plates and domes represent primitive shapes. The complexity of object geometries in real-world scenarios, with a combination of vertical and horizontal flows, will likely impact the haptic search effectiveness of the suction cup, making it challenging to identify suitable direction vectors. This may help us to understand why, at times, we observed certain unproductive haptic behaviors emerge during the bin-picking task.

We found in sensor characterization tests that thresholding reduced direction error, by eliminating cases where pressure differential measurements are too low to produce reliable estimates when sensor noise starts to dominate. At the same time, it is unlikely that perfect prediction accuracy is essential in effectively deploying Smart Suction Cup haptic search. Specifically, the prediction accuracy appears to improve as the cup gets closer to a successful grasp. During haptic search, if, as a result of noisy signals due to low pressures, the cup randomly reaches any state where a more accurate prediction can be better made, then the behavior will converge on a successful grasp over time. We posit that this will be especially true if, on average, predictions start from a place that are within 90° of the true direction

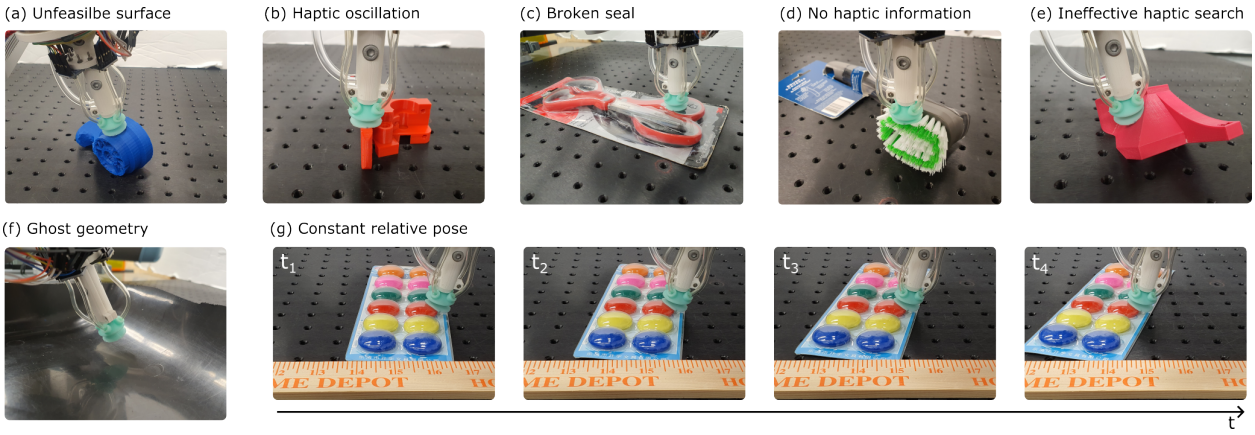

Figure 2.13: Representations of the failure modes for the Smart Suction Cup observed during the bin-picking experiments.

vector. In future work, conducting closed-loop control experiments, rather than stationary sensor characterization, would identify the highest possible offsets for which haptic search still yields a successful grasp, including on a wider variety of object shapes.

In the lateral search case and especially the rotational alignment case, we find that the compliant material and the bellows of the suction cup allows it to engage with objects even with postural errors to some extent. However, for objects with high curvature and critical features such as holes, the inherent tolerance of the suction cup may not be sufficient. In such cases, our proposed haptic search method is expected to enhance the operational tolerance even when the vision system fails to capture those features accurately.

Bin-picking observations

Bin-picking experiments suggest that a physical search phase after contact is made can improve grasp success, especially when employing autonomous haptic search methods that respond to measured contact conditions. The fact that all haptic search methods tested provided some increase in picking success rate as compared with experimental controls, including with random searching, shows how responding to contact pressures, even with a simple model-based controller, holds potential thus motivating ongoing investment in the Smart Suction Cup capability. We used a single suction cup prototype throughout all of these bin-picking-experiments, representing at least 1316 autonomous grasp attempts, without incurring damage to the cup or needing replacement. The Smart Suction Cup design, where the cup is fabricated in a single-step casting process and electronics are remote from the cup, thus appears to provides reliable and physically robust performance.

We saw the biggest performance increase with the α_2 haptic search method, whose motion is a mix of lateral positioning with a bit of rotational alignment. Though it matches our

expectations that a coupled motion would yield better results than purely sliding (α_1) or rotating (α_5), because most objects have both edges and curves, it is less obvious why α_2 outperforms α_3 and α_4. A possible theory is that the rotational alignment search counteracts the lateral search, so finding the optimal tuning between them is required. When the suction cup has partial contact, the lateral search attempts to reinforce contact on the contacted side by moving towards it, while the rotational alignment loosens the contact side and attempts to make balanced contact over all channels. Therefore, an appropriate balance between the two modes should be adjusted. We believe that α_2 provides the best balance among the five presets in general, but each geometry may require a different optimal balance between the two modes. We leave this local, object-specific controller optimization as a future work.

During the bin-picking trials with autonomous haptic search, we observed different common grasp failure modes. We classify them into seven categories, as shown in Fig. 2.13:

(a) *Unfeasible surface:* Haptic search starts at an infeasible surface, where possible grasp poses are beyond the searching boundary.

(b) *Haptic oscillation:* Haptic search oscillates in a region where haptic information makes the cup move back and forth without converging to a graspable point.

(c) *Broken seal:* The contact wrench applied to the cup is too large to lift an object. This typically occurs when the suction cup tries to grasp a heavy object from the edges, also reported in [9].

(d) *No haptic information:* The suction cup cannot get any distinguishable haptic data from a surface, such as the bristles of the brush (P<10 Pa).

(e) *Ineffective haptic search:* A surface is feasible and haptically searchable, but the system uses an ineffective behavior. The example shows a case where the suction cup is using lateral positioning but would benefit more from rotational alignment.

(f) *Ghost geometry:* Reflective and/or transparent materials yield artifacts, resulting in ghost geometries in a depth image. The example in the figure shows the suction cup is trying to grasp in the air because the light from the ceiling is reflected on the bin surface.

(g) *Constant relative pose:* During haptic search, a loose object can be pushed such that the relative position between the cup and object remains unchanged despite robot motion. Given the new position of the object, the next attempt may consider the same grasp point as a valid candidate as its pose in the world frame changed.

Several of these error types occur because the vision-based grasp planner initializes the grasp at a point in which a suction grasp is locally impossible. The cases in Fig. 2.13 (a), (c), and (f) are not recoverable using contact condition condition sensing. To combat these, the camera and/or visual planner performance would need to be improved. However, for cases in Fig. 2.13 (b), (d), (e), and (g), new adaptive haptic search controllers designed to identify

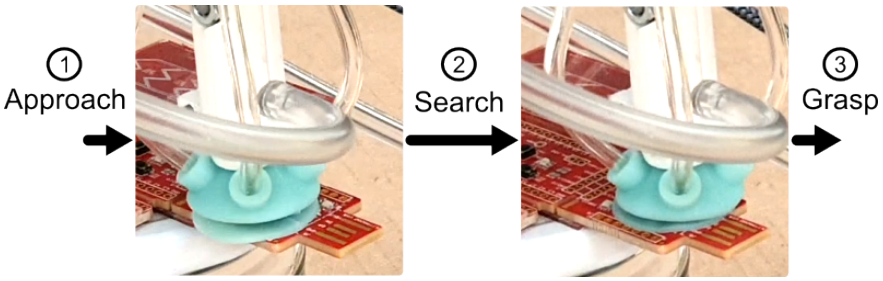

Figure 2.14: An example of lateral haptic search, α_1, on a stationary PCB adhered to a surface. ① "GQCNN" guides to the pose where there are several via holes. ② The suction cup adjusts its lateral pose given its pressure readings. ③ The haptic search succeeds in grasping the PCB within 2 seconds.

and overcome such failure cases could further improve grasping in future work. For instance, the failure mode (g) may be effectively addressed through a jumping haptic search approach. In this approach, the suction cup retracts from an object and then re-approaches with an adjusted pose. This prevents the suction cup from exerting continuous pressure on an object while making pose adjustments. We recommend also coupling vision with the haptic search process. For example, camera information could be used to select appropriate haptic search methods in response to case (e). Or vision could identify object movement in (g) to adapt behavior on the fly; for example, in [22], we propose that one could dynamically reduce the suction pressure of the vacuum in order to achieve more gentle sliding over objects.

In the present work, we made the deliberate choice not to re-train the GQCNN algorithm for our particular robot system, resulting in overall low planner performance. In our case, we use a different camera, robot arm, object set, room/lighting, gripper, and bin from the ones used in training. The purpose of this choice is to generate a scenario that emulates a quick-adopt case for such technology, since generalizability is an ongoing challenge for such planning algorithms [46]. The present work therefore shows that the use of a Smart Suction Cup can be one tool in ameliorating errors that arise specifically in previously unseen systems. Future work will investigate how planner optimization and hardware selection (e.g., higher spatial resolution camera) affects the role of autonomous haptic search.

Printed Circuit Board demonstration

In the bin-picking experiment, the tested objects all had at least one smooth graspable surface for the suction cup to grip. However, some real-world objects have bumpy surfaces without any obvious continuously-smooth regions. For example, a Printed Circuit Board (PCB) with Integrated Circuits (IC) soldered on it and via holes might prevent the use of a suction cup, if the cup would fail to grasp at most surface locations. However, haptic search behaviors can still enable the grasping of such surfaces, adapting around local features to

achieve a seal. To demonstrate this behavior, we fix a printed PCB to the table and allow the cup to search for a grasp point using only lateral positioning, or α_1. Fig. 2.14 shows how the cup is able to find a successful grasp point over one of the IC's. Future work will measure to what extent the cup can respond productively on surfaces with different types of porosity and rugosity profiles for real-world applications.

In Fig. 2.10, the directional errors in lateral search on a flat, smooth plate commonly reach almost 20° for the best case lateral offsets between 8 and 13 mm. These errors may appear unsatisfying and at times result in longer searching paths than desired. This directional error provides one reasonable explanation for the edge-following behavior that emerges at Grasp point 3 in Supplementary Video. However, the PCB demonstrations show how this error does not necessarily result in overall failure during smart suction haptic search; the controller continues to adjust its directional estimate every 0.5 mm as it moves, ultimately leading to a successful grasp. Regardless, future work should investigate how performance – such as time and distance to successful grasp – may be optimized through cup and algorithm design.

2.8 Conclusion

The four-chamber cup design of the Smart Suction Cup, with remote pressure transducers, provides a reliable solution for generating differential airflows and protecting sensitive electronics from physical damage. In this work, our proposed autonomous haptic search method – a model-based approach for estimating lateral positioning and rotational alignment – enables the suction cup to adjust to a successful pose for suction grasping, effectively increasing tolerance to positioning or misalignment error induced by errors from a vision-based grasp planner. The Smart Suction Cup holds the potential to improve gripping in various scenarios that already deploy vacuum grippers, such as recycling facilities, warehouses, manufacturing, and logistics robots.

Future work

This study presented a single implementation of the Smart Suction Cup and one particular model-based approach to generating haptic searching behaviors in response to pressure readings. In future work, we seek to explore new soft cup designs to both improve gripping performance while studying how parameters, like the number of chambers, affect sensing. Next steps include optimization and learning-based approaches for sensor characterization and mixing lateral positioning and rotational alignment. These adaptive methods may be informed by visual and haptic information, for example. Finally, the ultimate goals of this line of work is to explore the adoptability and lifetime of such technology in real-world application.

Chapter 3

The Smart Suction Cup: PCB regrasping

The disposal of waste electrical and electronic equipment (WEEE) presents a sustainability challenge, particularly for waste printed circuit boards (PCBs). PCBs are challenging to sort out from other waste materials in part because traditional industrial end-effectors struggle to reliably grip these irregularly shaped objects with unmodeled surface-mounted components. Vision-based separators, while effective for object categorization, face challenges with identifying precise grasp points on PCB surfaces. This paper studies regrasping control to enhance suction cup grasping performance on PCBs, addressing issues arising from uneven surfaces and intricate features that interfere with suction sealing. We categorize PCBs into two recycling levels – with large surface features intact or removed – and conduct experiments on both stationary and conveyor belt setups with realistic vision-based grasp planners. Results show that jumping regrasping improves pick-and-place success rate. Haptically driven jumping – using the Smart Suction Cup – is especially useful for unprocessed waste PCBs with large surface mount parts. The proposed method offers a promising solution to enhance the efficiency and reliability of robotic grasping in recycling applications.

3.1 Introduction

As of now, many waste printed circuit boards (PCBs) are not recycled[47, 48] and the rapid global growth of electronics industries has led to a surge in electronic waste[49, 50]. Resulting pollution harms both local ecosystems and the human populations residing in proximity to primary recycling facilities[51, 52]. PCBs present especially intricate designs with high metal contents and potential toxicity, making automated high-volume PCB recycling both difficult and important. The irregular shapes and sizes of PCBs with unmodeled surface mounted components makes reliable gripping difficult with conventional industrial end-effectors. Thus, sorting PCBs out from other waste materials using a pick-and-place process remains a bottleneck. Modern robotic manipulation technology suitable for PCB handling therefore has

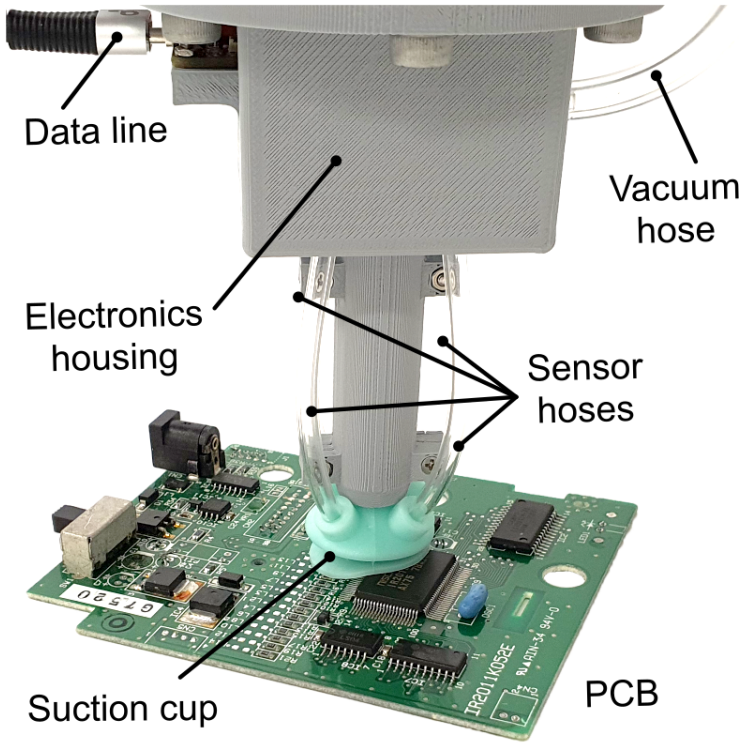

Figure 3.1: The multi-chamber Smart Suction Cup – equipped with four internal chambers, each linked to a pressure transducer for monitoring internal flow rate [22, 53] – touches a PCB on the edge of a surface mounted integrated circuit. The gripper can detect minor seal disruptions caused by physical interaction with such surface irregularities.

the potential to improve waste management practices.

Suction cups, also known as vacuum grippers, play a crucial and versatile role in various industrial robot applications[54][55]; they are fast, reliable, affordable, and effective on smooth, flat, and/or lightweight objects. Suction cups already enable the pick-and-place of some recyclable items[56], and facilitate the integration of robots into industrial recycling sorting applications [57, 58]. For objects that are too bumpy or difficult for suction cups to grip consistently, opposable grippers and multi-fingered hands enable fine adaptation to varied object shapes [44, 59]. However, suction grippers are typically simpler and cheaper in comparison to other articulated end-effectors. Our goal is to expand the capabilities of suction cups to grip irregular surfaces so that more complex end-effector hardware is not required.

Vision-based separator technology enables the identification of different mixed waste for sorting [60]. While vision-based planners have proven effective for object grasping, challenges arise when dealing with uneven surfaces and intricate features on objects [27]. PCBs, in

particular, pose difficulties for vision-based systems due to their complex array of small electronic components and vias, rendering suction performance difficult to predict accurately. This is especially true for fast-throughput conveyor systems, where the constantly moving belt may not provide enough time for the vision system to fully capture and process all the intricate features on the PCBs that affect suction cup gripper success. We therefore aim to provide fast, successful suction cup gripping on PCBs without accurate visual predictions or models of surface geometry.

Prior Work

In our previous work, Huh et al. (2021) introduced a custom-molded multi-chamber smart suction cup gripper capable of measuring four distinct pressure values corresponding to the sealing of individual chambers [22]. This cup is depicted in Fig. 3.1 with four sensor hoses each corresponding to its own chamber. We then introduced and tested continuously sliding and rotating control strategies to haptically search for graspable object locations in [53]; we found that this strategy can improve grasping of adversarial objects by up to 2.52x during bin picking. However, the sliding haptic search method was shown to fail when the object moves along with the gripper, such that the relative position with the suction cup remains unchanged as depicted in Fig. 3.2(a). While we demonstrated continuous sliding haptic search with a PCB in this prior work, the PCB was rigidly fixed to the table to prevent it from moving with the cup. We now introduce and test the use of jumping haptic regrasp as a viable alternative for preventing sliding failure with loose PCB handling – this involves releasing and regrasping the object at a new location, as seen in Fig. 3.2(b). In the present work, we also update the implementation of the end-effector assembly for easier mechanical integration with existing robotic manipulation systems.

Overview

Section 3.2 provides a description of the Smart Suction Cup with an updated end effector implementation. We also define the tested jumping haptic regrasping method that utilizes the pressure readings from each chamber to improve grasping on PCBs. In Section 3.3, we categorize PCBs into two levels according to their recycling status and perform two discrete experimental pick-and-place tests with this system – one test is for PCB's on a stationary table and the other is on a moving conveyor belt system and a realistic vision-based grasp planner. Section 3.4 presents the results of these experiments; we find that the use of jumping regrasping increases the success rate in both pick-and-place applications, and that haptically-guided regrasping is useful especially in non-processed waste PCBs with the largest surface features. Discussed in Section 3.5, transfering the haptic regrasping to real application encounters emerging issues that can be further improved in future work. We conclude that the jumping haptic method exhibits promising capabilities as corrective reflexes that complement traditional vision-based grasp planning approaches.

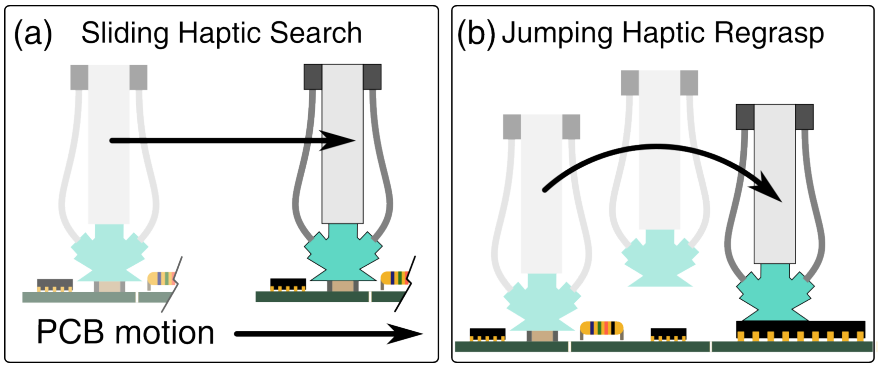

Figure 3.2: (a) In sliding haptic search, the object can slide with the gripper, making the strategy ineffective at leading to a successful grasp. (b) We study the utility of jumping haptic regrasping to find a better grasp location without sliding continuously across the object's surface.

3.2 Jumping Haptic Regrasp Implementation

End-Effector Hardware

In our prior work [22, 53], we provided comprehensive details regarding the fabrication, internal structure, and dimensions of the suction cups. To briefly summarize, these suction cups are fabricated using a customized mold, resulting in a specialized design with an internal structure comprising four identical chambers for the purpose of airflow monitoring. The manufactured suction cup is integrated into the underside of a 3D-printed fixture, as shown in Fig. 3.3(a). In this paper, we have made slight updates to the end-effector for the Smart Suction Cup to simplify its integration onto various robot arms. These updates include a newly designed fixture, a new microcontroller, and a multiplexer for communication with sensors. All electronic components required for pressure measurements are newly enclosed within this fixture, including four pressure sensors (MPRLS, Adafruit) securely affixed to the internal space facing the bottom. These sensors are connected to the four chambers through polyurethane tubes. Also updated in the current design, the pressure sensors are linked to an I2C multiplex (PCA9546, Adafruit), which interfaces with the microcontroller (ESP32-S3 feather, Adafruit). The microcontroller is securely fastened to the fixture, and positioned on the opposite side of the main vacuum hose. The vacuum hose is attached to a barbed tube fitting positioned on the fixture's side wall, with a hose extending through the fixture's guide hole to the suction cup, completing the integrated system.

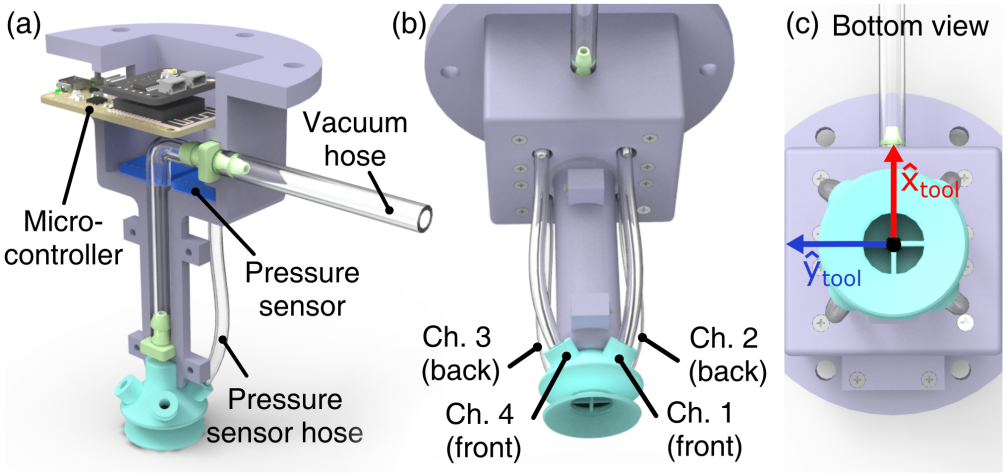

Figure 3.3: CAD images for the suction cup system. (a) Sectional view of the system showing four pressure sensors and a microcontroller for data acquisition. Assembled system showing vacuum hose and pressure sensor hoses. (b) Configuration of four channels and the coordinate of tool frame. (c) Axes are aligning with the inner chamber's walls, as illustrated in the bottom view.

Jumping Haptic Regrasping Algorithm

The aim of the haptic search controller is to adjust the end-effector pose of the robot arm until the suction cup becomes sealed against the surface. When this occurs, pressure sensors reach vacuum pressure levels, i.e. no flow conditions. We assume that the vacuum force is enough to lift any of the lightweight PCBs used in this study. During the haptic search, the robot conducts lateral pose adjustment to find a 'good' spot for grasping.[1] The direction for adjustment is calculated by the pressure difference between 4 channels, as seen in Fig. 3.3(b), at each grasping point. In order to calculate the pressure difference, we first define the vacuum pressure of each chamber as where $N = [1, 2, 3, 4]$ is the chamber number, P_{atm} is atmospheric pressure, and $P_{Ch.N}$ is the pressure reading from chamber N. A motion direction vector, v, is calculated as:

$$\begin{aligned}\vec{v} = &((P_1 + P_4) - (P_2 + P_3))\hat{x}_{tool} \\ &+ ((P_3 + P_4) - (P_1 + P_2))\hat{y}_{tool}\end{aligned} \tag{3.1}$$

to move towards the chambers with more vacuum pressure. We only consider the direction, not magnitude, of the pressure differences to move in the direction of the unit vector $\hat{v} = \vec{v}/\left\|\vec{v}\right\|$. We apply a threshold condition during the unit vector calculation, representing the

[1]While a smooth surface without via holes provides a suction seal, there are also good locations were chips or vias remain under the gripper.

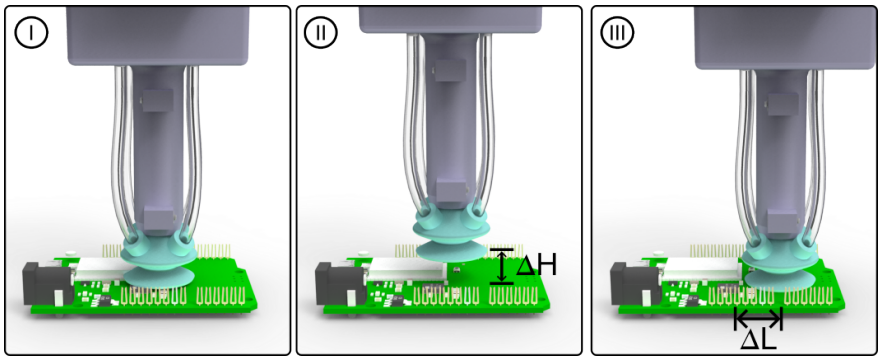

Figure 3.4: Schematic CAD image of jumping haptic regrasp.

noise floor of the pressure readings.[2] If the vacuum pressures from all chambers are below the threshold, the direction vector is set to $\vec{v} = \vec{0}$.

We employ a technique which we call "jumping haptic regrasp" (Fig. 3.4), during which the vacuum source is always ON. In this algorithm, the suction cup first approaches the object in an attempt to grip the PCB (I); it collects pressure information when in the target grasp position[3] to compute $\hat{v}$.[4] The robot arm then attempts to lift the PCB (II). Once the height of the gripper is lifted to ΔH above the grasp position, the pressure is again measured to detect whether the grasp was successful or not.[5] If unsuccessful, then the cup moves to a new position above the PCB, with a lateral step size ΔL (III), such that:

$$(x_{k+1}, y_{k+1}) = (x_k, y_k) + \Delta L \hat{v}(k) \quad k = 0, 1, 2... \tag{3.2}$$

where $\hat{v}(k)$ is the unit direction vector. For haptic search driven by the pressure readings of the Smart Suction Cup, we compute $\hat{v}(k)$ using the measurements at (x_k, y_k) and Equation 3.1. As an alternative experimental control case, we also conduct a random jumping search in which the unit direction vector $\hat{v}(k)$ in Equation 3.2 is chosen at random.

In the experiments conducted for this paper, we set ΔH to 15 mm and ΔL to 5 mm as selected through pilot testing. ΔH is selected in order to avoid interference with protruding components on PCBs. ΔL is selected in order to adjust the suction cup pose with the size of a single chamber. In order to find the initial grasp point (x_0, y_0), we use a vision system where to segment PCBs from the image and calculate a center point.

[2]The threshold is 10 Pa for the tabletop test, and 18 Pa for the conveyor belt system.

[3]The target grasp height is constant across all grasp attempts, a hardcoded value selected to make the cup lip flush with a flat PCB surface.

[4]The arm pauses for 50 ms to collect this data.

[5]Unsuccessful grasps are detected when the average of all chamber vacuum pressures is < 2000 Pa. Likewise a successful grasp is when average pressure is > 2000 Pa in the lifted pose.

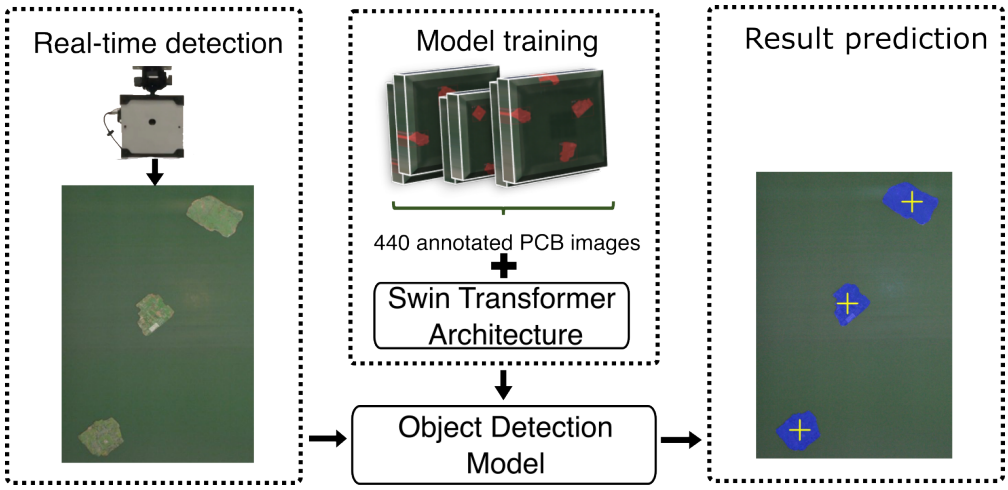

Figure 3.5: PCB detection using mechanical learning: We used 440 fully annotated PCB images as the dataset to train the PCB object detection model. We use it to achieve the PCB real-time detection. The PCB's location and its initial grasping point are predicted by the model.

3.3 Experimental Methods

Initial Grasp Position With Visual Segmentation

Data-driven vision approaches have been successfully applied to robot grasping planning[61]. The object recognition task involves object detection and semantic segmentation parts[62]. Beginning with the Swin Transformer architecture[63], transformer-based models have become the state-of-the-art object detection model. Hence, we utilize MMLab's MMDetection toolbox[64] to help us train a Swin Transformer object detection model to localize and segment PCB objects for the subsequent grasping point estimation (Fig. 3.5). We use 440 fully annotated RGB images of PCBs as the dataset to train the model. This dataset is designed to recognize different types of PCBs and predict their segmentation area and accurate edge with minimal error[65]. To annotate PCBs, we first use the Segment Anything Model (SAM) [66] to segment a rough area and use coco-annotator [67] to refine and accurately annotate them. The initial grasping point is derived from the segmentation results. Upon obtaining the predicted semantic segmentation mask, we can acquire its contour line points set X, composed of n points, with the assistance of OpenCV library[68]. The empirical mean of the contour line points set X is selected as the initial grasping point (x_0, y_0):

$$(x_0, y_0) = \frac{1}{n}\sum_{i=1}^{n} \mathrm{X}. \tag{3.3}$$

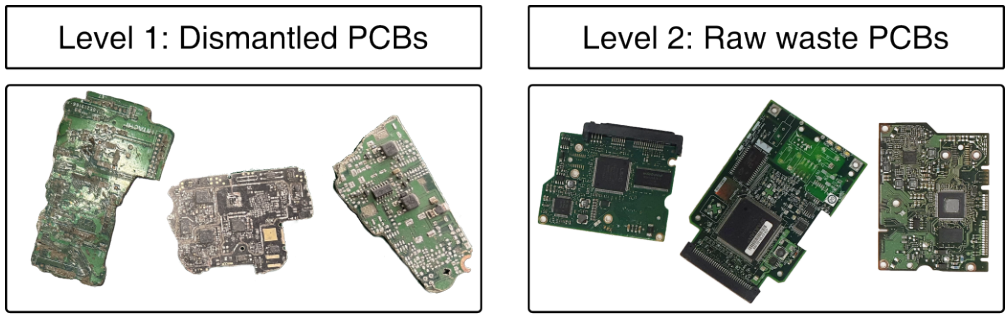

Figure 3.6: PCB categories according to difficulty levels

PCB Categories

To assess the effectiveness of our jumping haptic search method, we classify PCBs into two distinct difficulty levels based on their recycling status and surface complexity [47, 69], as illustrated in Fig. 3.6:

1. Level 1: Disassembled PCBs. These PCBs are processed using a mechanical dismantling machine, resulting in baseplate PCBs with little or no surface features. Baseplates may be warped by the dismantling process.

2. Level 2: Raw waste PCBs. These non-processed PCBs retain electronic components and are expected to pose a challenge for gripping using a suction cup.

Because Level 1 objects have been pre-processed, they have already been sorted out from other waste types at an earlier stage. However, we include both Levels in the current work because both may be present across varied applications, and Level 1 PCBs may still have surface features – vias, residual solder, warping, etc. – that hinder suction picking.

Tabletop Evaluation for PCB Haptic Regrasping

We establish a tabletop task involving the picking-up of PCBs to assess the performance of our proposed jumping haptic regrasping, as depicted in Fig. 3.7. The tabletop experiments are conducted using a desktop computer running Ubuntu 20.04, equipped with a Ryzen 5700X CPU and NVIDIA RTX 3090 GPU. We employ Robot Operating System (ROS, Noetic) to gather pressure sensor data and command the UR-10 robot to reach target poses. An RGB-D camera (Intel RealSense D435) is mounted on the robot arm's wrist, capturing photos at a resolution of 640x480 RGB, which are utilized for PCB segmentation. Additionally, we introduce a 3D-printed shock absorber made of TPU, strategically positioned between the robot arm and the suction cup system. This shock absorber serves to prevent the suction cup from exerting excessive force on electronic components as the height of surface mount components varies.

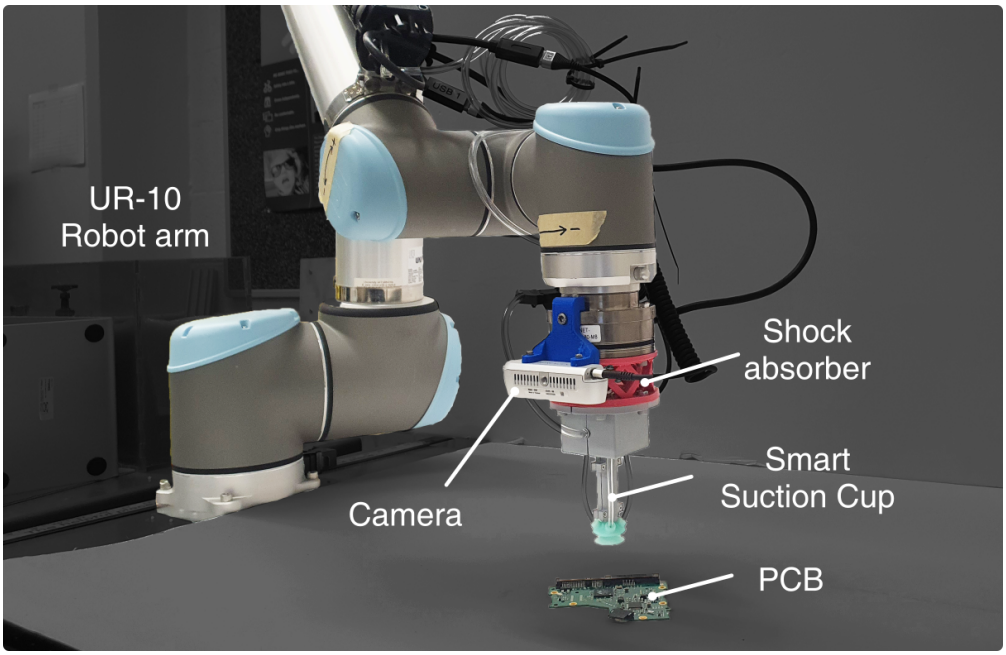

Figure 3.7: Experimental setup for the pick and place test on the tabletop system.

The robot system is programmed to employ either the haptic or random regrasping. Prior to commencing each grasping trial, the operator places a PCB on the tabletop with a random orientation. Subsequently, the robot attempts to grasp the PCB without researcher interference. First, the robot moves to an initial location to capture a photograph of the tabletop. After obtaining positional information from the visual segmentation, the robot approaches the target pose with a 15 mm height offset. It then starts the process of jumping regrasping, as described in Fig. 3.4. The robot continues to jump until either a successful grasp is achieved or the time limit of 10 seconds is reached. Following each trial, regardless of success or failure, the researcher removes the PCB and replaces it with a new PCB for the next trial.

Demonstration on Conveyor Belt System

To emulate an industrial recycling setup, we test PCBs grasping on a miniaturized industrial conveyor belt system, as illustrated in Fig. 3.8. The conveyor belt, measuring 0.4 meters in width and 1.5 meters in length, is placed on a table and powered by a 220V DC motor (120RGU-CF, TAITUO Technology). We integrate a 6-axis robotic arm (MZ-04, Nachi Robotics) to perform pick-and-place. The input end of the conveyor belt features a vision system comprising a photo booth equipped with white lights and an RGB camera (MV-SUA501GC-T, MindVision).[6] The open-loop speed of the conveyor belt is set to 94 mm/s

[6]The camera captures images at a rate of 5 Hz.

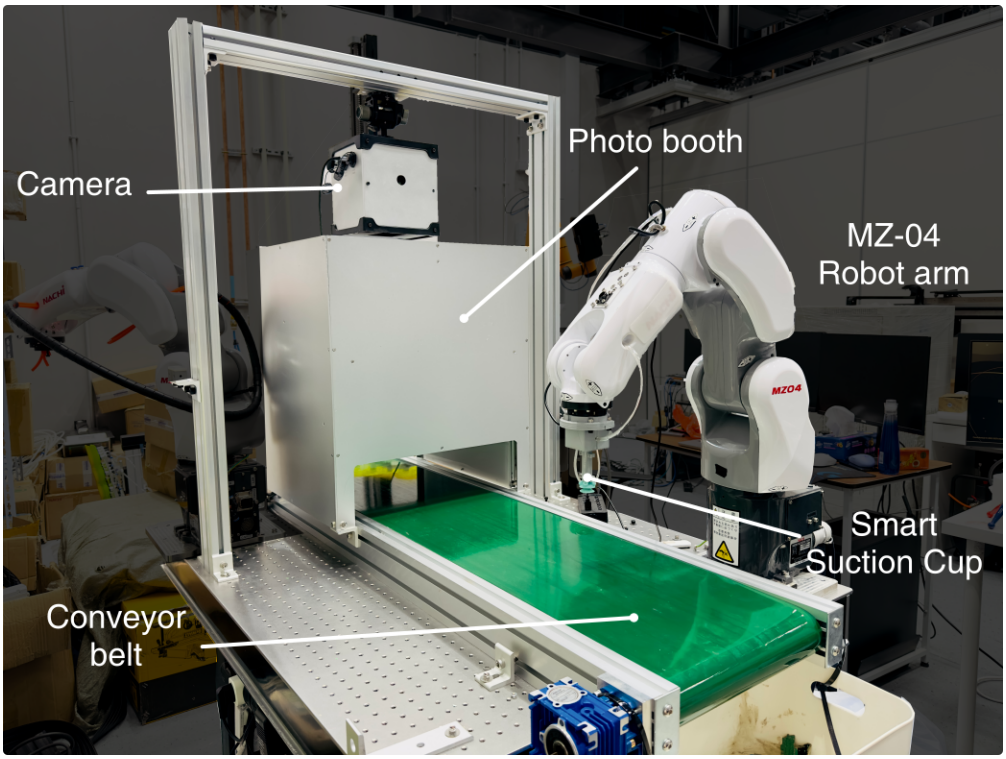

Figure 3.8: Experimental setup for tests on a miniaturized conveyor belt system.

at all times, without pause. Thus, to monitor the speed and absolute movement distance of the conveyor belt, we employ an encoder (E6B2-CWZ6C 2000PR, OMRON). The smart suction cup is attached to the robotic wrist. We establish a workspace measuring 0.53 meters in length, considering the robot arm's graspable area on the conveyor belt plane. Our computational setup consists of a desktop PC running Ubuntu 20.04, equipped with an NVIDIA 3060 graphics card, all managed by the Robot Operating System (ROS, Noetic) for model inference and robot control. Prior to conducting experiments, we perform calibration to determine the camera's position and orientation relative to the end-effector, adjusted for the conveyor belt's position using hand-eye calibration methods [70].

For each trial, the operator first places a PCB at the input of the conveyor belt with a random orientation. As the PCB traverses the belt and becomes visible to the camera, its segmentation mask and initial grasp point are predicted.[7] Once the initial grasping point is estimated, the robot moves to the starting line of the workspace with the predicted location, waiting for the PCB to pass directly beneath the suction cup. Subsequently, the robot commences jumping search on the PCB surface and continues until it successfully grips the

[7]If a segmentation result indicates that the same PCB detected in the previous image is still present, the robot system disregards the result.

PCB or reaches the end of the workspace on the conveyor belt. If the suction cup successfully grasps the PCB, the robot moves it to a designated location and released the PCB into a container.

Throughout the pick-and-place task, the robot continuously monitors the conveyor belt's speed and absolute location to ensure that the updated pose accurately reflects the relative location on the belt. The jumping search algorithm is modified from Equation 3.2 to include a compensation term representing the relative movement of the conveyor:

$$\Delta D = d_{k+1} - d_k \quad k = 0, 1, 2... \tag{3.4}$$

$$(x_{k+1}, y_{k+1}) = (x_{k+1}, y_{k+1} + \Delta D) \tag{3.5}$$

where d_k represents the conveyor's absolute location when the robot is approaching the location (x_k, y_k). During system setup, we aligned the direction of the conveyor with the robot's y-axis, such that we add the ΔD on the y_{k+1} to ensure accurate pose updating.

3.4 Results

Table-Top Pick and Release Test

The tabletop pick-and-release results are conducted for Level 1 PCBs (28 PCBs, 4 trials each) and Level 2 PCBs (21 PCBs, 4 trials each), presented in Fig. 3.9. For Level 1 PCBs, the random regrasping increases the success rate from 75.9 ± 4.5% to 91.1 ± 4.6% (Fig. 3.9a). The haptic regrasping exhibits a similar result with the success rate increasing from 75.0 ± 8.7% to 92.9 ± 5.1%. For the Level 2 PCBs (Fig. 3.9b), the initial attempts show lower success rates on the order of only 10%. While the random regrasping method only improved performance to 22.6 ± 2.4%, the haptically-driven regrasping increases success to 50.0 ± 4.8% representing a 370% performance increase.

Histograms depict the number of jumps required to achieve a successful grasp in each scenario (Fig. 3.9c, d). For Level 1 objects, the initial grasp is usually successful, and the grasp is likely to succeed with few additional grasps whether random or haptic control is used. However, in the case of Level 2 objects the chance of randomly finding a good grasp point is lower. Thus, only 4 cases are successfully gripped by random jumping within the first two regrasps. In contrast, haptic regrasping achieves 13 successes on the first regrasp and 8 cases on the second regrasp.

The overall trial success rate changes with respect to the number of jumps, depicted in Fig. 3.9e, f. For Level 1 PCBs, the success rate changes are nearly identical between random and haptic regrasping. However, as shown in Fig. 3.9f, haptic regrasping exhibits a logarithmic increase up to about 4 jumps, while random jumping shows a linear increase as the number of jumps increases. The effect of using haptically-driven direction estimation, as compared with random, appears most consequential for the first couple jumps.

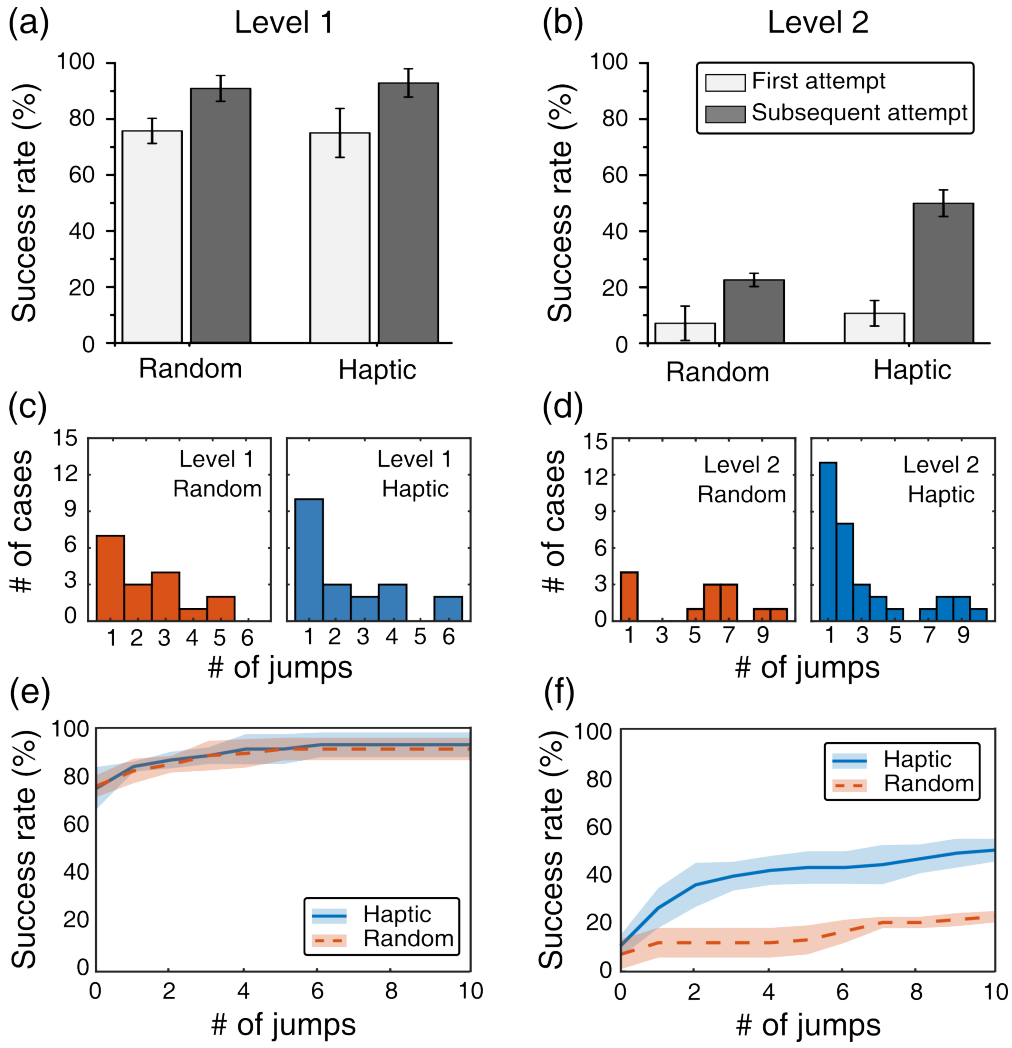

Figure 3.9: The results of pick-and-release from the table top experiment. The success rates for random and haptic regrasping with (a) level 1 and (b) level 2 PCBs. Lighter gray bars are the success rate from an initial attempt and darker grey bars are the increased success rate with subsequent jumping regrasping. Histograms for the number of cases according to the number of jumps for each type with (c) level 1 and (d) level 2 PCBs. The success rate changes according to the number of jumps with (e) level 1 and (f) level 2 PCBs. Data are presented as the mean ± s.d.

Demonstration on Conveyor Belt System

The results of the pick-and-place tests conducted on the conveyor belt system for Level 1 (52 PCBs, 4 trials each) PCBs and Level 2 PCBs (21 PCBS, 4 trials each) are presented in Fig. 3.10. For Level 1 PCBs (Fig. 3.10a), the random regrasping shows the success rate at

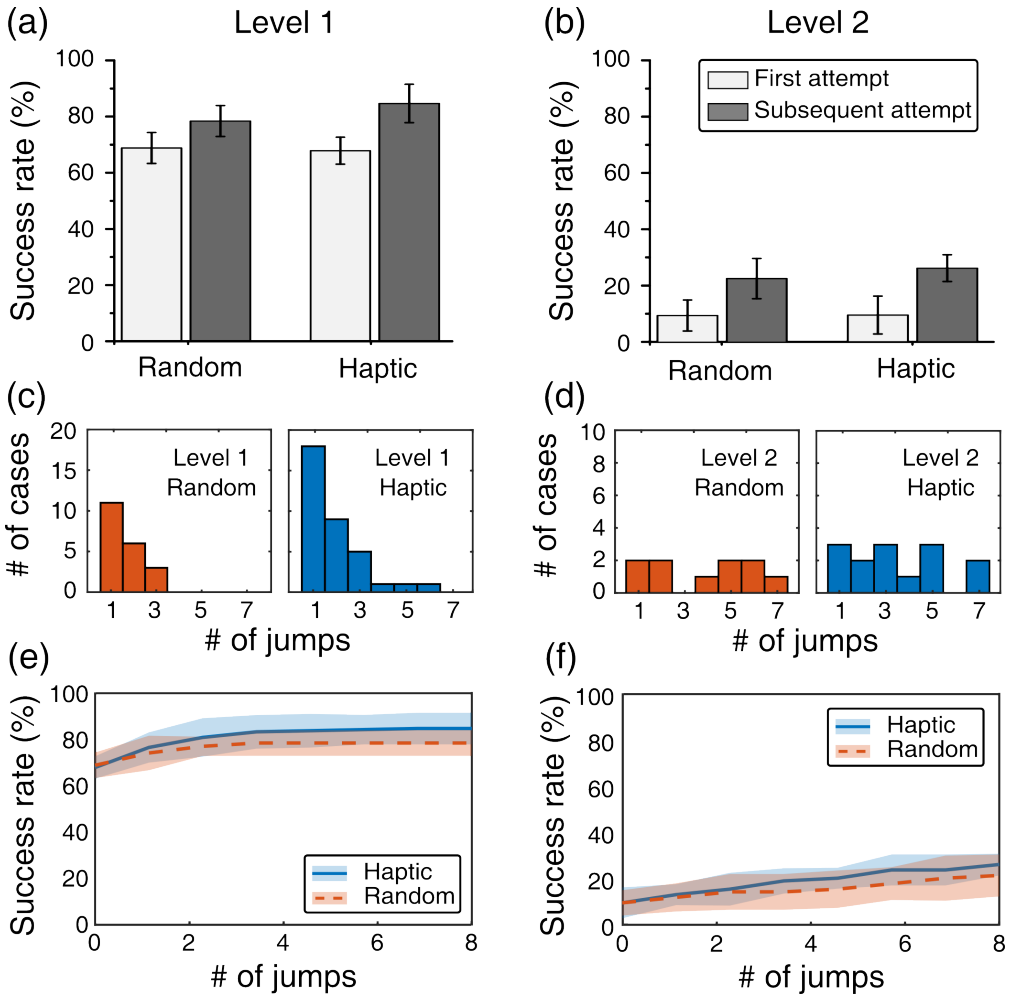

Figure 3.10: The results of pick and place tasks on the conveyor belt system. The success rate for random and haptic regrasping for each type with (a) level 1 and (b) level 2 PCBs. Histograms for the number of cases according to the number of jumps for random and haptic regrasping for each type with (c) level 1 and (d) level 2 PCBs. The success rate changes according to the number of jumps for each type with (e) level 1 and (f) level 2 PCBs. Data are presented as the mean ± s.d.

the initial attempt is 68.6 ± 5.5%, which increases to 78.4 ± 5.5%. The haptic regrasping demonstrates a success rate increase from 67.8 ± 4.8% to 84.6 ± 6.8%. While the random regrasping shows a 14.4% performance increase, a 25.0% performance increase is achieved with the haptically-driven regrasping. For the Level 2 PCBs Fig. 3.10b), the initial attempt presents a success rate of 9.5 ± 5.5%, which increases to 22.6 ± 7.3% with the random regrasping method. The haptically-driven regrasping increases the success rate from 9.5 ± 6.7% to 26.2 ± 4.8%. Performance increases by 134% and 176% for the random and haptic regrasping, respectively.

Histograms of successful grasping cases with respect to the number of jumps for each type are depicted in Fig. 3.10c, d. For the Level 1 PCBs, most successful grasps occur in the early stages of jumps in both cases, resulting in histograms that exhibit a plateauing trend. While, haptically-driven jumps show a higher number of successful cases, the difference with random search is small. In the case of Level 2 objects, both the random and haptic search show evenly distributed chances of finding a good grasp point. These trends are also shown in success rate changes (Fig. 3.10c, d); the success rate increases slightly faster in haptic regrasping, and keeps increasing slowly after the first three jumps for the Level 1 PCBs, while the success rate gradually increase in the case of Level 2 PCBs.

3.5 Discussion

We evaluated the performance of the proposed jumping haptic regrasping on the tabletop experimental setup. For table-top tests, we observed that the difficulty of the object to be gripped correlated with a more substantial performance improvement achieved through haptic regrasping, as compared with random search. In other words, haptic information is beneficial for the suction cup to regrasp more complex objects, like Level 2 PCBs. Interestingly, obstacles that prevent the suction cup from engaging with surfaces can help the system discern pressure differences between chambers, enabling the suction cup to know where to go for a better grasp. For instance, some PCBs have flat components such as microprocessors, which represent an ideal point for the suction cup to grip. If the suction cup touches the edge of the microprocessor, it tends to move in the direction of the microprocessor, even though this obstacle prevents it from grasping initially. In comparison, random jumps do not guarantee finding this prospective grasp point.

Although our regrasping algorithm enhances the probability of successful grasp on PCBs, the success rate doesn't reach 100% even for level 1 PCBs. This can be explained by failure cases discussed in the prior work [53]. One common failure mode is that an initial grasp point can be located in an area where there are a lot of electronic components, thereby it is impossible to be gripped in that region by the suction cup. The other common failure case is haptic oscillation, where the suction keeps moving back and forth without a successful grasp. One possible solution for this haptic oscillation is to use various step sizes (ΔL) from the pressure readings. Future work will include an adaptive choice of this parameter, which could be informed by further understanding of air flows on complex PCB surfaces.

Conducting robotic demonstrations in an industrial setup is crucial to translate manipulation methods initially developed in a laboratory environment. Thus, we evaluated our system using a scaled-down industrial conveyor belt setup. In these trials we find the null result: inconsequential differences between random and haptic regrasping methods on both Level 1 and 2 PCBs. The positive results from Level 2 table-top tests do not translate to the conveyor application in the current implementation. As of now, jumping haptic regrasp is only helpful when the object remains stationary.

Transitioning robotics technology from research labs to industrial settings faces challenges

due to the lab-to-industry gap[71]. This transition often involves adapting experimental setups with strictly controlled conditions to real-world industrial environments, which can introduce new complexities and uncertainties. We suspect the null outcome is in part due to relative motion between the cup and conveyor that unintentionally displaces the object, negating haptic information. In the tabletop experiment, the suction cup only moves vertically relative to the PCB during grasping. However, a short pause of the suction cup at the target grasp position to collect pressure data was observed to result in unwanted pose changes of PCBs due to the conveyor belt's motion. These disturbances likely decrease haptic regrasp direction estimate effectiveness. This essentially led to a haptic regrasp attempt resembling a random jump. To address these challenges, future work will incorporate real-time tracking of PCB orientations with a wrist-mounted camera to enable haptic regrasping between jumps that compensate for PCB motions.

3.6 Conclusion

In this study, we presented a jumping haptic regrasping for determining a searching direction with the Smart Suction Cup. This approach enables the suction cup to adjust its pose for more successful suction grasping of stationary Level 2 PCBs, with surface features difficult to capture by a vision-based planner. With ongoing development, the Smart Suction Cup is a promising tool for recycling sorting applications involving objects with intricate surface features, like PCBs.

Chapter 4

The Dorsal Grasper: Supernumerary grasping

The Dorsal Grasper, an assistive wearable grasping device, incorporates supernumerary fingers and an artificial palm with the forearm and back of the hand, respectively. It enables power wrap grasping and adduction pinching with its V-shaped soft fingers. Designed with C6/C7 spinal cord injury in mind, it takes advantage of active wrist extension that remains in this population after injury. We propose that allowing the operator to actively participate in applying grasp forces on the object, using the back of the hand, enables intuitive, fast and reliable grasping relevant for the execution of activities of daily living. Functional grasping is tested in three normative subjects and a person with C6 SCI using the Grasp and Release Test. Results indicate that this device provides promising performance on a subset of objects that complements the existing compensatory strategies used by people with C6/C7 SCI. We find that the addition of the artificial palm is important for increasing maximum grip strength, by increasing

4.1 Introduction

Spinal cord injury affects an estimated 40 million people worldwide every year[72]. Cervical-level spinal cord injury (SCI) results in tetraplegia, or paraplegia, and can dramatically reduce a person's ability to perform common activities of daily living (ADL), e.g., manipulating and grasping objects in the home necessary for cooking, donning cloths, inserting a catheter, etc., ultimately leading to loss of independence. When surveyed, people with cervical SCI report that hand and arm use has the highest functional importance in terms of research prioritization for improving quality of life [73], ranking above pain relief and walking.

People with SCI at the C6/C7 cervical levels generally lose voluntary flexion of the wrist and fingers [74], however wrist extension typically remains [75]. Active wrist extension elicits passive thumb-to-forefinger and finger-to-palm flexion, called "tenodesis" [76], as

demonstrated in Fig. 1. This flexion of the fingers enables passive tenodesis grasping [77], which is most effective for picking up light and small objects. However, tenodesis grasp is typically unsuitable for larger and heavier objects [78]. Empowering more dexterity with assistive devices, in this work through enabling power grasping, has the potential to improve psychosocial and economic outcomes after injury [79].

Related Work

Several assistive devices have been designed to support hand function for people with cervical SCI. One commonly prescribed device is the wrist-driven orthosis (WDO), which uses a mechanical linkage to assist tenodesis grasping [80, 81, 82]. Despite being body-powered and consequently lightweight, physically resilient and low cost, patients tend to abandon WDOs over time as they get used to unassisted tenodesis and opt to use a set of more specialized tools [83]. Constraining the hand to always use tenodesis grasping is problematic for the full set tasks required for ADL [84]. There are a wide number motor-articulated investigational devices [85], though few are commercially available. Recently, a number of new devices based on soft materials have received attention due to the potential benefits of creating compliant and light-weight structures, such as fabric-based actuators [86, 87] and soft linkages [88, 89, 90].

Instead of assisting the person to move their own fingers, another option is to add extra-fingers to the hand. Wu and Asada (2015) introduced a supernumerary robotic (SR) finger to perform "hold-and-manipulate" tasks for stroke survivors and other patients with limb impairments[17]; extra fingers are mounted on a wrist brace and primarily oppose the palm. Hussain, et al. (2016) separately reported on a soft-sixth finger for grasp compensation in chronic stroke patients [91]; the soft-sixth finger is worn like a bracelet and largely opposes the radial side of the hand during grasping. We explore how this supernumery finger concept may be adapted to grasping with the back of the hand.

Overview

We are expanding the concept of supernumerary fingers, taking into account the pathology of people with C6/C7 SCI. We expect that adding a set of supernumerary fingers on the opisthenar, or the back of the hand, can provide grasping on larger objects in a way that takes advantage of active wrist extension for intuitive and fast operation (Fig. 4.1). Importantly, by using the dorsal side of the hand, the device does not impede common use of the hand for other purposes such as palmar tenodesis grasping or the use of specialized tools. Often individuals with cervical SCI can extend the wrist, e.g., subjects with C5/C6 SCI can extend the wrist with approximately 1 N of force [92]. Thus, we expect dorsal grasps to be relatively gentle compared with normative power grasping.

Section 4.2 describes how the supernumerary fingers are constructed and how they function. These fingers are controlled via a joystick for initial testing with human subjects. The palm plays a role in human and animal grasping [93, 94], while the skin on the back of the

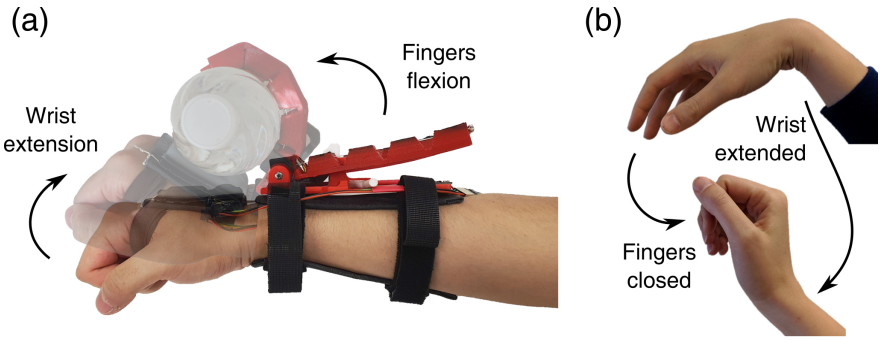

Figure 4.1: (a) The Dorsal Grasper includes a set of soft flexible fingers and an artificial palm on the dorsal part of the hand. Here, a water-bottle is grasped using both operator wrist extension and artificial finger flexion. (b) A tenodesis demonstration shows active wrist extension elicits passive finger flexion, from [82].

hand is thin, highly elastic and has little underlying tissue [95]. The opisthenar thus produces less friction and contact area with objects compared with the palm, and an artificial supernumerary palm is added to the back of the hand. We perform three discrete experimental tests with this system, described in Section 4.3: the grasping of different sized boxes, maximum grasp force, and a modified Grasp and Release Test. As described in Section 4.4, we find that the Dorsal Grasper enables both adduction pinching and palmar grasping, and that human subjects change grasp strategy depending on the object. The artificial palm, combined with active wrist extension, increases power grasp strength. Trials performed by a person with SCI indicate this device holds the potential to support the execution of ADLs, discussed in Section 4.5.

4.2 The Dorsal Grasper

The Dorsal Grasper is a compliant wearable device capable of grasping objects of various shapes and sizes. The mechanism is made of 3D printed plastic (PLA) and rubber (Ninjaflex) parts and a thermoplastic (Worbla sheet, TAP Plastics) cuff that provides a lightweight and flexible interface with the forearm. As shown in Fig. 4.2, the tendon-driven flexible fingers fit into a hinged finger-holder. The fingers rest two states: (1) the storage-stage, when the fingers lay back flat against the forearm, not in use, and (2) the ready-stage, when the fingers sit upright perpendicular to the forearm. A releasable latch holds the fingers in the storage-state, shown in Fig. 4.3.

When grasping, finger flexion is driven by a 0.4-mm-diameter rope (PE Braided line) on a 12 mm diameter winch with a DC motor (12V with a 156:1 metal gearbox). The brace and motor base are both fastened onto the soft cuff and the tendon is routed over a polished fixed pulley between these two elements.

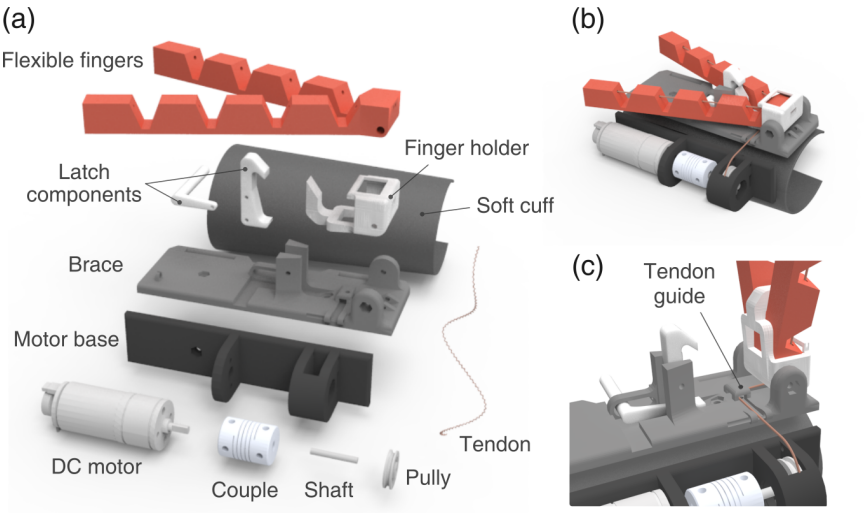

Figure 4.2: CAD images of the Dorsal Grasper: (a) exploded, (b) assembled, and (c) tendon routing details.

Soft Tendon-driven Finger

The soft tendon-driven fingers are 130 mm in length and the angle between the two fingers is 35.5 degrees (Fig. 4.2 and 4.4), which provides a balance between finger spread, for resisting object moments, and portability. V-shaped fingers were previously introduced for supernumerary applications in [96, 97]. Each finger consists of four equally sized phalanges with 4 mm gaps in between. A 2 mm diameter hole in the upper part of each phalanx (11.5 mm from the back of the finger) allows the tendon to route through each then terminates at the distal tip. The thickness of each interphalangeal flexure linearly increases from 2.5 to 4 mm, from proximal to distal, to generate a slight base-to-tip curling order. In order to increase the frictional coefficient between an object and the finger, rubber (Multipurpose rubber, Plasti-Dip) is coated onto the surface of each phalanx.

The V-shaped finger configuration in the Dorsal Grasper enables two separate grasp types: power palmar grasping (Fig. 4.1a) and gentle adduction pinching (Fig. 4.5c). In palmar grasping, the fingers press the object into the back of the person's hand. Alternatively, the user can pinch small objects as the fingers wrap inward towards the finger holder, approximating finger adduction. These two grasp classifications are qualitatively similar to grasping strategies of the human hand, defined in grasp taxonomies [98, 99] and demonstrated in Fig. 4.5a-b.

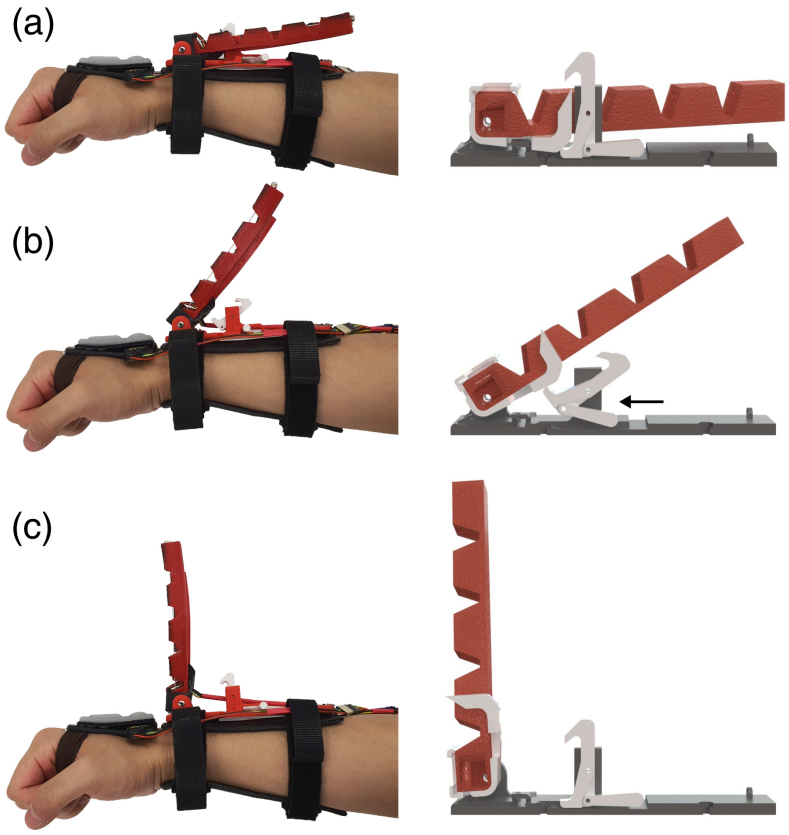

Figure 4.3: Deployment from "storage" (a) to "ready-to-grasp" (c). (a) The finger housing is held down with a releasable latch. (b) The user can deploy the fingers to the ready stage by pushing the positioning bar with his or her opposite hand. The base of the latch pushes the fingers forward towards the hand. (c) The Dorsal Grasper reaches its "ready" stage once the motor pulls the finger tendon taut in the upright position.

Artificial Palm

This device uses the back of the hand as a grasping surface. In the human hand, the skin of the opisthenar is relatively thin and fragile as compared to the palm, that regularly resists scratching and bruising. In contrast to the palmar surface, the skin of the opisthenar is also highly pliable and hairy [95]. In order to increase comfort, strength and friction during dorsal grasping, an artificial palm is attached to the opithenar using an elastic band. The palm is fabricated with a silicone rubber (Dragon Skin 10) molded onto Velcro[1] using a 3D printed negative. This artificial palm interfaces with the body using a soft cuff made of

[1]We find the loop side of the Velcro provides strong bonding with the silicone, while the hook side of the Velcro de-laminates easily and is not recommended.

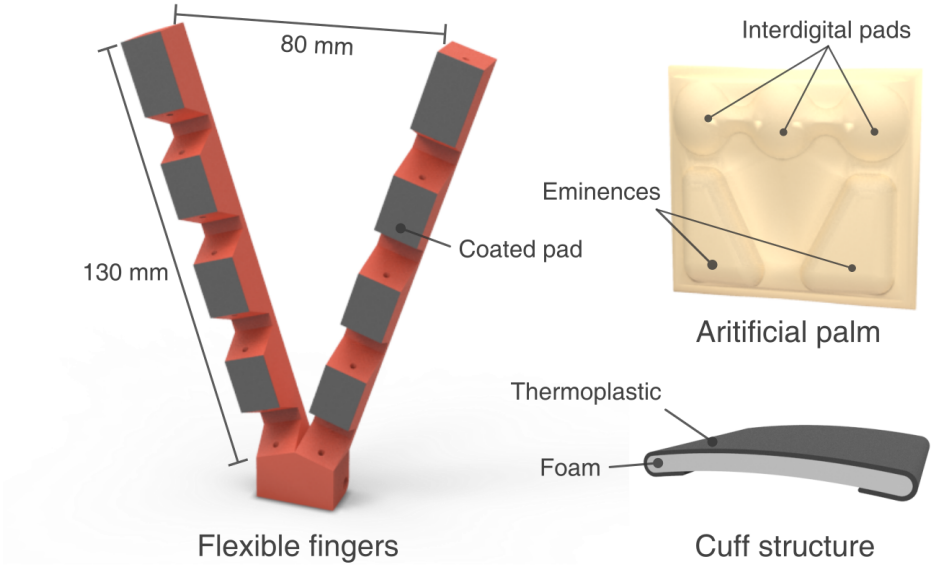

Figure 4.4: CAD images of the flexible fingers, artificial palm, and structure of the cuffs.

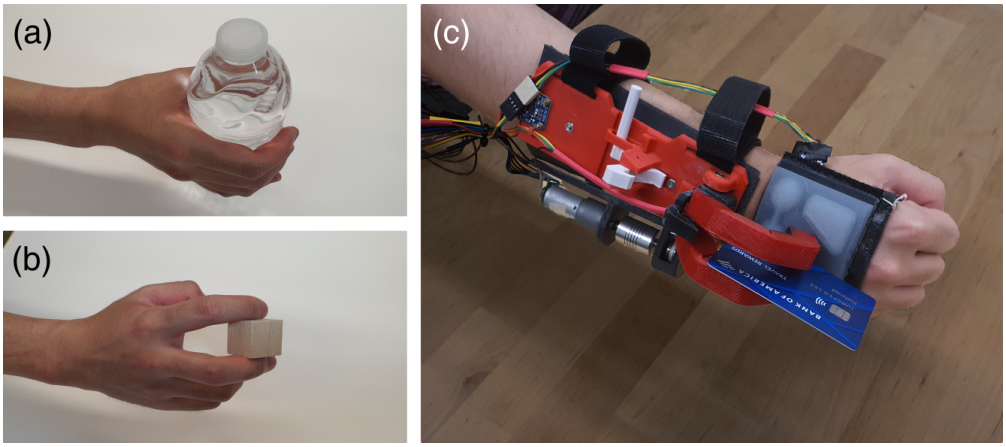

Figure 4.5: (a) Palmar grasping and (b) adduction pinching of the human hand. (c) Abduction pinching a credit card with the Dorsal Grasper.

thermoplastic shaped to fit the back of the hand. The compliant silicone pad is intended to conforms to various object shapes during grasping. The concave shape of the artificial palm (Fig. 4.4) is roughly inspired by the structure of the human hand, which has three interdigital pads positioned in between the thenar and hypothenar eminences on its palm [100].

Attachment to the body

In order to provide reliable grasping, the forearm attachment must be secure on the body, yet comfortable. The thermoplastic forearm cuff wraps around the ulna of the arm, allowing it to resist torsional forces. We use soft foam on the inside of the thermoplastic forearm cuff (Fig. 4.4) to protect the skin and distribute contact pressure. The flexible property of the thermoplastic allows it to fit onto forearms of various sizes. Velcro loops allow the wearer to fasten the device tightly to his or her own forearm. While the cuff can resist the forces due to grasping and lifting, and stays stationary on the skin, there is some motion of the device due to the soft nature of the underlying tissue of the forearm. The cuff for the artificial palm is fabricated in the same way as the forearm cuff. The elastic band attached to the artificial palm wraps around the person's palm and holds it in place on the back of the hand, visible in Fig. 4.3.

Control interface and data acquisition

Grasping commands are input by the wearer using their opposite hand through a control box fixed to the test-bench. The box is comprised of: i) a large arcade joystick, ii) an emergency stop button, iii) two LED indicators, and iv) the motor control electronics (Fig. 4.6). The left and right toggling of the joystick triggers grasping (finger flexion) and opening (finger extension) motions. A motor encoder measures finger actuation while a distance sensor, installed in the finger holder, measures the distance between the base of the finger and the object. An accelerometer on the artificial palm observes the motions of the hand. The wires for these on-board sensors are routed to the control box, but these signals are used only for data recording and not yet as inputs for control behavior.

4.3 Experimental Methods

We test the performance of the Dorsal Grasper under the University of California at Berkeley IRB-approved human subject protocol #2019-07-12348.

Grasping type comparison: block test

Anticipating that the ease of performing power grasping and adduction pinching with the Dorsal Grasper might change with object size, we prepare 3D printed cubes with a variety of sizes, from 10 to 60 mm length scale (Fig. 4.7a). Two normative subjects are asked to pick up the cube from an initial location on the table, 40 cm from the front edge of the table and in-line with person's shoulder. They then place it on a target location in-line with the opposite shoulder shown in Fig. 4.6. The time to complete the maneuver is recorded for both grasp methods over all cube sizes for 5 trials each. Since the experiment is conducted with light-weight cubes, results may vary if conducted with heavier objects.

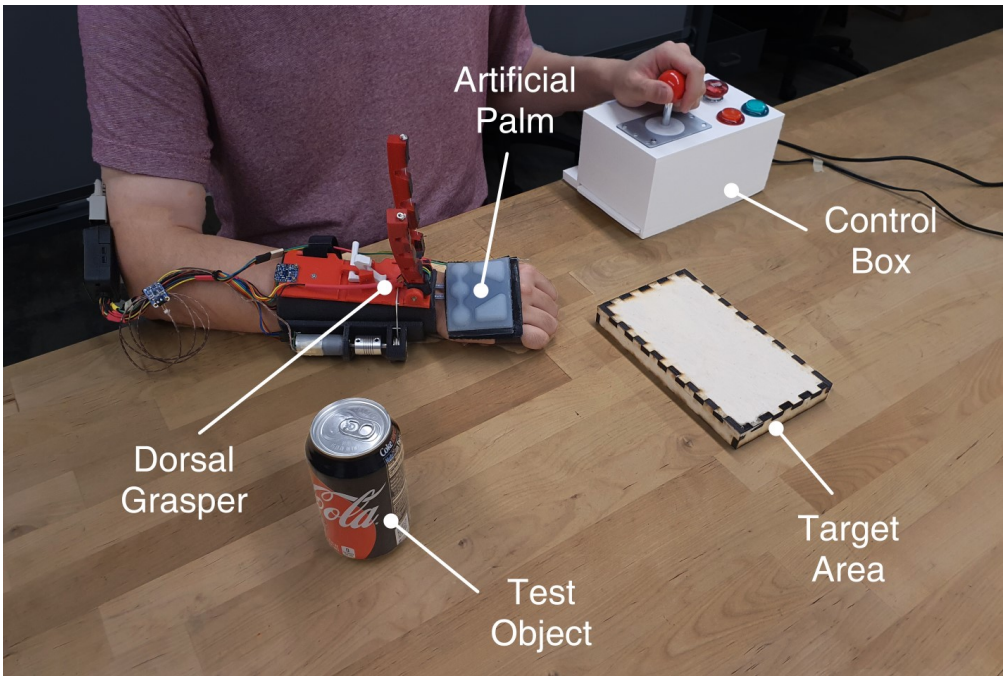

Figure 4.6: The experimental setup for the block test and the Grasp and Release Test, including the control box, object starting location and target area.

Maximum palmar grip strength

The artificial palm plays a role in both shielding the skin and increasing friction. Thus, we test the effect of the palm on the lift strength of the device. Three normative subjects are asked to grasp cylindrical objects then a hand-held force gauge (Mark-10 M4-50, MSI Viking) is used to pull the object out along the cylinder's axis, perpendicular to the finger plane of motion. The peak force needed to initiate any slip on the surface of either the artificial palm or the finger is recorded (Fig. 4.7b). Cylinders with 40, 50, and 60 mm diameters are each tested 10 times, both with and without the artificial palm. This entire set of trials is conducted (1) with the subject applying maximum wrist extension and (2) holding the wrist steady in a neutral pose.

The Grasp and Release Test

We utilize a modified Grasp and Release Test (GRT), which is specifically designed to quantitatively measure the grasping abilities in tetraplegic patients [101], to measure versatility and reliability of the Dorsal Grasper. Participants are asked to grasp, move, and release different objects, as shown in Fig. 4.6. If the subject completes the goal for a given object within 30-seconds, it is considered a success, otherwise it is considered a failure. We use five

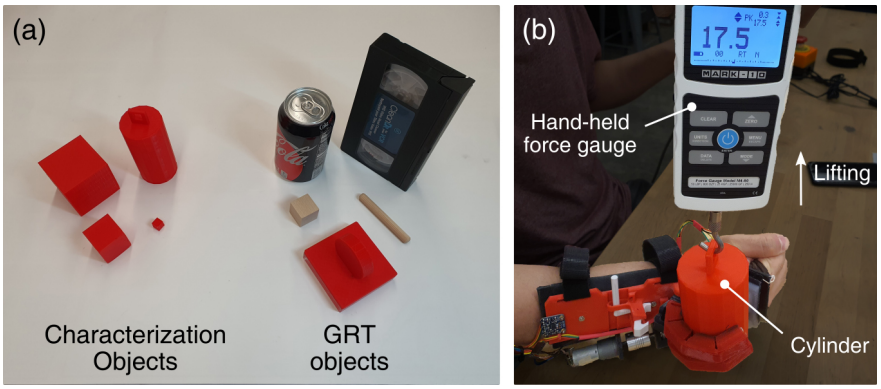

Figure 4.7: (a) Experimental objects for Dorsal Grasper testing include a cylinder with 50 mm diameter, cubes of 10, 35, and 60 mm edge length, and objects replicating the standard Grasp and Release Test kit. (b) The strength test setup uses a handheld force gauge to pull the object out of the grip.

objects from the original GRT, pictured in Fig. 4.7a, excluding the fork because the size does not fit the designed device. Object specifications are listed in Table 4.1. The objects are presented in the order: can, videotape, weight, block, and peg. The researcher first places the object on the start area in a random orientation. Then the subject is video recorded and timed during their attempts. For the block and peg, the object can be dropped into the target area with any orientation. For the can, paperweight, and videotape, the object must be placed in an upright orientation on the target area to be counted as a success. The participant is allowed to attempt the tasks as many times as possible within the 30-second time. Data is collected from four human subjects: two normative subjects are accustomed to using the device while one normative subject and one subject with C6 SCI are not familiar with using the device. Subjects unfamiliar with the device perform 10-minutes of grasping practice prior to data collection.

Table 4.1: Objects specification of The Grasp and Release Test

Test object	Object weight (N)	Object size (cm)
Can	3.48	12.3 x 6.6 (dia)
Videotape	1.28	19.3 x 10.9 x 2.8
Paperweight	2.32	5 x 1.4 (th)
Block	0.102	2.5 x 2.5 x 2.5
Peg	0.041	8.0 x 0.6 (dia)

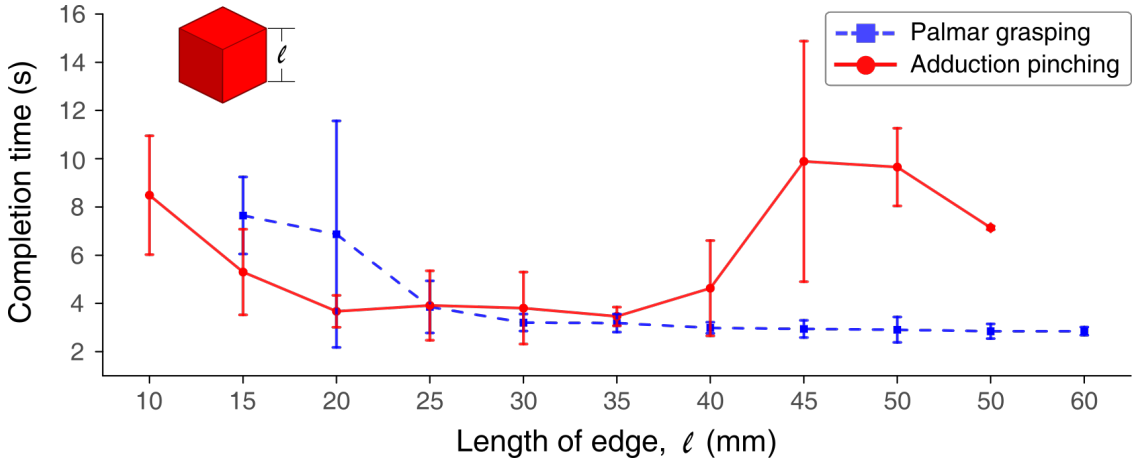

Figure 4.8: Comparison of completion time between palmar grasping and adduction pinching with the Dorsal Grasper on cubes of various sizes. Data is presented as the mean ± s.d. across all trials with two normative subjects.

4.4 Results and Discussion

Block test

Mean and standard deviation data from the block test is shown in Fig. 4.8, and indicates that the two different grasp types – palmar and adduction – provide different benefits based on object size. The 10 mm cube was too small to conduct the task with palmar grasping and the 60 mm cube was too large for adduction pinching, thus these data-points are excluded.

For cubes of size 25 mm to 35 mm, palmar grasping and adduction pinching have similar task completion times. For the small 15 mm and 20 mm cubes, palmar grasping requires more time to complete (7.6 ± 1.6 s & 6.9 ± 4.7 s respectively) than adduction pinching (5.3 ± 1.8 s & 3.7 ± 0.7 s respectively). Difficulty in performing palmar grasps on small objects occurs when the object is smaller than the fingers can curl; the object must be carefully pinched between the fingertip and the palm. Adduction pinching also becomes increasingly difficult as object size decreases because of limited adduction range of motion. For objects larger than 20 mm, palmar grasp completion times decrease monotonically from 25 mm (3.9 ± 1.1 s) to 60 mm (2.8 ± 0.2 s), and standard deviation diminishes. Palmar grasping outperforms adduction pinching for 40 mm cubes (4.6 ± 2.0 s) and bigger. Difficulty in performing adduction pinch with large objects emerges from limited adduction range of motion and curling behavior; when the finger starts to flex, the gap between the adjacent fingers closes rapidly and requires careful control to succeed.

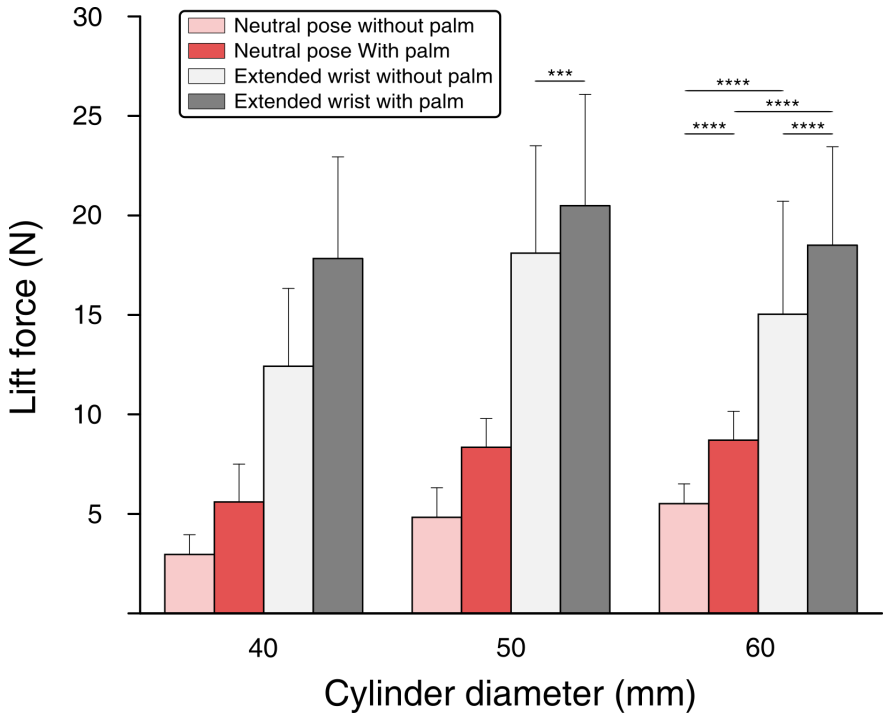

Figure 4.9: The lift force of the Dorsal Grasper both with and without the artificial palm and wrist extension over varying cylinder diameters. Statistical significance for all paired t-test comparisons for each object are ****$p < 0.0001$, as shown only for 60 mm. The only exception is the comparison between extended wrist with and without the palm with the 50 mm cylinder, which is ***$p < 0.001$. Data are presented as the mean ± s.d. (n = 30, 3 normative subjects for 10 trials each).

Grip strength

As shown in Fig. 4.9, there is a significant positive effect on lifting force with both the use of the artificial palm and wrist extension. For all three object diameters, holding the wrist neutral without the artificial palm is weakest while extending the wrist with the artificial palm is strongest. During trial observations, initial slip occurred at either the back of the hand or the fingers. One subject noted discomfort on the back of the hand when extending the wrist without wearing the artificial palm, caused by the fingertips of the device pushing into the dorsal skin, and this may have caused them to limit their wrist extension force. Regardless of whether the benefit is due extension strength or friction coefficient, wearing the artificial palm allows the operator to achieve greater grasp lifting forces. The difference between neutral pose and extended wrist trials indicate that an operator can actively moderate their maximum lift force using wrist extension, even after the fingers are fully actuated.

There appears to be a minor trend with object size. Cases that extend the wrist are

Table 4.2: Success rate of the Grasp and Release Test

Subject number	Can	Videotape	Paperweight	Block	Peg
Subject 1	7/9	8/9	9/9	9/9	0/9
Subject 2	9/9	8/9	9/9	9/9	2/9
Subject 3	9/9	9/9	8/9	9/9	8/9
SCI subject	5/5	5/5	4/5	5/5	2/5

maximized for the 50 mm cylinder, for both the bare hand (18.11 $\pm$ 5.39 N) and artificial palm (20.49 $\pm$ 5.58 N). Whereas, the results from the neutral wrist pose show gradual increases of lift force with cylinder size. This is likely caused by changes in soft finger pose with wrist pose.

The Grasp and Release Test

As shown in Fig. 4.10, the Dorsal Grasper enables grasping of all 5 GRT objects tested. Success rates out of 9 trials for each of the three normative subjects and 5 trials for the subject with C6 SCI are listed in Table 4.2. Examples of successful trials performed by the subject with SCI are included in the paper video extension. The soda can (b) and the paperweight (d) are grasped in approximately the same palmar method every time. One subject reported that the paperweight required maximum wrist strength due to its heavy weight and particular shape. For the videotape, subjects vary their palmar grasp orientation, shown in (c). The block is typically gripped in a palmar fashion, even though adduction pinch is possible, described in Sec. 4.4. The peg has the largest grasp strategy variability. While most successful trials are performed using adduction pinching (e), a couple successful trials are achieved using a palmar pinch with one finger (f). Only one subject consistently succeeds at the peg tasks (8/9 success rate) by orienting the hand as pictured in (e). Task failures occur if: (1) the paperweight is too heavy to lift, (2) the videotape or soda can is accidentally knocked over or dropped so it is no longer upright and isn't re-grasped, or (3) it takes too long to secure the peg in either a palmar or adduction grip. Completion times for each object across all subjects and successful trials are reported in Fig. 4.11. The subject with C6 SCI takes longer on average to complete tasks, except with the block. Observed grasping strategies and grasp success rates for the subject with SCI are otherwise similar to the normative subjects.

Recordings from the motor encoder, object distance sensor and palm accelerometer are plotted in Fig. 4.12 for a single representative grasp trial with the soda can. We divide the GRT trial into multiple steps: a coarse approach to the object, a fine approach, grasping and opening. During the coarse approach, the accelerometer captures the typical reaching-to-grasp acceleration and deceleration curves [102, 103]. During fine approach, the distance between the device and object closes gradually. The user then grasps and releases the object by operating the motor to flex the finger. Fluctuation of the acceleration during grasping

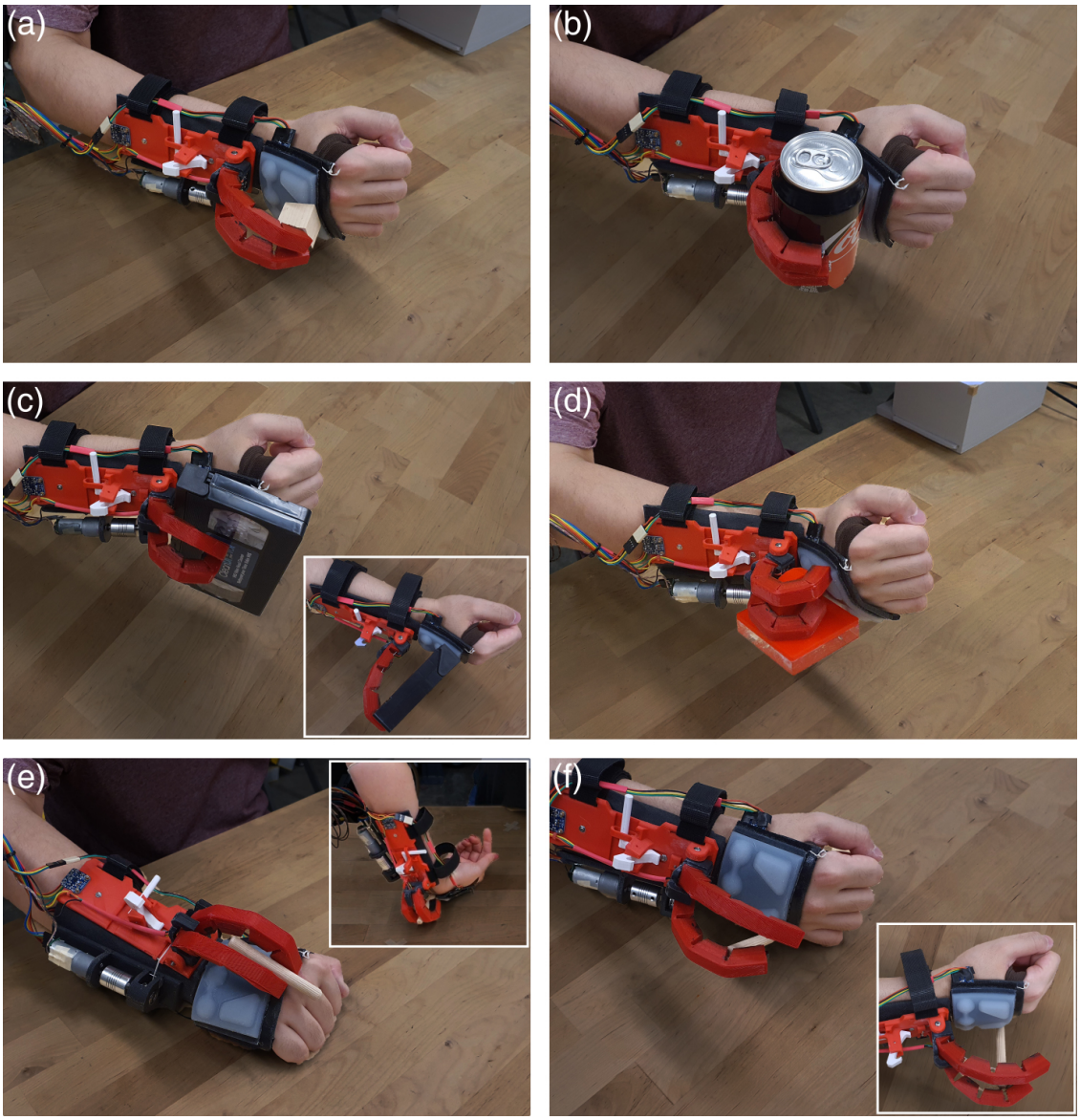

Figure 4.10: The Dorsal Grasper is used to perform the Grasp and Release Test on five objects: (a) a block, (b) a can, (c) a videotape, showing an inset image of an alternative object orientation, (d) a paperweight, and (e)-(f) a peg. (e) Pinching a peg is possible with finger-adduction and the inset shows the body pose of one subject's pinching strategy, where they place their opisthenar on the table with their fingers pointing toward their trunk. (f) Grasping a peg is also possible with a single finger against the palm.

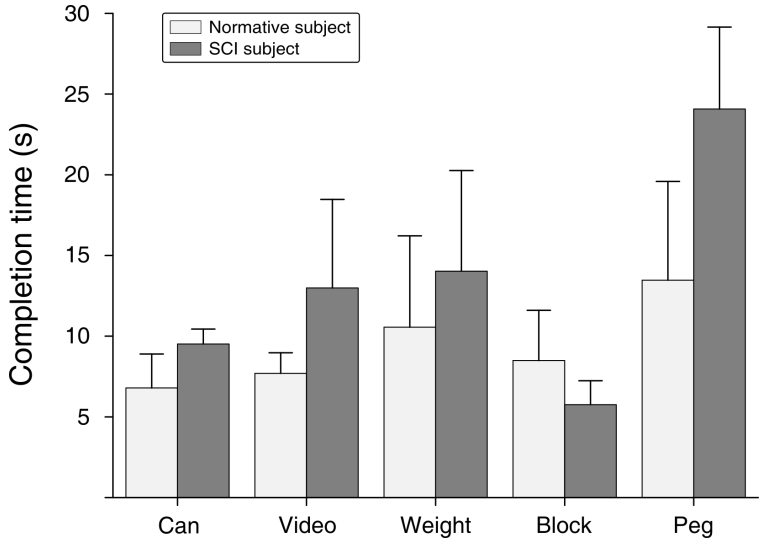

Figure 4.11: Completion times for successful trials in the modified Grasp and Release Test, showing the difference between the three normative subjects and a subject with C6 SCI. Data are presented as the mean ± s.d.

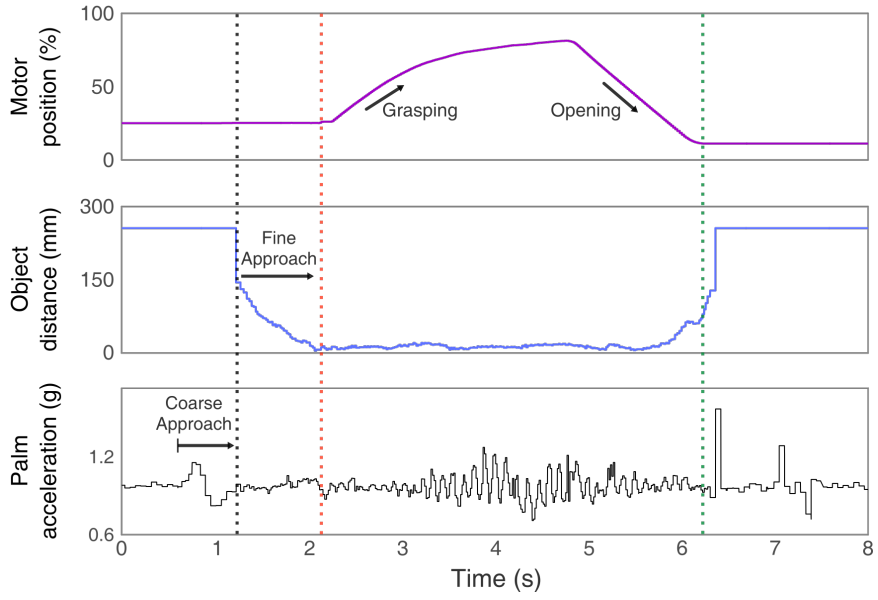

Figure 4.12: Representative real time recorded data during the execution of the Grasp and Release Test with the can. The black dotted line indicates the start time of fine approach. The red and green dotted lines indicate the start and end time point of the motor operation, respectively.

Figure 4.13: The subject with SCI picks up a water-bottle and pours water into a mug without spilling.

and opening phases may occur from the action of the person or vibrations of the motor. We aim to use these types of on-board readings to automate device behavior in future work, in lieu of the joystick.

ADL demonstration

To test the utility of the Dorsal Grasper in a more realistic ADL, the subject with SCI is asked to pour water from a 500 ml bottle into a mug (Fig. 4.13). The subject performs the task without spilling water, and a recording is included in the video extension associated with this paper. The extension also demonstrates the grasping of various ADL objects by a normative subject; it shows that the device can rapidly grasp different shapes.

4.5 Conclusion

The Dorsal Grasper enables operators to grasp objects with the opisthenar, using a set of supernumerary flexible fingers combined with an artificial palm. For strong palmar grasping, it benefits from extension of the wrist, which is commonly maintained in people after C6/C7 SCI. In addition to palmar grasping, adduction pinching exploits the V-shape of the fingers that adduct while curling. In part because this device empowers a number of different grasping strategies, preliminary data suggests that each person may demonstrate different preferences and performance when using it. Regardless, it provides intuitive operation for both experienced and inexperienced users, and both people with and without SCI.

We envision the Dorsal Grasper could serve as a candidate tool for people with SCI in performing activities of daily living, especially for larger objects that are difficult to secure in a tenodesis grasp. Because the device requires wrist extension to get the highest gripping forces, it may produce wrist fatigue with prolonged use, or encourage the strengthening extensor muscles. Future work should expand subject sample size and measure muscle

activation over longer periods during ADL. Prior supernumerary grasping works monitor muscle activation with EMG sensors [96] and finger movements with stretch sensors [104]. Future work will also incorporate wearable control input methods, by replacing the table-mounted controller box for more streamlined on-board inputs.

Chapter 5

The Dorsal Grasper: Enlarged workspace

Spinal cord injuries (SCI) substantially affect sensory, motor, and autonomous functions below the level of injury, reducing the independence and quality of life for affected individuals. Specifically, people with SCI between C5 and C7 cervical levels encounter limitations in voluntary finger and wrist flexion, reducing grasp capability. Compensatory strategies like tenodesis grasp, whereby wrist extension passively closes the fingers, remain; this is effective for lighter objects but insufficient for heavier ones. Typically, wearable assistive exoskeletons are designed to actuate a person's fingers, however, such devices are sensitive to anatomical variability, such as hand size and joint contractures. Addressing this challenge, here we present a new version of the *Dorsal Grasper*, a wearable device designed for those with voluntary wrist extension, providing human-robot collaborative grasping capabilities with underactuated supernumerary fingers on the back of the hand. We show that the *Dorsal Grasper* expands the graspable workspace and reduces trunk motion, especially in situations where the use of a wheelchair restricts the individual's posture. Our experiments with SCI participants demonstrate the *Dorsal Grasper*'s potential as a versatile assistive solution for enhancing grasping capability in individuals with distinct SCI profiles.

5.1 Introduction

Spinal cord injury (SCI) causes dysfunction of the body's sensory, motor, and autonomic systems below the level of injury[105]. This generates challenges for the individual and their care providers due to reduced function, high cost of treatment, and prolonged recovery period [106]. Individuals with SCI also often endure a concurrent impact on their psychological and social well-being, as well as an overall decrease in quality of life[107]. According to estimates, there are between 10.4 and 83 cases per million people every year[108], and the incidence of SCI is gradually increasing [106].

The most common category of SCI is at the cervical level, causing tetraplegia[109]. People

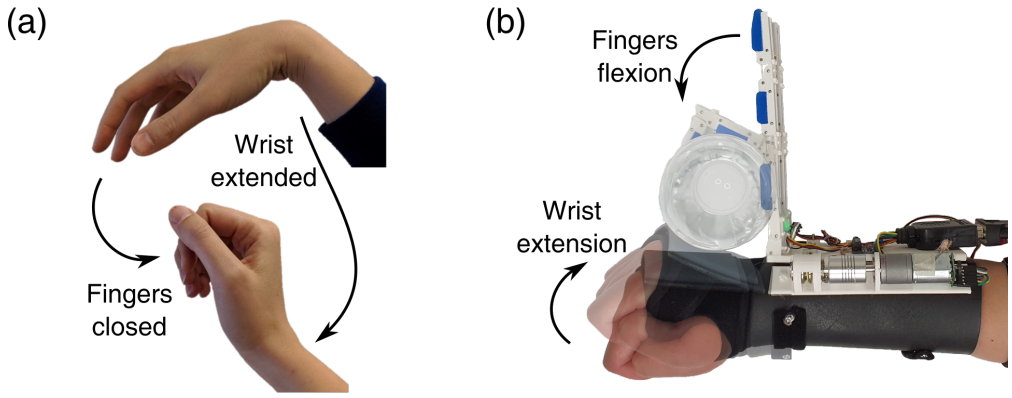

Figure 5.1: (a) Demonstration of tenodesis finger motion from [15]. Active wrist extension causes passive finger flexion. (b) The *Dorsal Grasper* includes a set of underactuated fingers and an artificial palm on the back of the hand. Here, a water-bottle is grasped using both active wrist extension and supernumerary finger flexion.

with SCI between C5 and C7 cervical levels generally lose the ability to voluntarily flex their fingers and wrist, thus reducing grasp function[110]. Studies of individuals with cervical level SCI found they believed restoring arm and hand function would considerably enhance their quality of life; they scored hand and arm function above all other functions (e.g., walking, bowel/bladder control, etc.) as the primary research priority [23, 111].

People with SCI below C5 are commonly able to actively extend their wrist (extensor carpi radialis longus and brevis), which, fortunately, can elicit passive thumb-to-forefinger motion for lateral gripping and finger-to-palm flexion for whole hand gripping due to shortening of the muscles (flexor pollicis longus, flexor digitorium superficialis and profundus)[110]. This compensatory hand skill is called "tenodesis grasp," as demonstrated in Fig. 5.1(a). Tenodesis grasp allows for picking up light and small objects, however it is less suitable for heavier and larger ones[112]. In addition, compensatory strategies like tenodesis grasp may lead to overuse injury[113] and limit the reachable workspace[114]. For heavier and larger objects, bimanual manipulation is often used, however, this limits the workspace even further. A limited workspace may lead to increased body compensation, posing challenges for tetraplegic individuals whose body motion and orientation are constrained by their kinematic limitations and the use of essential tools, such as a wheelchair.

To address these challenges, we explore a potential expansion of the tenodesis grasp using a supernumerary device that expands the range of graspable objects while mitigating exertion. The device is specifically designed to complement the limitations of the tenodesis grasp by performing power grasping for heavier and larger objects, thereby reducing reliance on bimanual grasping and extending the graspable workspace. Consequently, the use of the device can reduce body compensation and enhance overall functionality in individuals with

SCI.

Background: Re-enabling grasp function

Several methods have been proposed to restore lost grasping function in the SCI population. Functional electrical stimulation (FES) [115] is a non-invasive method that artificially stimulates peripheral nerves to restore contraction of the paralyzed muscle [116]. However, FES faces several ongoing challenges, such as skin discomfort [117], low muscle selectivity [118], and muscle fatigue [119]. More invasive approaches have included nerve transfer [120] and tendon transfer [121]. Although these surgeries have shown positive results, they are nonetheless underutilized [122, 123]. On the other hand, wearable assistive orthotics provide a practical non-invasive pathway to improve daily function [124] as well as enabling rapid prototyping for early studies on normative populations [125].

Over the past several years, various wearable devices for the upper extremities have been developed, reviewed in [126, 127, 85]. Rigid exoskeletons benefit from a precise analysis of power transmission to various joints. One common device is the wrist-driven orthosis (WDO) with a mechanical linkage to enhance tenodesis grasping[15, 114]. However, difficulties associated with these devices include comfort and fitting to different individuals [128, 129]. Thus, SCI patients frequently abandon these devices over time as they get accustomed to doing tenodesis without assistance and instead choose to utilize a set of more specialized instruments[130]. Soft devices with compliant, lightweight structures provide more comfort and adaptability. Recent soft wearable research aims at developing soft actuators, such as fabric-based actuators[18, 131] and elastomeric chambers[132, 133]. Others develop interfaces taking advantage of compliant properties. Soft-linkage or hybrid devices [16, 134, 135] are relatively easy to align with humans anatomy, enabling users to wear them for long periods in various environments [136, 137]. All of these devices – rigid or soft – actuate or support the person's fingers to enable prehensile gripping. Nonetheless, all of these approaches have their drawbacks. Instead of harnessing the user's body power, they may unintentionally restrict it. Additionally, they have the potential to constrain the wearer's remaining dexterity and present challenges in adapting to individuals with substantial anatomical variations in their joints.

Supernumerary devices offer another solution, where the user/device is not required to actuate the person's fingers[138]. One such device, developed for stroke survivors and other patients with limb impairment, included supernumerary robotic fingers mounted on a wrist brace that oppose the palm [17]. Another device applied to chronic stroke patients consisted of a soft-sixth finger that opposed the hand's radial side for grasp compensation [139]. We propose that supernumerary grasping with the back of the hand may be helpful for people with C5-C7 SCI who maintain voluntary wrist extension but limited or no finger function. This dorsal format works independently of the finger state, such that users' fingers can be either soft or stiff and passively either open or close due to variability in muscle stiffness and contractures [140, 128], as well as changes in daily activity. Such dorsal grasping would mimic power palmar grasping, and could therefore replace bimanual grasping for heavier

and larger objects, thereby expanding the reachable workspace. Additionally, the user can utilize residual dexterity, as this format doesn't constrain the hand.

Overview

A preliminary version of the device, hereby referred to as the *Dorsal Grasper*, was presented in [141]. In the present work, we perform a design iteration and a comprehensive analysis of device performance. Notably, we expand on the subject population to include SCI participants, in hopes of translating the device to a more real-world setting. Analysis is expanded to include both quantitative kinematic performance across different device conditions during Grasp and Release testing, as well as post hoc qualitative device perception that includes device usage with real-world objects.

In Section 5.2, we present the implementation and performance characterization of the updated *Dorsal Grasper* (Fig. 5.1(b)). Then, in Section 5.3, we describe the experimental methods used to measure body kinematics during reach-to-grasp trials in human subjects, both with and without SCI. Experimental results presented in Section 5.4 include both qualitative and quantitative device assessments. Observations are discussed in Section 5.5, followed by a conclusion in Section 5.6.

5.2 The *Dorsal Grasper*

The *Dorsal Grasper* is capable of grasping objects of various shapes and sizes through supernumerary grasping with the back of the hand by taking advantage of the user's active wrist extension; while complete SCI at C5 prevents wrist extension, people with SCI at C6 or C7 can extend their wrists up to 1.92 ± 0.82 Nm at $29.4° \pm 11.5°$ [124]. The device is comprised of 3D printed plastic (PLA) base situated on top of a soft cuff that is both lightweight and flexible, and holds the motor, electrical components, and updated finger design. The brace and motor base are securely fastened with L-brackets to reduce the bending force applied to the cuff during grasping. Dowel pins (2mm) are used throughout the design for cable routing to reduce friction and wear.

Tendon-driven Supernumerary Finger

In the design of the *Dorsal Grasper*, one of the key components is the supernumerary fingers. These tendon-driven fingers are 156 mm in length and 12 mm in width, arranged in a parallel configuration with a 40 mm distance between the finger centers. Each finger consists of a proximal, middle, and distal phalanx, with lengths of 64, 50, and 42 mm, respectively (Fig. 5.2). These dimensions were chosen following pilot testing to ensure that fingers can effectively grasp objects ranging in diameter from 4 to 10 cm.

The fingers are driven by tendons and are positioned upright, perpendicular to the forearm for grasping. A 0.4-mm-diameter rope (PE Braided line) on a 12 mm diameter winch

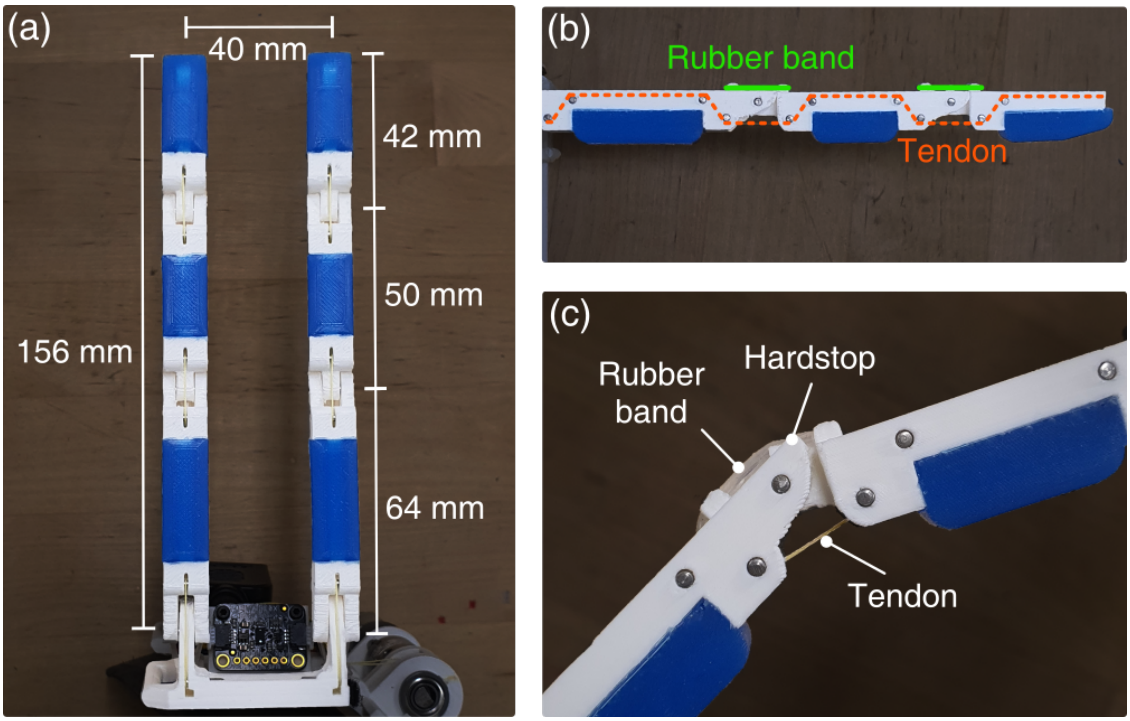

Figure 5.2: Tendon driven fingers. (a) Two three-phalanx fingers in a parallel position. (b) Tendon routing (orange) and rubber band (green). (c) Proximal joint details, showing tendon and rubber band for flexion/extension of the finger joint. The geometrical hardstop to prevent the joint from overextending.

with a DC motor (12V with a 391:1 metal gearbox) drives finger flexion during the grasping motion. In order to increase the frictional coefficient and compliance between an object and the finger, finger pads made of silicone rubber (Dragon Skin 10) are integrated onto the surface of each phalanx through casting. The thickness of each phalange is 13 mm including the finger pad.

The *Dorsal Grasper* utilizes a hinge mechanism for its joints, with two phalanges being connected by a dowel pin. Unlike the preliminary version [141], the new hinge design ensures the fingers are more rigid laterally and will not deflect when lifting heavier objects. Rubber bands (Sonic Dental Supply, Bradenton, FL, USA) are preloaded across each joint to keep the fingers passively open. The shape of the fingers has been designed to prevent overextending[1], and the rubber band preloads are selected to generate a slight base-to-tip, proximal to distal curling order.

[1]This iteration of the *Dorsal Grasper* is designed for the test in laboratory conditions. The 'stow-ablity' function in [141] weakened the grasp, so it has been removed from the current version of the *Dorsal Grasper*.

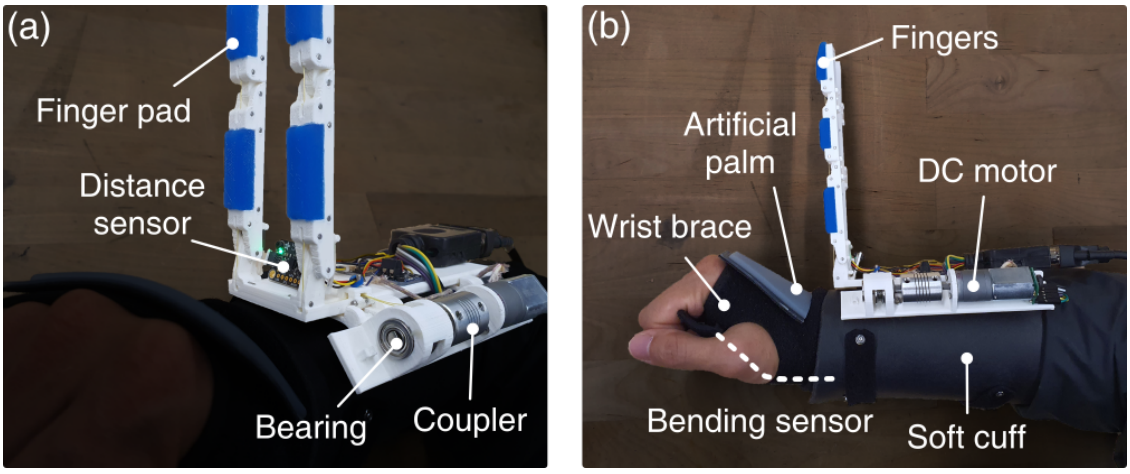

Figure 5.3: The image of the *Dorsal Grasper* while wearing the device. (a) The front side of the fingers, brace, and drive-train. (b) The right side of the device, showing the bending sensor is located on the palm side of the wrist (white dotted line) embeded within the brace.

Attachment to the Body

The attachment of the device to the forearm must be secure and comfortable to ensure effective grasping. To achieve this, as described in our previous study[141], a thermoplastic (Worbla sheet, TAP Plastics) forearm cuff is used with soft foam padding to protect the skin and distribute contact pressure. The cuff is secured onto the wearer's forearm using Velcro loops for a tight fit. The two bones (radius and ulna) in the forearm provide the capability to resist torsional rotation, thereby enhancing stability and support. The device should remain stationary on the skin, resisting the forces associated with grasping and lifting, though some slight motion may still occur due to the soft nature of the underlying tissue of the forearm and the torsional motion during supination or pronation.

Our device utilizes a commercially available wrist brace (HiRui, Xiamen, China) to integrate both an artificial palm and 1-axis flexible bending sensor (Nitto Bend Technologies, Inc., Farmington, UT, USA). The artificial palm features Velcro hooks that attach to the surface of the wrist brace (Fig. 5.3), and protects the opisthenar while increasing grasp friction. The bending sensor is embedded inside a small pocket on the palm of the wrist brace and measures the angle of wrist extension for both data acquisition and device control (Fig. 5.4). In order to compensate for individual hand shape and size variability, we calibrate the bending sensor at 0° and 45° for each participant.

Control Interface and Data Acquisition

The *Dorsal Grasper* uses a control box to collect data and control the device. This box includes a large arcade joystick, an emergency stop button, two LED indicators, and an

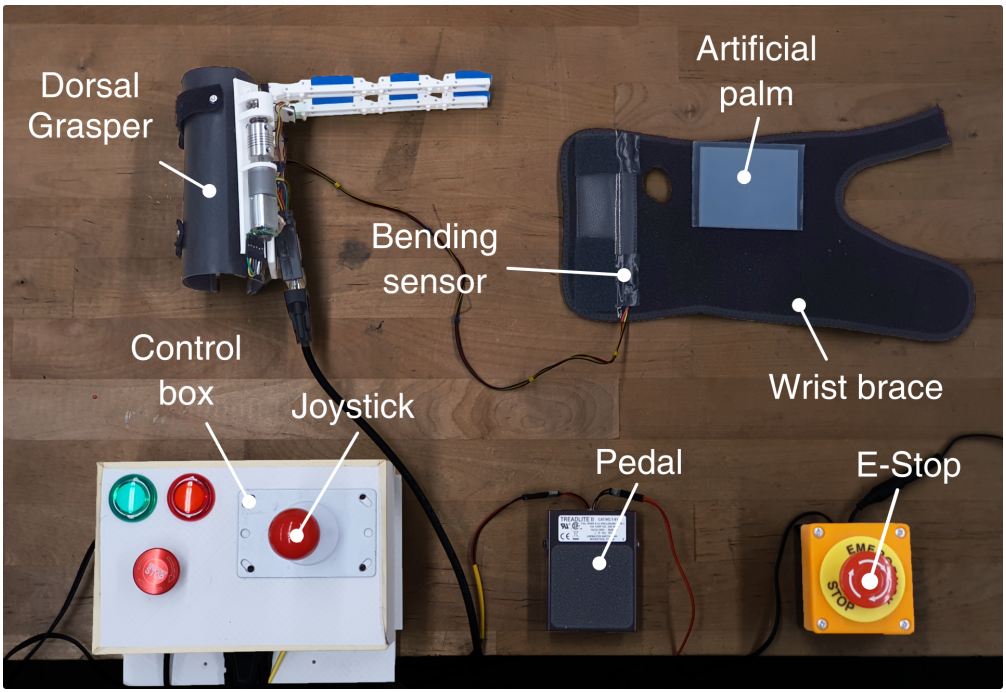

Figure 5.4: The image of the *Dorsal Grasper* system, showing the device and wrist brace with the artificial palm and bending sensor. The test bed includes the control box, synchronizing pedal, and E-Stop button.

ESP32 microcontroller (Adafruit, New York, NY, USA). A DB9 serial connector enables two-way communication between a PC, the device, and the control box.

The *Dorsal Grasper* provides two control methods – joystick control and wrist angle control – manually selected by the researcher during the experiment. In the joystick control mode, the wearer inputs the grasping commands using an arcade joystick (Adafruit, New York, NY, USA) on the control box attached to the test-bench. The joystick can be toggled left and right to initiate finger flexion (grasping) and finger extension (opening), respectively, to move at a predefined speed.

In the wrist angle control mode, the device is equipped with various sensors that serve as inputs. First, the bending sensor in the palm is used to detect wrist angle. The fingers begin to close at a predefined speed when the user extends their wrist past the close-threshold angle (20∘). In addition, a VL53L0X distance sensor (Adafruit, New York, NY, USA), placed at the base between the two supernumerary fingers, is used to prevent unexpected finger motion by determining when an object is within 60 mm of the gripper that the user may be attempting to grasp (Fig. 5.3a). To avoid detecting the back of the user's hand as an object, the sensor is angled away by 15∘. Finally, the motor's magnetic encoder (part #3499, Pololu, Las Vegas, NV, USA) is used to measure motor speed and, during stall, to

determine if grasping is complete, during which the device stops the motor to maintain the grasp with a non-backdrivable transmission. When the user relaxes their wrist extension below the open-threshold angle (10°), the supernumerary fingers move toward their original open position.

5.3 Experimental Methods

To assess the effect of the *Dorsal Grasper*, we compare its performance to conventional unassisted tenodesis (unimanual) and bimanual grasping. We administer two experiments involving normative subjects (control group) and subjects with SCI. First, we measure their graspable workspace. Then, we ask subjects to perform a series of grasp and release tasks aimed at emulating real-world conditions. We evaluate the performance of each grasping strategy with and without the device in terms of success rate, task completion time, and wrist travel distance. As the altered grasp workspace by the device could affect body kinematics, we also measure three distinct torso rotations: Flexion/Extension in the sagittal plane, transverse rotation in the transverse plane, and lateral bending in the coronal plane. It takes participants approximately 2 hours to complete the study over a single session.

Population

Four participants with SCI are recruited in the experiment group; all four had SCI between C5-C6 level. Three of the four participants are female and all are right handed. The ages of the subjects are 64, 35 (male), 62, and 42, later referenced by S1-S4, respectively. They are initially screened to have active wrist extension capability and use of tenodesis grasping. Six right-handed normative participants (5 males), aged 22-30, with unimpaired hand function, are included in the control group. All experiments with human subjects were conducted under the IRB-approved protocol #2019-07-12348 (approved 10/04/2019) from the University of California at Berkeley. Informed consent was received from all human subjects before experimentation.

Motion Capture System and Markers

Three-dimensional kinematic analysis of the upper-limb and body movements are made using the Impulse X2 motion capture system (PhaseSpace Inc., San Leandro, CA, USA), sampled at 60 Hz. Five motion cameras around an experimental area capture the body's and an object's motion by tracking the position of light-emitting diodes (LEDs). LED markers are placed on the following locations (Fig. 5.5): a body harness, a strap around the upper-arm, on the *Dorsal Grasper* around the forearm, the experiment table, and the experimental objects. One LED marker on the table is electrically connected to the synchronizing pedal in order to sync the motion capture system to the *Dorsal Grasper*.

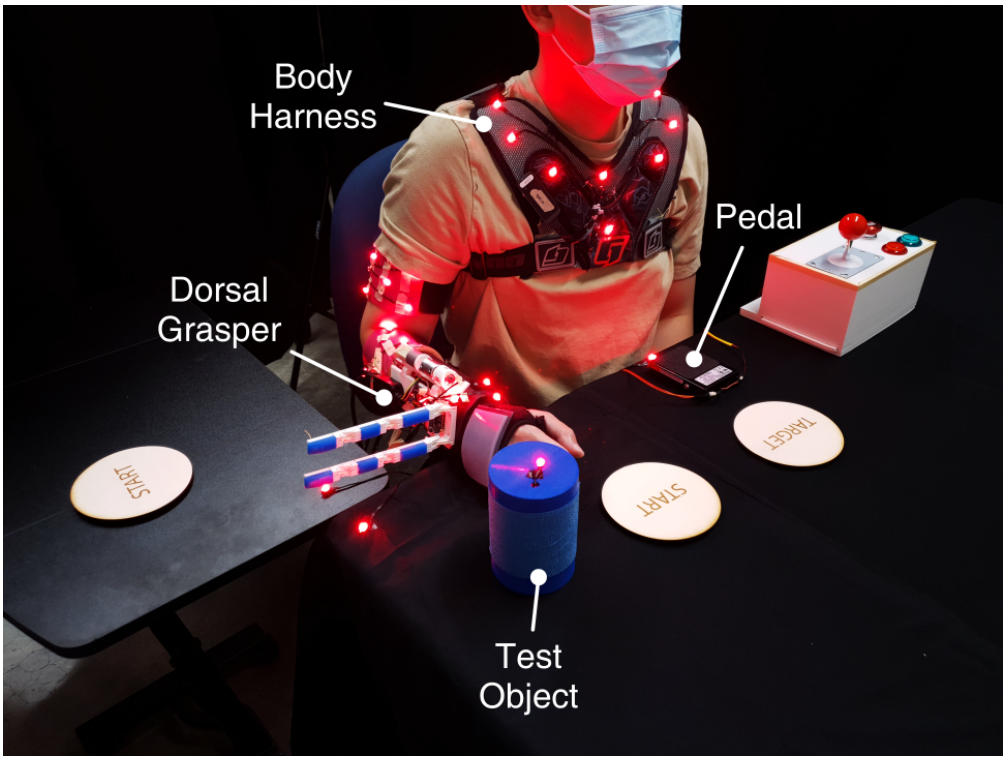

Figure 5.5: The table setup and LED markers for the experiment. LEDs are attached to the body and the table.

For accurate capture of markers during the experiment, motion capture recordings are reviewed using Recap2 post-processing software (PhaseSpace Inc., San Leandro, CA, USA). The body's neutral posture is determined by calculating averages from a calibration trial.

Graspable Workspace

We define a graspable workspace as the distance from the origin on the table in which the person can grasp and lift an object (Fig. 5.6a); the user's sitting position is fixed. We use a cylindrical object with 15 cm height, 5 cm diameter, and 80 g in weight; its edges are additionally tapered to make the object easier to slide into the hand. We put the object in a specific direction and distance from the reference origin point on the table and ask participants to grasp and lift the object. If the participant successfully performs the task, we increase the object's distance until they can no longer grasp and lift it, thus defining the graspable workspace in 2-dimensional space. Workspace measurements are performed in six directions within the extended first quadrant.

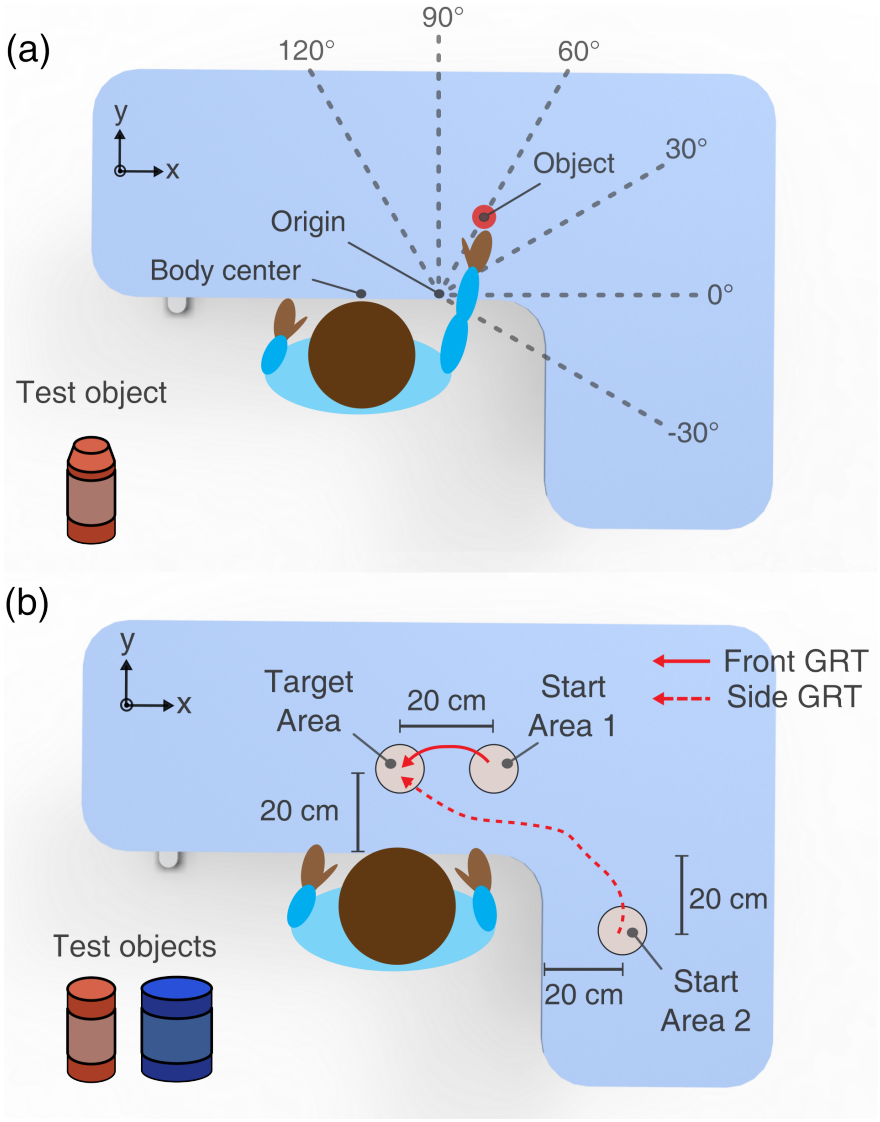

Figure 5.6: Diagram of experiments. (a) Graspable workspace measurement, showing six different directions from the origin. (b) The experimental setup for the modified Grasp and Release Test, showing two different tasks: *front GRT* and *side GRT*.

Modified Grasp and Release Test

We design a modified Grasp and Release Test (GRT) to quantitatively evaluate the *Dorsal Grasper*'s grasping success rate and how the device influences users' motion at two different points of the workspace (Fig. 5.6b). Participants are asked to grasp, lift, transfer, and release the experimental object from one of the two start areas to the target area. When the subjects are asked to grasp the object from start area 1 and release it on the target area, we call this

task *front GRT*. When an object is grasped from the start area 2 to the target area, we call that task *side GRT*. This later setup specifically places the objects on the right side of the bodies to emulate the scenario where the wheelchair cannot access the table from the front. The subjects are asked to place the objects in an upright orientation on the target area. They are also asked to push the synchronizing pedal before and after performing each task. The task is considered successful if it is completed within 30 seconds, otherwise it is considered a failure; failed tasks are not repeated. We use two 3D-printed cylindrical objects for the modified GRT. The small object is 15 cm in height, 5 cm in diameter, and 150 g in weight; the large object is 15 cm in height, 8 cm in diameter, and 500 g in weight. While the large object is only suitable for bimanual grasping, the small object can be grasped unimanually (using tenodesis grasp) by some; both objects can be unimanully grasped by the normative participants. Both objects have self-adhesive bandages wrapped around the middle to increase friction between the plastic material and the hand. All tasks are repeated three times, self-paced, and performed after pre-training prior to trial recordings.

Experimental Condition

For both evaluations, we prepare a height-adjustable L-shaped desk so that participants' upper limbs are at a comfortable elevation from the table. They are asked to fix their wheelchair position during the experiment after adjusting their body position. However, they are allowed to rotate and lean their body in their chair. In both workspace and GRT experiments, participants are asked to perform the tasks with four different grasping methods (Fig. 5.7): *unimanual* (one hand) and *bimanual* (two hands) grasping without the device; *joystick* and *wrist angle* control mode with the device. After completing the tasks using the device, participants are then asked to repeat unimanual and bimanual GRT while now wearing the device (but not using it) to evaluate how the device's weight and presence influence a non-device functional outcome in terms of success rate. Normative participants are not asked to perform bimanual grasping in the workspace experiment, while they are asked to do so in the GRT experiment to allow us to compare body kinematics between the two populations.

Interview Analysis

Following the completion of all tasks, we conduct semi-structured interviews with each participant with SCI. The interview guide covers a range of topics, including the participants' perceptions of and experiences with the *Dorsal Grasper*, their preferences regarding control modes, the comfort and usability of the device, as well as its potential for commercialization and adaptability.

Figure 5.7: Four different grasping methods performed by the subject with SCI. (a) Unimanual (one hand) and (b) bimanual (two hands) grasping without the device. (c) joystick and (d) wrist angle control mode with the device.

5.4 Results

Graspable Workspace

The graspable workspace measurements are shown in Fig. 5.8. The participants with SCI exhibit diverse tendencies across individuals and grasp methods, while normative participants show more consistent workspaces across methods, whether with or without the device. Participant S1, whose fingers are substantially flexed, displays no graspable workspace data for unimanual grasping, rendering it impossible to grip even the 50 mm object. Notably, this subject utilized the left hand (device not worn) on the table for body balance, resulting in a larger workspace for the wrist angle control mode compared to the joystick control mode, which necessitates using the left hand to operate the device.

Participant S2 exhibits the largest graspable workspace among participants with SCI in both unimanual and device-assisted grasping. For the S3 subject, the results indicate that unassisted grasping yields a larger workspace in certain directions compared to device-

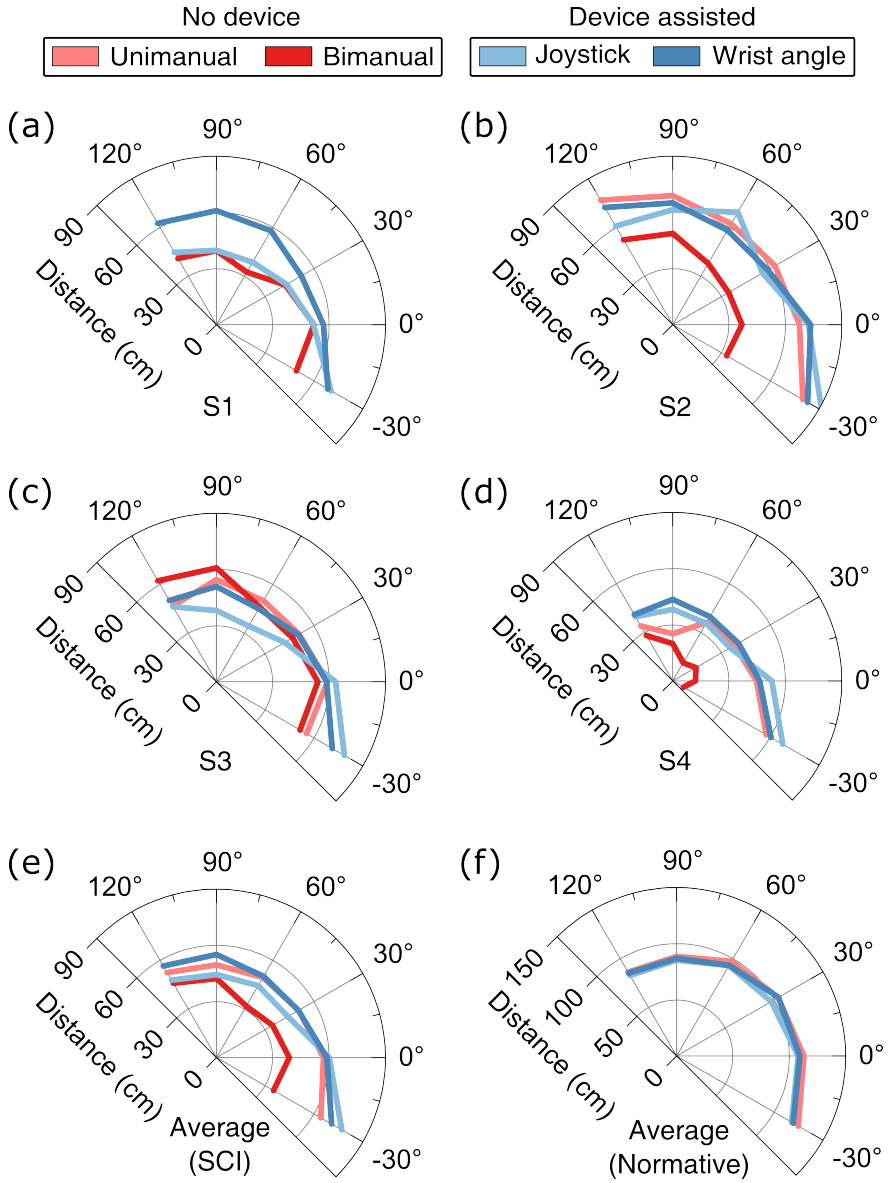

Figure 5.8: Results of graspable workspace. (a-d) Workspace results from individuals with SCI S1-S4, respectively. Average graspable workspace area from subjects with SCI (e) and normative subjects (f).

assisted grasping. Interestingly, subject S3 exhibits the largest workspace in bimanual grasping when reaching in front (120° and 90°). This participant leaned forward substantially and used their elbows to support their body, allowing them to reach and grasp objects over 60 cm from the origin. However, other participants with SCI show that bimanual grasping generally has the smallest workspace among all the grasping methods tested. Subject S4 exhibits the smallest workspace among all participants with SCI across all grasping methods measured.

On average (Fig. 5.8e), individuals with SCI demonstrate similar results between unimanual grasping and device-assisted grasping, while bimanual grasping yields the smallest workspace. In general, graspable workspaces with one hand grasping (unimanual grasping, joystick, and wrist angle control mode) tend to increase as the reaching angle decreased, which is expected considering that a lower reaching angle corresponds to reaching to the side of the body. This trend is also observed in the normative subjects' results (Fig. 5.8f). In contrast, bimanual grasping shows a tendency to decrease its workspace with lower reaching angle. Thus, the difference between bimanual grasping and the other methods increases as the angle decreases.

Modified Grasp and Release Test

Success rate

Fig. 5.9 presents the success rates of the modified GRT for subjects with SCI; normative participants achieved success in every task and are thus omitted. The average success rate for conditions without the device, representing grasping with the participants' own hand(s), is $64.7 \pm 17.3\%$. Most notably, upon wearing the device, no failures occur in performing the GRT using the 'Device assisted' modes. However, in 'Device unassisted', unimanual grasping success rate drops significantly from $41.7 \pm 31.2\%$ to $12.5 \pm 25.0\%$ while bimanual grasping success rate remains the same. This difference is attributed to subjects S2 (87.5% dropping to 50%) and S4 (45.8% dropping to 25%); the participants fail to grasp the large object in all tasks when wearing the device but using their own hand, despite successfully performing the *front GRT* task with the large object using unimanual grasping in the 'No device' condition. Subjects S1 and S3 success rates for both 'No device' and 'Device unassisted' remain the same at 50% and 75%, respectively. Thus, for some subjects and objects, the device (possibly the wrist brace) may impede the tenodesis grasp.

Completion time and travel distance

The results for the completion time and wrist trajectory of the GRT, along with the mean difference between the two populations, are presented in Fig. 5.10. The normative population demonstrates more consistent completion times and travel distances across the different grasping methods than subjects with SCI; mean standard deviations of 0.84 compared to 3.30 s for completion times and 81.1 compared to 294.7 mm for travel distances, respectively. Unimanual and bimanual grasping methods exhibit shorter completion times compared to

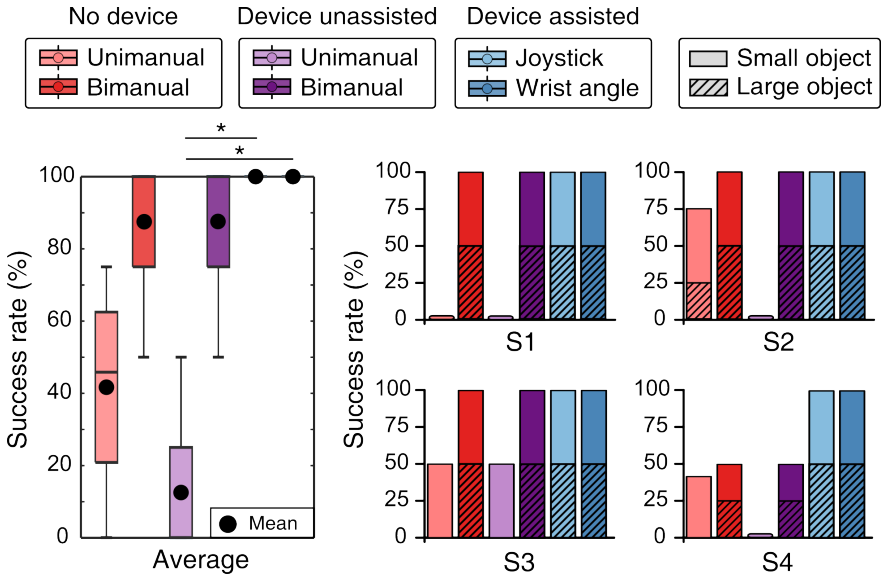

Figure 5.9: Success rate of the grasp and release test from SCI population. Unassisted grasping includes both unimanual and bimanual grasping without assistance from the worn device. Asterisks denote statistical significance after paired t-tests with Bonferroni correction for multiple comparisons (*p < 0.05).

the joystick and wrist angle control modes in normative subjects; this can be attributed to the fact that using the device requires additional time to operate fingers with fixed speeds, whereas bare hands can accomplish a grasp very quickly. In normative participants, unimanual grasping without a device exhibits the shortest wrist travel distance, while bimanual grasping displays the largest, despite similar completion times. From observation, participants maintained an unusually rigid posture during bimanual grasping; their elbows were largely extended and they rotated the whole torso rather than just their arms as in unimanual grasping, leading to the observed longer distances.

The results obtained from subjects with SCI exhibit greater variability across participants and grasping methods. Specifically, when attempting to grasp the large object using unimanual grasping (i.e. without the device), only one SCI subject successfully, though slowly, performed the *front GRT*, while none of the participants could perform the unassisted unimanual *side GRT*. On the other hand, the utilization of the *Dorsal Grasper* resulted in successful grasps across all participants during the 'large object Side GRT' task, indicating a performance improvement and normalization across subjects. This suggests that the device is beneficial even for individuals with severe and varied hand dysfunction due to SCI impairment. However, device-assisted grasping did not consistently lead to reduced completion times. In addition to needing to first orient the gripper around the object and then operate the fingers, SCI participants in particular also face mobility challenges that require them to

spend more time rotating their bodies towards the object. Conversely, device-assisted grasping did result in the shortest travel distances. Although time is not significantly affected, the device enables a more efficient grasping action for the SCI participants.

To compare the two subject groups, we calculated the mean differences between them (Fig. 5.10, bottom row). Notably, the differences in completion times and wrist travel distance exhibit a decreasing trend across the grasping methods, with unimanual, bimanual grasping, and device-assisted modes, in that order. While participants with SCI display substantial variability across grasping methods, the mean difference results, for both travel distance and completion time, suggest that performance in GRT using the device is approaching that of normative participants. However, the observed diminishing differences are also in part due to a worsening grasp performance with the device in the normative population.

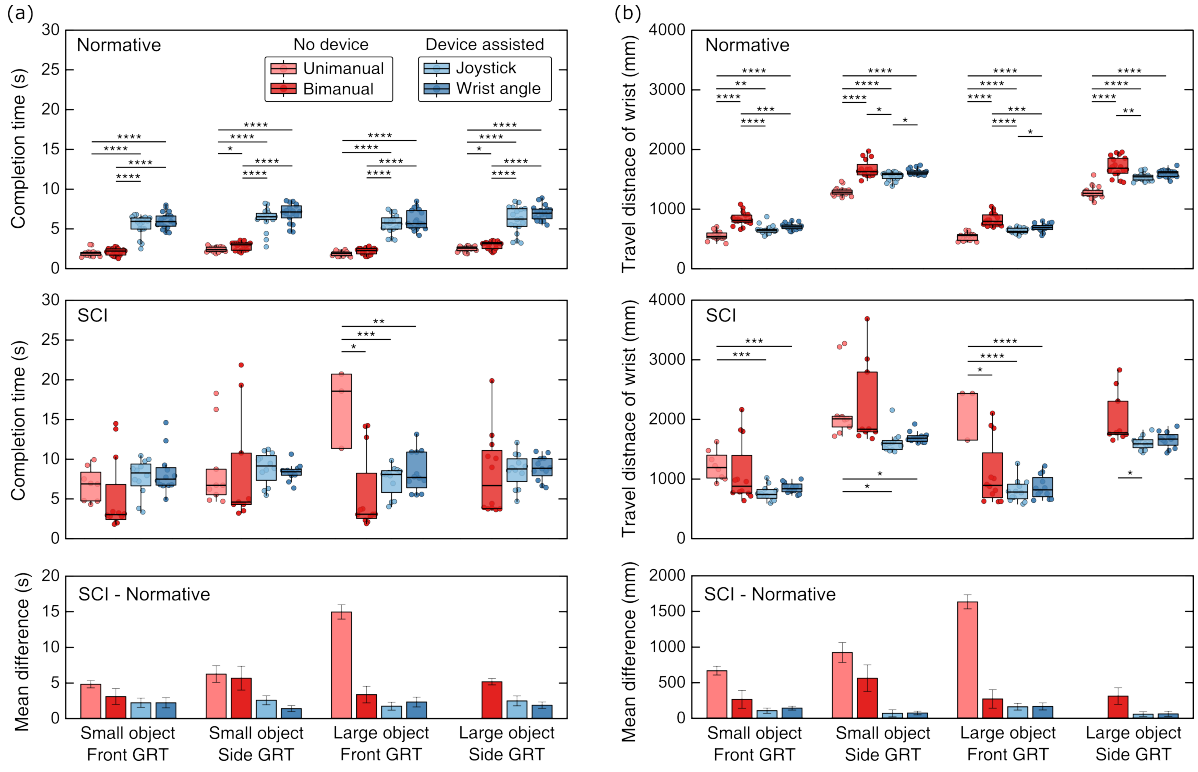

Figure 5.10: Results of the (a) completion time and (b) wrist travel distance of the GRT. The results include data from the normative population, subjects with SCI, and the mean differences between the two populations, shown from top to bottom, respectively. The mean differences are presented as the mean difference ± standard error of the mean. Asterisks denote statistical significance after two-sampled t-tests with Bonferroni correction for multiple comparisons (*p $<$ 0.05, **p $<$ 0.01, ***p $<$ 0.001, ****p $<$ 0.0001).

Torso rotation

The results of torso rotations during the GRT are presented in Fig. 5.11. We defined the range of motion as the angular difference between the maximum and minimum angles during each GRT task. Due to kinematic constraints, during *side GRT* with bimanual grasping, both subject populations exhibit notably larger ranges of motion compared to *front GRT*. Among normative subjects, unimanual grasping consistently exhibits the least body rotation across all task configurations, even when comparing *side GRT* tasks to *front GRT*. In contrast, among SCI subjects, device-assisted modes often result in significantly lower torso rotation compared to modes without the device. Therefore, the device assisted modes consistently provide significant reductions in transverse and lateral compared with bimanual grasping, and sometimes unimanual grasping as well. While normative subjects tend to show larger ranges of motion with bimanual grasping than with unimanual grasping, SCI subjects during the 'large object Front GRT' task exhibit median values for unimanual grasping larger than those for bimanual grasping. For both populations, differences between the joystick and wrist angle control modes are not substantial, except for the 'large object Side GRT' task in flexion/extension from the SCI subjects.

The mean difference of the range of motions between SCI and normative subjects is shown at the bottom of Fig. 5.11c-e. In unimanual grasping, SCI subjects exhibit a larger range of motion across all torso rotations. Due to weaker arm and hand strength, SCI subjects may require further body adjustments to successfully perform the tasks. During bimanual grasping for *side GRT*, both subject groups rotated their torsos to face the start area, but likely owing to greater body mobility, normative subjects had greater flexion/extension and transverse rotations than that of SCI subjects. On the other hand, subjects with SCI had to leverage more lateral bending for these tasks. However, with device-assisted modes, subjects with SCI are able to reach objects without large lateral bending resulting in smaller differences ($<5°$) between the two populations.

Common Interview Theme from Subjects with SCI

All subjects expressed a preference for using the device over their own hand(s) for GRT tasks. Subject S3 specifically noted, "This [the device] is definitely better for things that are super heavy." Also, subject S4 commented, "I felt like I didn't have to extend my body as much and I didn't have to use as many muscles with the device. So that's the benefit." Regarding comfort, subjects S1, S2, and S4 rated the device a 4 out of 5, while subject S3 rated it 2.5 out of 5, with 0 being uncomfortable and 5 being very comfortable. Subject S4 mentioned that the weight of the device was the only complaint, and subject S3 remarked, "It's not the most comfortable thing, but now I don't know if it was the device or the sensors and the vest [body harness]." Generally, subjects preferred using the joystick control mode for the heavier object, stating that it felt less dependent on their wrist and stronger, as they could apply grasp force from the device toward the object and back of the hand. However, they found the wrist angle mode easier to learn, with subject S1 commenting, "The wrist

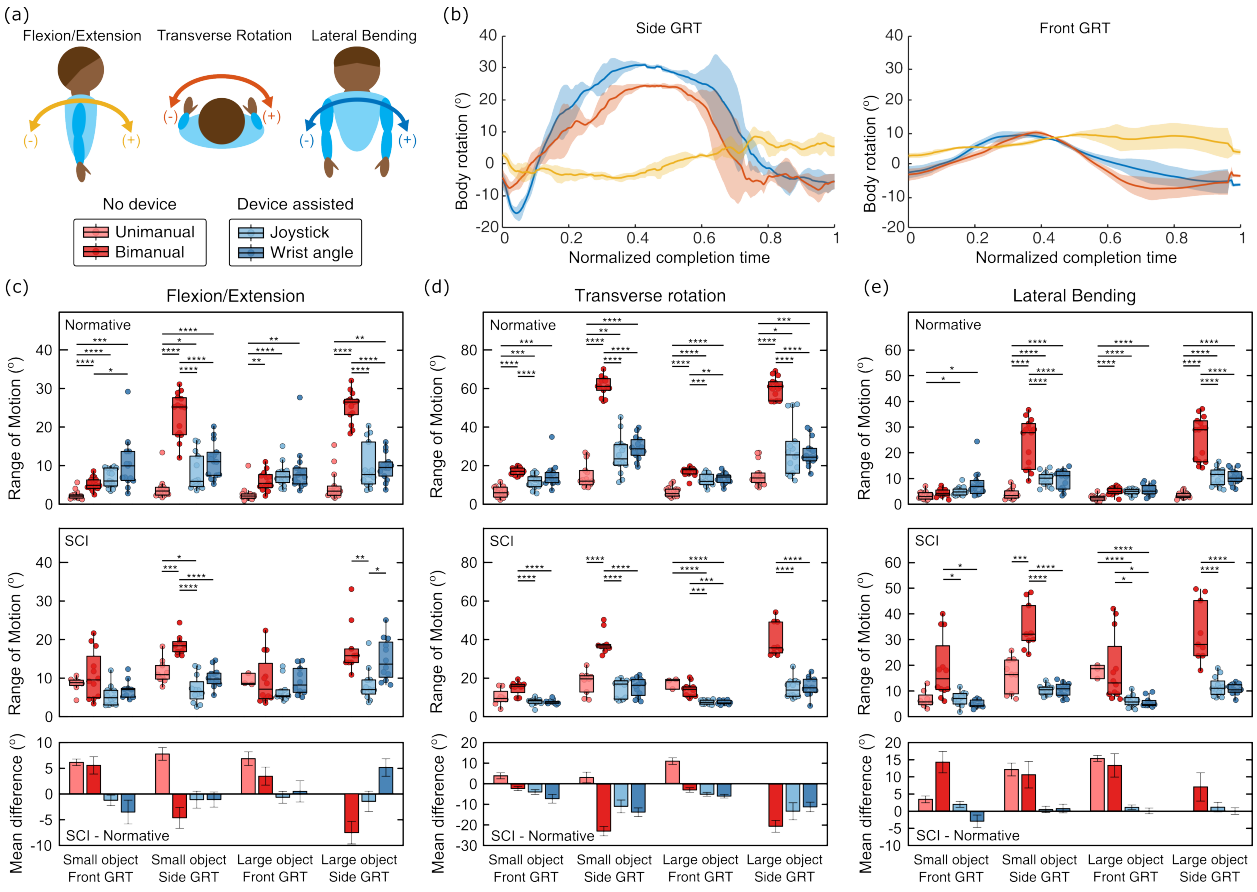

Figure 5.11: Torso rotation results during the GRT. (a) Three torso rotations and their sign convention. (b-c) Representative torso rotation during GRT with the large object using bimanual grasping, with solid colored lines indicating the average and colored areas representing the standard deviation. Data represented here are from all three trial repetitions from one subject with SCI. (d-f) The average range of torso rotations during the GRT. Asterisks denote statistical significance after two-sampled t-tests with Bonferroni correction for multiple comparisons (*p $<$ 0.05, **p $<$ 0.01, ***p $<$ 0.001, ****p $<$ 0.0001).

angle was more intuitive than the joystick."

Observations of Onboard Device Sensor Data

Throughout the study, we observed variations in the grasping phase between the test objects in the wrist angle control mode. To further investigate, we segmented the GRT data into five distinct phases: approach, grasp, transport, release, and return. We illustrate one subject performing the *front GRT* in Fig. 5.12). Following the hand's approach to the start area, the subject extends the wrist to close the supernumerary fingers around the object, then transports it to the target area, releases the object, and finally returns to the origin. In the case of the smaller object, the subject completed the grasping phase when the motor stopped and moved the object to the target area. However, for the larger object, the subject attempted further wrist extension (indicated by the red arrow) after the motor stopped, before starting the transport phase. This second wrist extension effort was observed in two subjects with SCI in the GRT with the larger object. From this observation, we hypothesize that some subjects can perceive and intuitively increase grasp security as needed while using the device.

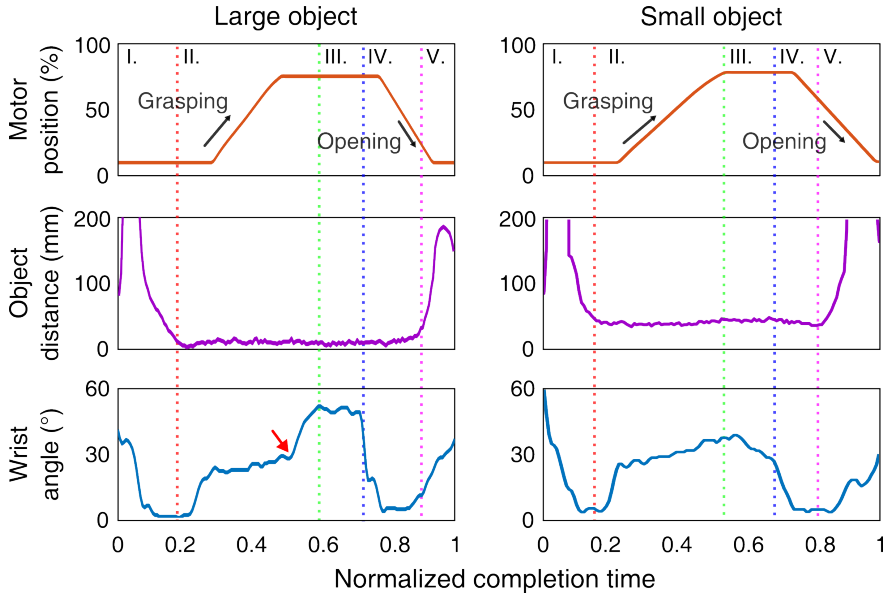

Figure 5.12: Representative sensor readings from *front GRT*. Dotted lines show transitions between grasping phases: I. approach, II. grasp, III. transport, IV. release, and V. return.

5.5 Discussion

For individuals with SCI, unimanual and bimanual grasping have complementary strengths and weaknesses. Unimanual grasping provides a larger graspable workspace (Fig. 5.8e) but is largely limited to small and light objects (Fig. 5.9). In contrast, bimanual grasping can handle larger and heavier objects but has a smaller workspace. The *Dorsal Grasper* combines the strengths of both approaches, offering a large graspable workspace and the capability to grasp large and heavy objects, making it a versatile option for a wide range of tasks. In this work, we quantify the efficiency of the movement by tracking completion times and wrist travel distances (Fig. 5.10) and trunk movements (Fig. 5.11), comparing 'no device' to 'device assisted' test conditions. All three measures confirm that the *Dorsal Grasper* provides either neutral outcomes – unchanged completion times – or benefits – reduced wrist travel distances and trunk motions – for subjects with SCI. In comparing these measures from subjects with SCI to subjects with normative hand and arm function, we find that these groups perform more similarly when using the device; while this is associated with improved performance in subjects with SCI, it also amplified by a reduction in performance by normative subjects.

One of the goals of the device is to enable supernumerary grasping for heavier and larger objects without limiting people from using tenodesis grasping for small, light objects. However, according to the results of the GRT, using tenodesis grasping under 'Device unassisted' shows decreased success rate compared to 'No device' (Fig. 5.9), specifically for S2 and S4. The added weight of the device requires more effort for individuals with reduced arm strength. The material around the wrist may also impede wrist extension motion, and the resulting grasp aperture control. Regardless, we note that device presence had no measured negative effect on S1 and S3, thus some individuals can still perform typical unimanual tenodesis grasping with the device on. Future work will explore device customization to reduce weight and minimize interference with tenodesis grasping across individual variability.

Both the joystick and wrist angle control modes of the device show similar results in terms of workspace and GRT performance. Despite this similarity, these control modes offer distinct functionalities tailored to different user requirements, with each appealing to SCI subjects for different applications. The joystick control mode allows for precise manual control over the device, enabling users to adjust their grasp according to the object's shape and size. The wrist angle control mode offers an intuitive approach, using wrist extension like in tenodesis grasp. One of the advantages of wrist angle mode over joystick mode is the liberation of the opposite hand; the left hand can brace the body during reaching tasks, for example. In some cases, the joystick mode exhibited a larger workspace than the wrist control mode, which motivates future work generating adaptable user inputs.

The supernumerary fingers squeeze an object against the back of the hand, thus, both the user and device simultaneously act on the object with opposing grasp forces. As a result, we observe that people with SCI can perceive and respond to changes in object mass to improve grasp security with additional wrist extension (Fig. 5.12). As opposed to devices that constrain the fingers, people now compensate for grasp state with body-power without

latency or physical resistance. Further study of user participation in such collaborative grasping is left to future work.

5.6 Conclusion

Supernumerary grasping with the back of the hand enables people – with varied hand muscle stiffness or contracture in the fingers resulting from SCI – to grasp more objects across a larger workspace. It is not uncommon for tables to be wheelchair inaccessible, highlighting the *Dorsal Grasper*'s important capability to expand the reachable workspace of users while avoiding the need to perform large torso movements. This laboratory study motivates future device development for translation and testing of utility in the home. This will provide valuable insights into the device's performance and usability in real-world settings, potentially uncovering new challenges and opportunities for improvement.

Chapter 6

Conclusion

The overarching research goal for the dissertation is to design efficient grippers for robotic and human-robot systems by leveraging the intrinsic functions of the systems. To achieve this goal, I introduce two different grippers for robotic and human-robot systems, addressing significant challenges in both fields. Both grippers leverage intrinsic functionality within these systems, thereby reducing the need for supplementary components such as actuators, sensors, or complicated control algorithms. I demonstrate how this strategy, despite differences in application, provides intuitive control methods in both cases. The main contributions of this work are as follows:

The design of model-based haptic search algorithm with the Smart Suction Cup

I highlight how a simple and intuitive model-based algorithm, where the suction cup adjusts its pose toward higher vacuum pressure, successfully enhances robotic grasping that previously relied solely on vision-based methods.

Enhancement of robotic grasping in industrial pick-and-place applications

In Chapter 2, the Smart Suction Cup shows a performance increase of 2.5 times in a bin-picking application compared to state-of-the-art vision-based algorithms, although there are still many failure cases with the proposed control method. In Chapter 3, I demonstrate the feasibility of industrial transfer of the developed technology despite the lab-to-industry gap.

Development of a new assistive wearable device

The Dorsal Grasper utilizes the remaining wrist extension capabilities of individuals with SCI as well as various sensory modalities in the body. By maximizing and utilizing inherent functionality, the device provides intuitive and effortless control methods for users. Additionally, due to the device's form factor, which enables supernumerary grasping with the back of the hand, it is versatile enough to accommodate the variability among individuals with disabilities, allowing every subject to operate the device effectively.

Evaluation of the device with targeted population

In Chapter 4, this new form factor (supernumerary dorsal grasping with the back of the hand) is evaluated, demonstrating its potential as an assistive wearable device for the targeted population. Chapter 5 expands on the Dorsal Grasper with an updated design and experiments for real-world scenarios. The results show that the device successfully increases the graspable workspace, thereby reducing body compensation in scenarios where the object's location is offset.

Future work

In the era of the recent AI boom, there is a growing trend to apply data-driven approaches to high-dimensional data spaces. Researchers often gather extensive data from various sensors and train models to perform desired robotic actions. However, by simply leveraging intrinsic capabilities, we can reduce the system's dimensionality and the amount of data required. This approach not only reduces computational effort but also lowers the overall cost of the robotic system. Future work will include how to integrate embodied intelligence into the system. By embedding mechanical intelligence, we can further enhance the system's efficiency and effectiveness, allowing for more intuitive and adaptive robotic actions, ultimately leading to more cost-effective and efficient solutions.

The Smart Suction cup

The design aspects of the Smart Suction Cup offer extended possibilities for further exploration. Currently, the Smart Suction Cup uses four internal chambers. Future research could investigate the impact of varying the number of chambers, such as increasing to eight or reducing to three. This variation could affect the direction error and deformation properties, providing insights into optimal configurations or design requirements for multi-chamber suction cups.

As shown in our experiments, the current haptic search method exhibits several failure modes. While some issues may be mitigated by the jumping haptic search introduced in Chapter 3, many other failure modes persist. For example, the current method employs fixed weight values between lateral positioning and rotational alignment, leading to ineffective haptic searches in certain scenarios. A more sophisticated approach would involve adaptable weight values based on various factors, such as the curvature of the contact point. Additionally, the fixed step size and yaw angle used in experiments could be refined through more adaptive control methods.

The current model-based haptic search cannot fully utilize all sensor information. So far, only normalized direction vectors from pressure differences have been utilized. However, incorporating more information from data, such as the amplitude of the vacuum pressure, and time-series pressure changes, could provide further control inputs. For instance, the ampli-

tude could indicate the distance of the suction cup from the object, allowing for adjustments in step size during the haptic search.

Additionally, the Smart Suction Cup will be able to further leverage suction airflow by integrating mechanical intelligence into the system. By utilizing the pressure difference between chambers and a fluidic computation circuit [142], an adaptive haptic response can be achieved. This system will be capable of dynamically adjusting to varying conditions, enhancing its effectiveness in complex environments without requiring additional computational effort or even reducing it.

The Dorsal Grasper

Currently, the Dorsal Grasper has only been evaluated in laboratory setups. To ensure its effectiveness for actual users in real-world scenarios, it is essential to evaluate the device in a fully unstructured environment, such as the user's home. This would involve testing the device during actual daily living tasks, providing insights into its practical usability and effectiveness. By examining how the device influences the user's grasping patterns compared to their natural grasping taxonomy without the device, we can identify its strengths and weaknesses. This will guide further refinements and improvements, enhancing its functionality as an assistive technology.

The current active version of the Dorsal Grasper, while effective, has limitations due to its electronics and drive trains, which contribute to its bulk and weight. Considering that the device is intended for individuals with spinal cord injuries, it needs to be compact and lightweight. Active components also introduce potential failure points, such as sensors and motors, complicating long-term use without professional supervision. One solution for addressing these issues would be to develop a fully passive version of the Dorsal Grasper that does not use active components like sensors and motors. The supernumerary fingers remain in position on the back of the hand, and users perform grasping actions by extending their wrists. Although this passive version may offer lower grasping strength compared to the active version, its form factor ensures that it is easy to don and doff, lightweight, and suitable for prolonged use. Additionally, this passive Dorsal Grasper can be further reinforced with a mechanical system that magnifies grasping force. For example, when the user extends their wrist, the tendon connected to the wrist can flex the supernumerary fingers with a mechanical advantage, thereby achieving additional grasp force with the device.

Bibliography

[1] H. Duan, P. Wang, Y. Huang, G. Xu, W. Wei, and X. Shen, "Robotics dexterous grasping: The methods based on point cloud and deep learning," *Frontiers in Neurorobotics*, vol. 15, p. 658280, 2021.

[2] A. Billard and D. Kragic, "Trends and challenges in robot manipulation," *Science*, vol. 364, no. 6446, p. eaat8414, 2019.

[3] K. Hsiao, L. P. Kaelbling, and T. Lozano-Pérez, "Robust grasping under object pose uncertainty," *Autonomous Robots*, vol. 31, pp. 253–268, 2011.

[4] K. Kleeberger, R. Bormann, W. Kraus, and M. F. Huber, "A survey on learning-based robotic grasping," *Current Robotics Reports*, vol. 1, pp. 239–249, 2020.

[5] J. M. Romano, K. Hsiao, G. Niemeyer, S. Chitta, and K. J. Kuchenbecker, "Human-inspired robotic grasp control with tactile sensing," *IEEE Transactions on Robotics*, vol. 27, no. 6, pp. 1067–1079, 2011.

[6] E. Brown, N. Rodenberg, J. Amend, A. Mozeika, E. Steltz, M. R. Zakin, H. Lipson, and H. M. Jaeger, "Universal robotic gripper based on the jamming of granular material," *Proceedings of the National Academy of Sciences*, vol. 107, no. 44, pp. 18 809–18 814, 2010.

[7] K. Becker, C. Teeple, N. Charles, Y. Jung, D. Baum, J. C. Weaver, L. Mahadevan, and R. Wood, "Active entanglement enables stochastic, topological grasping," *Proceedings of the National Academy of Sciences*, vol. 119, no. 42, p. e2209819119, 2022.

[8] T. Feix, J. Romero, C. H. Ek, H.-B. Schmiedmayer, and D. Kragic, "A metric for comparing the anthropomorphic motion capability of artificial hands," *IEEE transactions on robotics*, vol. 29, no. 1, pp. 82–93, 2012.

[9] K. Sanders, M. Danielczuk, J. Mahler, A. Tanwani, and K. Goldberg, "Non-markov policies to reduce sequential failures in robot bin picking," in *2020 IEEE 16th International Conference on Automation Science and Engineering (CASE)*. IEEE, 2020, pp. 1141–1148.

[10] M. Guo, D. V. Gealy, J. Liang, J. Mahler, A. Goncalves, S. McKinley, J. A. Ojea, and K. Goldberg, "Design of parallel-jaw gripper tip surfaces for robust grasping," in *2017 IEEE international conference on robotics and automation (ICRA)*. IEEE, 2017, pp. 2831–2838.

[11] H. Zhang, J. Peeters, E. Demeester, and K. Kellens, "A cnn-based grasp planning method for random picking of unknown objects with a vacuum gripper," *Journal of Intelligent & Robotic Systems*, vol. 103, pp. 1–19, 2021.

[12] A. Namiki, T. Komuro, and M. Ishikawa, "High-speed sensory–motor fusion for robotic grasping," *Measurement Science and Technology*, vol. 13, no. 11, p. 1767, 2002.

[13] J. Tegin and J. Wikander, "Tactile sensing in intelligent robotic manipulation–a review," *Industrial Robot: An International Journal*, vol. 32, no. 1, pp. 64–70, 2005.

[14] Z. Kappassov, J.-A. Corrales, and V. Perdereau, "Tactile sensing in dexterous robot hands," *Robotics and Autonomous Systems*, vol. 74, pp. 195–220, 2015.

[15] A. I. McPherson, V. V. Patel, P. R. Downey, A. A. Alvi, M. E. Abbott, and H. S. Stuart, "Motor-augmented wrist-driven orthosis: Flexible grasp assistance for people with spinal cord injury," in *2020 42nd Annual Int Conf of the IEEE Engineering in Medicine & Biology Society (EMBC)*. IEEE, 2020, pp. 4936–4940.

[16] B. B. Kang, H. Choi, H. Lee, and K.-J. Cho, "Exo-glove poly ii: A polymer-based soft wearable robot for the hand with a tendon-driven actuation system," *Soft robotics*, vol. 6, no. 2, pp. 214–227, 2019.

[17] F. Y. Wu and H. H. Asada, ""Hold-and-Manipulate" with a Single Hand Being Assisted by Wearable Extra Fingers," *2015 IEEE International Conference on Robotics and Automation (ICRA)*, p. 6205–6212, 2015.

[18] L. Cappello, J. T. Meyer, K. C. Galloway, J. D. Peisner, R. Granberry, D. A. Wagner, S. Engelhardt, S. Paganoni, and C. J. Walsh, "Assisting hand function after spinal cord injury with a fabric-based soft robotic glove," *J of neuroengineering and rehabilitation*, vol. 15, no. 1, pp. 1–10, 2018.

[19] A. Furui, S. Eto, K. Nakagaki, K. Shimada, G. Nakamura, A. Masuda, T. Chin, and T. Tsuji, "A myoelectric prosthetic hand with muscle synergy–based motion determination and impedance model–based biomimetic control," *Science Robotics*, vol. 4, no. 31, p. eaaw6339, 2019.

[20] L. H. Huinink, H. Bouwsema, D. H. Plettenburg, C. K. Van der Sluis, and R. M. Bongers, "Learning to use a body-powered prosthesis: changes in functionality and kinematics," *Journal of neuroengineering and rehabilitation*, vol. 13, pp. 1–12, 2016.

[21] C. J. Haarman, E. E. Hekman, E. M. Maas, J. S. Rietman, and H. Van Der Kooij, "Design and feasibility of the t-grip thumb exoskeleton to support the lateral pinch grasp of spinal cord injury patients," in *2022 International Conference on Rehabilitation Robotics (ICORR)*. IEEE, 2022, pp. 1–6.

[22] T. M. Huh, K. Sanders, M. Danielczuk, M. Li, Y. Chen, K. Goldberg, and H. S. Stuart, "A multi-chamber smart suction cup for adaptive gripping and haptic exploration," in *2021 IEEE/RSJ International Conference on Intelligent Robots and Systems (IROS)*. IEEE, 2021, pp. 1786–1793.

[23] K. D. Anderson, "Targeting recovery: priorities of the spinal cord-injured population," *J of neurotrauma*, vol. 21, no. 10, pp. 1371–1383, 2004.

[24] D. Morrison, A. W. Tow, M. Mctaggart, R. Smith, N. Kelly-Boxall, S. Wade-Mccue, J. Erskine, R. Grinover, A. Gurman, T. Hunn, *et al.*, "Cartman: The low-cost cartesian manipulator that won the amazon robotics challenge," in *2018 IEEE International Conference on Robotics and Automation (ICRA)*. IEEE, 2018, pp. 7757–7764.

[25] A. Zeng, S. Song, K.-T. Yu, E. Donlon, F. R. Hogan, M. Bauza, D. Ma, O. Taylor, M. Liu, E. Romo, *et al.*, "Robotic pick-and-place of novel objects in clutter with multi-affordance grasping and cross-domain image matching," *The International Journal of Robotics Research*, vol. 41, no. 7, pp. 690–705, 2022.

[26] W. Wan, K. Harada, and F. Kanehiro, "Planning grasps with suction cups and parallel grippers using superimposed segmentation of object meshes," *IEEE Transactions on Robotics*, vol. 37, no. 1, pp. 166–184, 2020.

[27] J. Mahler, M. Matl, X. Liu, A. Li, D. Gealy, and K. Goldberg, "Dex-net 3.0: Computing robust vacuum suction grasp targets in point clouds using a new analytic model and deep learning," in *2018 IEEE International Conference on robotics and automation (ICRA)*. IEEE, 2018, pp. 5620–5627.

[28] H. Cao, H.-S. Fang, W. Liu, and C. Lu, "Suctionnet-1billion: A large-scale benchmark for suction grasping," *IEEE Robotics and Automation Letters*, vol. 6, no. 4, pp. 8718–8725, 2021.

[29] Q. Shao, J. Hu, W. Wang, Y. Fang, W. Liu, J. Qi, and J. Ma, "Suction grasp region prediction using self-supervised learning for object picking in dense clutter," in *2019 IEEE 5th International Conference on Mechatronics System and Robots (ICMSR)*. IEEE, 2019, pp. 7–12.

[30] H.-G. Cao, W. Zeng, and I.-C. Wu, "Reinforcement learning for picking cluttered general objects with dense object descriptors," in *2022 International Conference on Robotics and Automation (ICRA)*. IEEE, 2022, pp. 6358–6364.

[31] S. Aoyagi, M. Suzuki, T. Morita, T. Takahashi, and H. Takise, "Bellows suction cup equipped with force sensing ability by direct coating thin-film resistor for vacuum type robotic hand," *IEEE/ASME Transactions on Mechatronics*, vol. 25, no. 5, pp. 2501–2512, 2020.

[32] H. J. Lee, S. Baik, G. W. Hwang, J. H. Song, D. W. Kim, B.-y. Park, H. Min, J. K. Kim, J.-s. Koh, T.-H. Yang, *et al.*, "An electronically perceptive bioinspired soft wet-adhesion actuator with carbon nanotube-based strain sensors," *ACS nano*, vol. 15, no. 9, pp. 14 137–14 148, 2021.

[33] E. Shahabi, F. Visentin, A. Mondini, and B. Mazzolai, "Octopus-inspired suction cups with embedded strain sensors for object recognition," *Advanced Intelligent Systems*, vol. 5, no. 2, p. 2200201, 2023.

[34] S. Doi, H. Koga, T. Seki, and Y. Okuno, "Novel proximity sensor for realizing tactile sense in suction cups," in *2020 IEEE International Conference on Robotics and Automation (ICRA)*. IEEE, 2020, pp. 638–643.

[35] S. Sareh, K. Althoefer, M. Li, Y. Noh, F. Tramacere, P. Sareh, B. Mazzolai, and M. Kovac, "Anchoring like octopus: biologically inspired soft artificial sucker," *Journal of the royal society interface*, vol. 14, no. 135, p. 20170395, 2017.

[36] S. T. Frey, A. T. Haque, R. Tutika, E. V. Krotz, C. Lee, C. B. Haverkamp, E. J. Markvicka, and M. D. Bartlett, "Octopus-inspired adhesive skins for intelligent and rapidly switchable underwater adhesion," *Science Advances*, vol. 8, no. 28, p. eabq1905, 2022.

[37] V. Müller, T.-L. Lam, and N. Elkmann, "Sensor design and model-based tactile feature recognition," in *2017 IEEE SENSORS*. IEEE, 2017, pp. 1–3.

[38] C. Eppner, S. Höfer, R. Jonschkowski, R. Martín-Martín, A. Sieverling, V. Wall, and O. Brock, "Lessons from the amazon picking challenge: Four aspects of building robotic systems." pp. 4831–4835, 2016.

[39] K. Hang, M. Li, J. A. Stork, Y. Bekiroglu, F. T. Pokorny, A. Billard, and D. Kragic, "Hierarchical fingertip space: A unified framework for grasp planning and in-hand grasp adaptation," *IEEE Transactions on robotics*, vol. 32, no. 4, pp. 960–972, 2016.

[40] Y. Chebotar, K. Hausman, Z. Su, G. S. Sukhatme, and S. Schaal, "Self-supervised regrasping using spatio-temporal tactile features and reinforcement learning," in *2016 IEEE/RSJ International Conference on Intelligent Robots and Systems (IROS)*. IEEE, 2016, pp. 1960–1966.

[41] B. Wu, I. Akinola, J. Varley, and P. Allen, "Mat: Multi-fingered adaptive tactile grasping via deep reinforcement learning," *arXiv preprint arXiv:1909.04787*, 2019.

[42] F. R. Hogan, M. Bauza, O. Canal, E. Donlon, and A. Rodriguez, "Tactile regrasp: Grasp adjustments via simulated tactile transformations," in *2018 IEEE/RSJ International Conference on Intelligent Robots and Systems (IROS)*. IEEE, 2018, pp. 2963–2970.

[43] R. Calandra, A. Owens, D. Jayaraman, J. Lin, W. Yuan, J. Malik, E. H. Adelson, and S. Levine, "More than a feeling: Learning to grasp and regrasp using vision and touch," *IEEE Robotics and Automation Letters*, vol. 3, no. 4, pp. 3300–3307, 2018.

[44] J. Mahler, M. Matl, V. Satish, M. Danielczuk, B. DeRose, S. McKinley, and K. Goldberg, "Learning ambidextrous robot grasping policies," *Science Robotics*, vol. 4, no. 26, p. eaau4984, 2019.

[45] V. Satish, J. Mahler, and K. Goldberg, "On-policy dataset synthesis for learning robot grasping policies using fully convolutional deep networks," *IEEE Robotics and Automation Letters*, 2019.

[46] S. Dasari, F. Ebert, S. Tian, S. Nair, B. Bucher, K. Schmeckpeper, S. Singh, S. Levine, and C. Finn, "Robonet: Large-scale multi-robot learning," *arXiv preprint arXiv:1910.11215*, 2019.

[47] X. Zeng, L. Zheng, H. Xie, B. Lu, K. Xia, K. Chao, W. Li, J. Yang, S. Lin, and J. Li, "Current status and future perspective of waste printed circuit boards recycling," *Procedia Environmental Sciences*, vol. 16, pp. 590–597, 2012.

[48] J. Li, P. Shrivastava, Z. Gao, and H.-C. Zhang, "Printed circuit board recycling: a state-of-the-art survey," *IEEE transactions on electronics packaging manufacturing*, vol. 27, no. 1, pp. 33–42, 2004.

[49] S. B. Wath, A. N. Vaidya, P. Dutt, and T. Chakrabarti, "A roadmap for development of sustainable e-waste management system in india," *Science of the Total Environment*, vol. 409, no. 1, pp. 19–32, 2010.

[50] J. Li, B. Tian, T. Liu, H. Liu, X. Wen, and S. Honda, "Status quo of e-waste management in mainland china," *Journal of Material Cycles and Waste Management*, vol. 8, pp. 13–20, 2006.

[51] R. Khanna, R. Cayumil, P. Mukherjee, and V. Sahajwalla, "A novel recycling approach for transforming waste printed circuit boards into a material resource," *Procedia environmental sciences*, vol. 21, pp. 42–54, 2014.

[52] Y. Lu, B. Yang, Y. Gao, and Z. Xu, "An automatic sorting system for electronic components detached from waste printed circuit boards," *Waste Management*, vol. 137, pp. 1–8, 2022.

[53] J. Lee, S. D. Lee, T. M. Huh, and H. S. Stuart, "Haptic search with the smart suction cup on adversarial objects," *IEEE Transactions on Robotics*, vol. 40, pp. 226–239, 2024.

[54] A. Jaiswal and B. Kumar, "Vacuum gripper-an important material handling tool," *Int J Sci Technol*, vol. 7, pp. 1–8, 2017.

[55] Y. Yoo, J. Eom, M. Park, and K.-J. Cho, "Compliant suction gripper with seamless deployment and retraction for robust picking against depth and tilt errors," *IEEE Robotics and Automation Letters*, vol. 8, no. 3, pp. 1311–1318, 2023.

[56] E. Papadakis, F. Raptopoulos, M. Koskinopoulou, and M. Maniadakis, "On the use of vacuum technology for applied robotic systems," in *2020 6th International Conference on Mechatronics and Robotics Engineering (ICMRE)*. IEEE, 2020, pp. 73–77.

[57] D. Pham and S. Yeo, "Strategies for gripper design and selection in robotic assembly," *The International Journal of Production Research*, vol. 29, no. 2, pp. 303–316, 1991.

[58] F. Raptopoulos, M. Koskinopoulou, and M. Maniadakis, "Robotic pick-and-toss facilitates urban waste sorting," in *2020 IEEE 16th International Conference on Automation Science and Engineering (CASE)*. IEEE, 2020, pp. 1149–1154.

[59] B. Sauvet, F. Lévesque, S. Park, P. Cardou, and C. Gosselin, "Model-based grasping of unknown objects from a random pile," *Robotics*, vol. 8, no. 3, p. 79, 2019.

[60] S. P. Gundupalli, S. Hait, and A. Thakur, "A review on automated sorting of source-separated municipal solid waste for recycling," *Waste management*, vol. 60, pp. 56–74, 2017.

[61] R. Newbury, M. Gu, L. Chumbley, A. Mousavian, C. Eppner, J. Leitner, J. Bohg, A. Morales, T. Asfour, D. Kragic, *et al.*, "Deep learning approaches to grasp synthesis: A review," *IEEE Transactions on Robotics*, 2023.

[62] L. Yu and M. T. Orchard, "Accurate edge location identification based on location-directed image modeling," in *2019 IEEE International Conference on Image Processing (ICIP)*. IEEE, 2019, pp. 2971–2975.

[63] Z. Liu, Y. Lin, Y. Cao, H. Hu, Y. Wei, Z. Zhang, S. Lin, and B. Guo, "Swin transformer: Hierarchical vision transformer using shifted windows," in *Proceedings of the IEEE/CVF international conference on computer vision*, 2021, pp. 10 012–10 022.

[64] K. Chen, J. Wang, J. Pang, Y. Cao, Y. Xiong, X. Li, S. Sun, W. Feng, Z. Liu, J. Xu, Z. Zhang, D. Cheng, C. Zhu, T. Cheng, Q. Zhao, B. Li, X. Lu, R. Zhu, Y. Wu, J. Dai, J. Wang, J. Shi, W. Ouyang, C. C. Loy, and D. Lin, "MMDetection: Open mmlab detection toolbox and benchmark," *arXiv preprint arXiv:1906.07155*, 2019.

[65] L. Yu and M. T. Orchard, "Location-directed image modeling and its application to image interpolation," in *2018 25th IEEE International Conference on Image Processing (ICIP)*. IEEE, 2018, pp. 2192–2196.

[66] A. Kirillov, E. Mintun, N. Ravi, H. Mao, C. Rolland, L. Gustafson, T. Xiao, S. Whitehead, A. C. Berg, W.-Y. Lo, *et al.*, "Segment anything," *arXiv preprint arXiv:2304.02643*, 2023.

[67] J. Brooks, "COCO Annotator," https://github.com/jsbroks/coco-annotator/, 2019.

[68] G. Bradski, "The OpenCV Library," *Dr. Dobb's Journal of Software Tools*, 2000.

[69] J. Cui and E. Forssberg, "Mechanical recycling of waste electric and electronic equipment: a review," *Journal of hazardous materials*, vol. 99, no. 3, pp. 243–263, 2003.

[70] A. Tabb and K. M. Ahmad Yousef, "Solving the robot-world hand-eye (s) calibration problem with iterative methods," *Machine Vision and Applications*, vol. 28, no. 5-6, pp. 569–590, 2017.

[71] G. Vekinis, "Out into the real world: Scaling up," in *Mastering Technology Transfer: From Invention to Innovation: A Step-by-Step Guide for Researchers and Inventors*. Springer, 2023, pp. 141–161.

[72] P. K. Yip and A. Malaspina, "Spinal cord trauma and the molecular point of no return." *Molecular neurodegeneration*, vol. 7, no. 1, p. 6, 2012.

[73] C. Lo, Y. Tran, K. Anderson, A. Craig, and J. Middleton, "Functional priorities in persons with spinal cord injury: using discrete choice experiments to determine preferences," *Journal of neurotrauma*, vol. 33, no. 21, pp. 1958–1968, 2016.

[74] G. J. Snoek, M. J. IJzerman, H. J. Hermens, D. Maxwell, and F. Biering-Sorensen, "Survey of the needs of patients with spinal cord injury: impact and priority for improvement in hand function in tetraplegics," *Spinal Cord*, vol. 42, no. 9, p. 526–532, 2004.

[75] K. Nas, L. Yazmalar, V. Şah, A. Aydın, and K. Öneş, "Rehabilitation of spinal cord injuries," *World journal of orthopedics*, vol. 6, no. 1, p. 8, 2015.

[76] S. Mateo, F. Di Rienzo, K. T. Reilly, P. Revol, C. Delpuech, S. Daligault, A. Guillot, S. Jacquin-Courtois, J. Luaute, Y. Rossetti, *et al.*, "Improvement of grasping after motor imagery in C6-C7 tetraplegia: a kinematic and MEG pilot study," *Restorative neurology and neuroscience*, vol. 33, no. 4, pp. 543–555, 2015.

[77] S. Mateo, P. Revol, M. Fourtassi, Y. Rossetti, C. Collet, and G. Rode, "Kinematic characteristics of tenodesis grasp in C6 quadriplegia," *Spinal Cord*, vol. 51, no. 2, p. 144–149, 2013.

[78] B. T. Smith, M. J. Mulcahey, and R. R. Betz, "Quantitative comparison of grasp and release abilities with and without functional neuromuscular stimulation in adolescents with tetraplegia," *Spinal Cord*, vol. 34, no. 1, p. 16–23, 1996.

[79] L. Harvey, J. Batty, R. Jones, and J. Crosbie, "Hand function of C6 and C7 tetraplegics 1–16 years following injury," *Spinal Cord*, vol. 39, no. 1, p. 37–43, 2001.

[80] A. A. Portnova, G. Mukherjee, K. M. Peters, A. Yamane, and K. M. Steele, "Design of a 3d-printed, open-source wrist-driven orthosis for individuals with spinal cord injury," *PLOS ONE*, vol. 13, no. 2, p. e0193106, 2018.

[81] Y. S. Kang, Y. G. Park, B. S. Lee, and H. S. Park, "Biomechanical evaluation of wrist-driven flexor hinge orthosis in persons with spinal cord injury," *Journal of Rehabilitation Research and Development*, vol. 50, no. 8, p. 1129–38, 2013.

[82] A. I. McPherson, V. V. Patel, P. R. Downey, A. A. Alvi, M. E. Abbott, and H. S. Stuart, "Motor-augmented wrist-driven orthosis: Flexible grasp assistance for people with spinal cord injury," in *2020 42nd Annual International Conference of the IEEE Engineering in Medicine & Biology Society (EMBC)*. IEEE, 2020, pp. 4936–4940.

[83] C. Shepherd and S. Ruzicka, "Tenodesis brace use by persons with spinal cord injuries." *American Journal of Occupational Therapy*, vol. 45, no. 1, pp. 81 – 83, 1991.

[84] D. Kaneishi, R. P. Matthew, J. E. Leu, J. O'Donnell, B. Zhang, M. Tomizuka, and H. Stuart, "Hybrid control interface of a semi-soft assistive glove for people with spinal cord injuries," in *2019 IEEE 16th International Conference on Rehabilitation Robotics (ICORR)*. IEEE, 2019, pp. 132–138.

[85] M. Sarac, M. Solazzi, and A. Frisoli, "Design requirements of generic hand exoskeletons and survey of hand exoskeletons for rehabilitation, assistive, or haptic use," *IEEE Transactions on Haptics*, vol. 12, no. 4, pp. 400–413, 2019.

[86] L. Cappello, J. T. Meyer, K. C. Galloway, J. D. Peisner, R. Granberry, D. A. Wagner, S. Engelhardt, S. Paganoni, and C. J. Walsh, "Assisting hand function after spinal cord injury with a fabric-based soft robotic glove," *Journal of NeuroEngineering and Rehabilitation*, vol. 15, no. 1, p. 59, 2018.

[87] H. K. Yap, P. M. Khin, T. H. Koh, Y. Sun, X. Liang, J. H. Lim, and C. H. Yeow, "A fully fabric-based bidirectional soft robotic glove for assistance and rehabilitation of hand impaired patients," *IEEE Robotics and Automation Letters*, vol. 2, no. 3, p. 1383–1390, 2017.

[88] P. Tran, S. Jeong, S. L. Wolf, and J. P. Desai, "Patient-Specific, Voice-Controlled, Robotic FLEXotendon Glove-II System for Spinal Cord Injury," *IEEE Robotics and Automation Letters*, vol. 5, no. 2, p. 898–905, 2020.

[89] B. B. Kang, H. Choi, H. Lee, and K. J. Cho, "Exo-Glove Poly II: A Polymer-Based Soft Wearable Robot for the Hand with a Tendon-Driven Actuation System," *Soft Robotics*, vol. 6, no. 2, p. 214–227, 2019.

[90] D. Kaneishi, J. E. S. Leu, J. A. O'Donnell, C. Affleck, R. P. Matthew, A. McPherson, M. Tomizuka, and H. Stuart, "Design and preliminary assessment of a semi-soft assistive glove for people with spinal cord injuries," in *2019 IEEE/RSJ International Conference on Intelligent Robots and Systems (IROS)*, 2019.

[91] I. Hussain, G. Salvietti, G. Spagnoletti, and D. Prattichizzo, "The Soft-SixthFinger: a Wearable EMG Controlled Robotic Extra-Finger for Grasp Compensation in Chronic Stroke Patients," *IEEE Robotics and Automation Letters*, vol. 1, no. 2, p. 1000–1006, 2016.

[92] P. Taylor, J. Esnouf, and J. Hobby, "The functional impact of the Freehand System on tetraplegic hand function. Clinical Results," *Spinal Cord*, vol. 40, no. 11, p. 560–566, 2002.

[93] J. R. Napier, "The prehensile movements of the human hand," *The Journal of Bone and Joint Surgery. British volume*, vol. 38-B, no. 4, p. 902–913, 1956.

[94] A. Bicchi, "Hands for dexterous manipulation and robust grasping: a difficult road toward simplicity," *IEEE Transactions on Robotics and Automation*, vol. 16, no. 6, p. 652–662, 2020.

[95] L. A. Jones and S. J. Lederman, *Human hand function*. Oxford University Press, 2006.

[96] I. Hussain, G. Spagnoletti, G. Salvietti, and D. Prattichizzo, "Toward wearable supernumerary robotic fingers to compensate missing grasping abilities in hemiparetic upper limb," *The International Journal of Robotics Research*, vol. 36, no. 13-14, pp. 1414–1436, 2017.

[97] M. Malvezzi, Z. Iqbal, M. C. Valigi, M. Pozzi, D. Prattichizzo, and G. Salvietti, "Design of multiple wearable robotic extra fingers for human hand augmentation," *Robotics*, vol. 8, no. 4, p. 102, 2019.

[98] T. Feix, J. Romero, H.-B. Schmiedmayer, A. M. Dollar, and D. Kragic, "The grasp taxonomy of human grasp types," *IEEE Transactions on Human-Machine Systems*, vol. 46, no. 1, p. 66–77, 2016.

[99] M. R. Cutkosky, "On grasp choice, grasp models, and the design of hands for manufacturing tasks," *IEEE Transactions on Robotics and Automation*, vol. 5, no. 3, p. 269–279, 1989.

[100] M. Kücken, "Models for fingerprint pattern formation," *Forensic Science International*, vol. 171, no. 2–3, p. 85–96, 2007.

[101] K. S. Wuolle, C. L. Van Doren, G. B. Thrope, M. W. Keith, and P. H. Peckham, "Development of a quantitative hand grasp and release test for patients with tetraplegia using a hand neuroprosthesis," *The journal of hand surgery*, vol. 19, no. 2, pp. 209–218, 1994.

[102] A. Schuboe, A. Maldonado, S. Stork, and M. Beetz, "Subsequent actions influence motor control parameters of a current grasping action," in *RO-MAN 2008-The 17th IEEE International Symposium on Robot and Human Interactive Communication*. IEEE, 2008, pp. 389–394.

[103] S. M. Michaelsen, R. P. Gomes, A. P. Marques, L. C. Rodrigues, N. G. Borges Junior, R. Claudino, and M. J. d. Santos, "Using an accelerometer for analyzing a reach-to-grasp movement after stroke," *Motriz: Revista de Educação Física*, vol. 19, no. 4, pp. 746–752, 2013.

[104] F. Y. Wu and H. Asada, "Bio-artificial synergies for grasp posture control of supernumerary robotic fingers," 2014.

[105] A. Krassioukov, "Autonomic function following cervical spinal cord injury," *Respiratory physiology & neurobiology*, vol. 169, no. 2, pp. 157–164, 2009.

[106] Y. Kang, H. Ding, H. Zhou, Z. Wei, L. Liu, D. Pan, and S. Feng, "Epidemiology of worldwide spinal cord injury: a literature review," *J of Neurorestoratology*, vol. 6, no. 1, p. 3, 2018.

[107] J. R. Tomasone, N. N. Wesch, K. A. M. Ginis, and L. Noreau, "Spinal cord injury, physical activity, and quality of life: a systematic review," *Kinesiology Review*, vol. 2, no. 2, pp. 113–129, 2013.

[108] M. Wyndaele and J.-J. Wyndaele, "Incidence, prevalence and epidemiology of spinal cord injury: what learns a worldwide literature survey?" *Spinal cord*, vol. 44, no. 9, pp. 523–529, 2006.

[109] N. S. C. I. S. Center *et al.*, "Traumatic spinal cord injury facts and figures at a glance," *Birmingham, AL.*, 2022.

[110] S. Mateo, A. Roby-Brami, K. T. Reilly, Y. Rossetti, C. Collet, and G. Rode, "Upper limb kinematics after cervical spinal cord injury: a review," *J of neuroengineering and rehabilitation*, vol. 12, no. 1, pp. 1–12, 2015.

[111] A. Bryden, A. Peljovich, H. Hoyen, G. Nemunaitis, K. Kilgore, and M. Keith, "Surgical restoration of arm and hand function in people with tetraplegia," *Topics in Spinal Cord Injury Rehabilitation*, vol. 18, no. 1, pp. 43–49, 2012.

[112] B. Smith, M. Mulcahey, and R. Betz, "Quantitative comparison of grasp and release abilities with and without functional neuromuscular stimulation in adolescents with tetraplegia," *Spinal Cord*, vol. 34, no. 1, pp. 16–23, 1996.

[113] D. Apple, R. Cody, and A. Allen, "Overuse syndrome of the upper limb in people with spinal cord injury," *Physical fitness: a guide for individuals with spinal cord injury. J Rehabil Res Dev*, vol. 26, pp. 97–108, 1996.

[114] E. Y. Chang, A. I. McPherson, R. C. Adolf, Y. Gloumakov, and H. S. Stuart, "Modulating wrist-hand kinematics in motorized assisted grasping with c5-6 spinal cord injury," *IEEE Transactions on Medical Robotics and Bionics*, 2023.

[115] M. W. Keith, P. H. Peckham, G. B. Thrope, J. R. Buckett, K. C. Stroh, and V. Menger, "Functional neuromuscular stimulation neuroprostheses for the tetraplegic hand." *Clinical orthopaedics and related research*, no. 233, pp. 25–33, 1988.

[116] K. L. Kilgore, K. D. Anderson, and P. H. Peckham, "Neuroprosthesis for individuals with spinal cord injury," *Neurological Research*, pp. 1–13, 2020.

[117] E. d. L. d. Santos, M. C. Gelain, E. Krueger, G. N. Nogueira-Neto, and P. Nohama, "Artificial motor control for electrically stimulated upper limbs of plegic or paretic people," *Research on Biomedical Engineering*, vol. 32, pp. 199–211, 2016.

[118] S. Micera, T. Keller, M. Lawrence, M. Morari, and D. B. Popovic, "Wearable neural prostheses," *IEEE Engineering in Medicine and Biology Magazine*, vol. 29, no. 3, pp. 64–69, 2010.

[119] M. Stokes and R. Cooper, "Muscle fatigue as a limiting factor in functional electrical stimulation: A review," *Physiotherapy Practice*, vol. 5, no. 2, pp. 83–90, 1989.

[120] J. M. Khalifeh, C. F. Dibble, A. Van Voorhis, M. Doering, M. I. Boyer, M. A. Mahan, T. J. Wilson, R. Midha, L. J. Yang, and W. Z. Ray, "Nerve transfers in the upper extremity following cervical spinal cord injury. part 1: systematic review of the literature," *J of Neurosurgery: Spine*, vol. 31, no. 5, pp. 629–640, 2019.

[121] J. A. Dunn, K. A. Sinnott, A. G. Rothwell, K. D. Mohammed, and J. W. Simcock, "Tendon transfer surgery for people with tetraplegia: an overview," *Archives of physical medicine and rehabilitation*, vol. 97, no. 6, pp. S75–S80, 2016.

[122] J. Fridén and A. Gohritz, "Tetraplegia management update," *The J of hand surgery*, vol. 40, no. 12, pp. 2489–2500, 2015.

[123] C. M. Curtin, D. R. Gater, and K. C. Chung, "Upper extremity reconstruction in the tetraplegic population, a national epidemiologic study," *The J of hand surgery*, vol. 30, no. 1, pp. 94–99, 2005.

[124] Y.-S. Kang, Y.-G. Park, B.-S. Lee, and H.-S. Park, "Biomechanical evaluation of wrist-driven flexor hinge orthosis in persons with spinal cord injury," *Journal OF Rehabilitation Research and Development*, 2013.

[125] E. Y. Chang, R. Mardini, A. I. McPherson, Y. Gloumakov, and H. S. Stuart, "Tenodesis grasp emulator: Kinematic assessment of wrist-driven orthotic control," in *2022 Int Conf on Robotics and Automation (ICRA)*. IEEE, 2022, pp. 5679–5685.

[126] S. Khalid, F. Alnajjar, M. Gochoo, A. Renawi, and S. Shimoda, "Robotic assistive and rehabilitation devices leading to motor recovery in upper limb: a systematic review," *Disability and Rehabilitation: Assistive Technology*, pp. 1–15, 2021.

[127] R. Readioff, Z. K. Siddiqui, C. Stewart, L. Fulbrook, R. J. O'Connor, and E. K. Chadwick, "Use and evaluation of assistive technologies for upper limb function in tetraplegia," *The J of Spinal Cord Medicine*, pp. 1–12, 2021.

[128] A. S. Gorgey, "Robotic exoskeletons: The current pros and cons," *World J of orthopedics*, vol. 9, no. 9, p. 112, 2018.

[129] N. Jarrassé and G. Morel, "Connecting a human limb to an exoskeleton," *IEEE Transactions on Robotics*, vol. 28, no. 3, pp. 697–709, 2011.

[130] C. C. Shepherd and S. H. Ruzicka, "Tenodesis brace use by persons with spinal cord injuries," *The American J of Occupational Therapy*, vol. 45, no. 1, pp. 81–83, 1991.

[131] H. K. Yap, P. M. Khin, T. H. Koh, Y. Sun, X. Liang, J. H. Lim, and C.-H. Yeow, "A fully fabric-based bidirectional soft robotic glove for assistance and rehabilitation of hand impaired patients," *IEEE Robotics and Automation Letters*, vol. 2, no. 3, pp. 1383–1390, 2017.

[132] P. Polygerinos, S. Lyne, Z. Wang, L. F. Nicolini, B. Mosadegh, G. M. Whitesides, and C. J. Walsh, "Towards a soft pneumatic glove for hand rehabilitation," in *2013 IEEE/RSJ Int Conf on Intelligent Robots and Systems*. IEEE, 2013, pp. 1512–1517.

[133] C. Venugopal, G. Pak, S. Florea, J. Perkins, and C. Anderson, "Assistive hand device using silicone actuators," in *2021 IEEE Industrial Electronics and Applications Conf (IEACon)*. IEEE, 2021, pp. 242–245.

[134] D. Kaneishi, J. E. Leu, J. O'Donnell, C. Affleck, R. P. Matthew, A. McPherson, M. Tomizuka, and H. S. Stuart, "Design and assessment of a single-size semi-soft assistive mitten for people with cervical spinal cord injuries," in *2019 IEEE-RAS 19th Int Conf on Humanoid Robots (Humanoids)*. IEEE, 2019, pp. 614–621.

[135] C. G. Rose and M. K. O'Malley, "Hybrid rigid-soft hand exoskeleton to assist functional dexterity," *IEEE Robotics and Automation Letters*, vol. 4, no. 1, pp. 73–80, 2018.

[136] A. T. Asbeck, S. M. De Rossi, I. Galiana, Y. Ding, and C. J. Walsh, "Stronger, smarter, softer: next-generation wearable robots," *IEEE Robotics & Automation Magazine*, vol. 21, no. 4, pp. 22–33, 2014.

[137] C. Walsh, "Recent results from evaluation of soft wearable robots in clinical populations," in *Int Symposium on Wearable Robotics*. Springer, 2018, pp. 58–62.

[138] B. Yang, J. Huang, X. Chen, C. Xiong, and Y. Hasegawa, "Supernumerary robotic limbs: a review and future outlook," *IEEE Transactions on Medical Robotics and Bionics*, vol. 3, no. 3, pp. 623–639, 2021.

[139] I. Hussain, G. Salvietti, G. Spagnoletti, and D. Prattichizzo, "The soft-sixthfinger: a wearable emg controlled robotic extra-finger for grasp compensation in chronic stroke patients," *IEEE Robotics and Automation Letters*, vol. 1, no. 2, pp. 1000–1006, 2016.

[140] G. M. Yarkony, L. M. Bass, V. Keenan, and P. R. Meyer, "Contractures complicating spinal cord injury: incidence and comparison between spinal cord centre and general hospital acute care," *Spinal Cord*, vol. 23, no. 5, pp. 265–271, 1985.

[141] J. Lee, L. Yu, L. Derbier, and H. S. Stuart, "Assistive supernumerary grasping with the back of the hand," in *2021 IEEE Int Conf on Robotics and Automation (ICRA)*. IEEE, 2021, pp. 6154–6160.

[142] Q. Lu, H. Xu, Y. Guo, J. Y. Wang, and L. Yao, "Fluidic computation kit: Towards electronic-free shape-changing interfaces," in *Proceedings of the 2023 CHI Conference on Human Factors in Computing Systems*, 2023, pp. 1–21.